PREFERRED ORIENTATION IN 18/10, 18/12 AND 18/14 CHROMIUM/NICKEL STEELS AND ITS RELATION TO TENSILE AND PRESS FORMING PROPERTIES

BY

MALCOLM JOHN DICKSON

A thesis submitted for the degree of Master of Science in the Department of Metallurgy, The University of Aston in Birmingham, July 1967.

SUMMARY

The cold rolling and primary recrystallisation textures of 18% chromium steels containing 10%, 12% and 14% nickel have been determined, and tensile and press forming properties have been compared in sheet processed to obtain (a) a randomly oriented grain structure and (b) a strong primary recrystallisation texture.

During cold rolling to 93% reduction all the steels partly transform to α' martensite, the extent of transformation increasing with decreasing nickel content. The 18/10 steel exhibits a texture consisting mainly of $\{111\}\langle 11\bar{2}\rangle_{\alpha'}$, $\{112\}\langle \bar{1}10\rangle_{\alpha'}$ and $\{001\}\langle 110\rangle_{\alpha'}$ orientations with a small amount of untransformed austenite having the orientation $\{110\}\langle \bar{1}12\rangle$. In the cold rolling texture of the 18/12 and 18/14 steels the $\{110\}\langle \bar{1}12\rangle_{\gamma}$ orientation is predominant. The primary recrystallisation texture of the 18/10 steel consists of two orientations, $\sim\{230\}\langle 3\bar{2}1\rangle$ and $\sim\{230\}\langle 3\bar{2},13\rangle$, whereas the recrystallisation texture of the 18/12 and 18/14 steels may be described as $\sim\{113\}\langle \bar{2}\bar{1}1\rangle$. The effect of the martensite transformation on the cold rolling and annealing textures is discussed.

The recrystallisation textures are associated with marked planar variations in the strain ratio, R, and a mean strain ratio, $\bar{R}$, only slightly greater than that in randomly oriented material. Deep drawability is not significantly affected by the presence of the textures. The amount of earing associated with the texture in 18/10

steel is the same as that in randomly oriented material (~3%), whereas the texture in 18/12 and 18/14 steels gives rise to a larger amount of earing (6-8%).

In a fully annealed condition, the rate of work hardening, the extent of uniform elongation and the stretch formability increase with decreasing nickel content. Stretch formability is not significantly affected by the presence of strong preferred orientation.

Neither temper annealing for ½h at 800°C (instead of full annealing) nor cold reductions of up to 12.5% have any marked effect on deep drawability, but both treatments lower the stretch formability.

CONTENTS

1. INTRODUCTION

Press forming may be defined as a means of altering the shape of a flat blank and making from it some article of tubular form or one containing deep cavities. To achieve this, pressure is applied to the blank in sufficient amount to cause plastic flow, but insufficient to rupture the metal before plastic flow has taken place.

A variety of shapes are made on industrial presses, but in all cases the maximum depth of pressing which can be formed without failure depends on the inherent formability of the material itself, and also on such factors as tool configuration, frictional forces and efficiency of lubrication. Although a greater depth of pressing can be obtained by using intermediate annealing, there is usually an economical limit to the number of intermediate anneals which can be allowed.

In the past 20 years or so, both manufacturers and users of thin sheets have expressed interest in identifying the main factors which control a material's inherent formability. Most of the work has been directed towards mild steel, but F.C.C. metals and to a lesser extent C.P.H. metals have also received some attention. F.C.C. metals are particularly interesting from a research point of view because it has so far been impossible to obtain in these metals a drawability equivalent to that in some B.C.C. or C.P.H. metals.

Before describing the present work, which aims to analyse the factors affecting the inherent formability of austenitic stainless steels, it is relevant to review the available literature in this field with particular reference to F.C.C. metals and alloys, although certain parts of the review include data on B.C.C. and C.P.H. metals. An emphasis is placed on current theories concerning the factors which influence deep

drawability and stretch formability and the development of rolling and recrystallisation textures, and how this information may be used to develop good press forming properties.

2. REVIEW OF LITERATURE

2.1. Principles of Press Forming Operations

The deformation mechanisms involved in industrial pressing operations are generally considered to lie between the two extremes of deep drawing and stretch forming. Most commonly one of these processes will predominate, but both will be taking place simultaneously. However, in order to analyse the factors which influence pressing behaviour it is necessary to consider their effect on simple deep drawing and stretch forming operations.

2.1.1. Deep Drawing

a) Flat-bottomed cup drawing

The tool configuration during simple flat-bottomed cup drawing starting with a circular blank is shown in Figure 1(a). The pressure on the blank holder is insufficient to prevent inward movement of material in the flange, so that as the punch descends it causes material to flow inwards over the die profile radius to form the walls of the cup. The operation is completed when the periphery of the blank is reduced to the circumference of the cup wall. Since there occurs a zone of material which is stretched over the punch profile radius the operation is, strictly speaking, not pure drawing. The extent of this zone depends on the tool geometry.

The requirement of blank holder pressure becomes apparent from the following argument. In Figure 1(b) is shown a sector from the round blank prior to drawing. It can be seen that during movement into the die mouth, arc L_1 and radius R_1 will have to reduce to L_2 and R_2, so causing a displacement of material in the shaded areas. Since this

condition prevails throughout a circular blank, a hoop compressive stress is set up around the annular rim outside the die aperture. Without some blank holder pressure this stress would cause buckling or wrinkling.

The blank holder also restricts the tendency of the metal to thicken uniformly around the annular rim and progressively between the die mouth and outside edge, and so produces an elongation outwards. A differential speed of movement is thus set up, with material near to the die mouth moving over the die face at a greater speed than the metal at the outer edge of the blank.

Theoretically, the area of the final surface of a deep drawn cup should be equal to the area of flat blank from which it was produced.

b) Stress-strain conditions during cup drawing

The two regions of importance are the flange, where deformation occurs and force requirements originate, and the cup wall, which must support the necessary forces without tearing. Figure 1(c) shows the directions of the principal stresses in these regions. Certain simplifications are necessary to rationalise the stress-strain conditions.

In the flange, the effect of blank holder pressure is relatively small and can be ignored ($\sigma_z = 0$). The important stresses operating are therefore σ_x (radial tension) and $-\sigma_y$ (circumferential compression). Also, since little thickening occurs, $d\varepsilon_z = 0$, and a condition of plane strain is imposed.

2.1.2. Stretch Forming

a) Simple biaxial stretching

The tool configuration for simple biaxial stretching from a circular blank is shown in Figure 2. In contrast to the cup drawing operation shown in Figure 1(a), the blank holder pressure is now sufficient to prevent the inward movement of material in the flange. When pressure is applied, either hydraulically or via a round nosed punch, the material over the die becomes stretched biaxially to form a dome shaped cup. The operation is completed when the maximum or required depth of cup is obtained.

b) Stress-strain conditions during cup stretching

Using hydraulic pressure the stress system is pure biaxial tension, with the principal stresses in the plane of the sheet, σ_x and σ_y, being of equal magnitude, and the normal stress $\sigma_z = 0$. Also, since $d\varepsilon_x = d\varepsilon_y = \frac{-d\varepsilon_z}{2}$, deformation and failure can occur only by sheet thinning. When a punch is used, the material which is in contact with the punch is restrained and the stress system is not one of pure biaxial tension.

2.2 Factors Influencing the Inherent Formability of Metals

For a given tool configuration and lubrication conditions, the forming limit is governed by the inherent formability of the metal itself. Theories are able to predict only how various factors will affect performance during simple cup drawing or simple punch stretching, so that application to industrial forming operations is necessarily limited to situations which approach these two extremes. No theory can yet be visualised which would predict performance

under a complex stress system involving both deep drawing and stretch forming and where the relative amounts of these processes may vary throughout a component.

2.2.1. Plastic Anisotropy

Plastic anisotropy is a basic property of a metal that can sometimes be an asset in metal forming. The three main causes of directionality in sheet are:-

a) the anisotropy of individual crystals when there is preferred orientation.

b) the distribution and orientation of the various constituents and defects in the material, usually referred to as mechanical fibering.

c) internal stresses resulting from directionality and inhomogeneity in plastic flow (which are not usually important in annealed material).

Internal stresses and mechanical fibering produce more or less isolated anisotropic effects. The Bauschinger effect and low transverse ductility are the principal manifestations of anisotropy arising from these two sources, respectively. On the other hand, anisotropy due to crystallographic texture is reflected in the entire deformation behaviour, and in certain cases fracture behaviour as well. It is this form of anisotropy which is the most important in metal processing.

a) The strain ratio, R

The ratio of the width to thickness strains in uniaxial tension provides a useful index of plastic anisotropy normal to the plane of the sheet, and is defined as

$$R = \frac{\ln\left(\frac{w_o}{w_x}\right)}{\ln\left(\frac{t_o}{t_x}\right)} \qquad \ldots\ldots\ldots\ldots(1)$$

where w_o and w_x are the initial and final gauge width respectively and t_o and t_x are the initial and final gauge thickness respectively. In practice the change in thickness of a flat tensile specimen is difficult to measure accurately, but by assuming constant volume conditions in the gauge length, R may be calculated from measurements of the gauge width and gauge length only. It is then given by

$$R = \frac{\ln\left(\frac{w_o}{w_x}\right)}{\ln\left(\frac{l_x w_x}{l_o w_o}\right)} \qquad \ldots\ldots\ldots\ldots(2)$$

where l_o and l_x are the initial and final gauge length respectively.

Complete isotropy occurs when R = 1 in all directions of the sheet. When there is preferred orientation R may be $\gtrless$ 1 and will usually vary with the direction of testing in the plane of the sheet. In either case, a mean value, $\bar{R}$, is used as an index of normal anisotropy. $\bar{R}$ is calculated from values determined in at least three directions:-

$$\bar{R} = \frac{1}{4}\left(R_{0^o} + 2R_{45^o} + R_{90^o}\right) \qquad \ldots\ldots\ldots\ldots(3)$$

Generally $R_0^o \neq R_{45}^o \neq R_{90}^o$, which indicates a state of planar anisotropy. This is reflected in differences in strength and ductility in different directions in the plane of the sheet. Planar anisotropy is usually associated with some degree of normal anisotropy.

When $\bar{R} = \infty$, there is little or no strain in the thickness direction and maximum resistance to thinning is achieved. Conversely, when $\bar{R} = 0$, thinning occurs very easily. Neither of these extremes is realized in practice.

b) Effect of anisotropy on deep drawability

Several theories of plastic deformation incorporating anisotropic behaviour have been proposed. Application of these has been limited and only the theory due to Hill[1,2] has received appreciable attention. By analogy with the Huber-Mises yield criterion for isotropic behaviour, Hill defined a plastic potential or effective stress for anisotropic behaviour assuming the uniaxial yield stress to vary with direction.

Hosford and Backofen[3] have applied Hill's theory[1,2] to sheet materials by assuming rotational symmetry about the sheet normal and an absence of the Bauschinger effect. Hill's yield criterion then becomes

$$(\sigma_y-\sigma_z)^2+(\sigma_z-\sigma_x)^2+\bar{R}(\sigma_x-\sigma_y)^2 = 2Z^2 \qquad \text{.....(4)}$$

with $$Z = X\sqrt{\frac{1+\bar{R}}{2}} \qquad \text{.....(5)}$$

and $d\varepsilon_x : d\varepsilon_y : d\varepsilon_z =$

$$(\bar{R}+1)\sigma_x-\sigma_y-\sigma_z:(\bar{R}+1)\sigma_y-\sigma_x-\sigma_z:2\sigma_z-\sigma_x-\sigma_y \quad \ldots\ldots\ldots\ldots(6)$$

where x and y are the two directions of principal stress in the plane of the sheet and z is the sheet normal. X, Y and Z are the uniaxial yield stresses in the x, y, and z directions.

For loading in the plane of the sheet $\sigma_z = 0$, and equations (4) and (6) become

$$\sigma_x^2+\sigma_y^2-\sigma_x\sigma_y\left(\frac{2\bar{R}}{\bar{R}+1}\right)= X^2 \quad \ldots\ldots\ldots\ldots(7)$$

$$d\varepsilon_x:d\varepsilon_y:d\varepsilon_z = (\bar{R}+1)\sigma_x-\sigma_y:(\bar{R}+1)\sigma_y-\sigma_x:-\sigma_x-\sigma_y \quad \ldots\ldots\ldots\ldots(8)$$

Putting $\alpha = \frac{\sigma_y}{\sigma_x}$, equation (7) becomes

$$\sigma_x^2\left[1+\alpha^2-\alpha\left(\frac{2\bar{R}}{\bar{R}+1}\right)\right] = X^2 \quad \ldots\ldots\ldots\ldots(9)$$

Under balanced biaxial tension $\alpha = 1$, and equation (9) predicts yielding in an isotropic material ($X=Y=Z;\bar{R}=1$) when $\sigma_x = X$. In this case, yielding is equivalent yielding in pure compression with a stress $\sigma_z = Z$, the uniaxial yield strength in the thickness direction.

The significance of normal anisotropy now becomes apparent. The strength in biaxial tension is determined not by the uniaxial planar strength but by the thickness strength. Increasing thickness strength, i.e. increasing $\bar{R}$, increases planar strength for all stress ratios >0 but decreases planar strength for $\alpha<0$. The effect is more marked in the former case. Differentiating equation (9) gives $\alpha = \frac{\bar{R}}{\bar{R}+1}$ as the condition for maximum σ_x at yielding.

For an isotropic material ($\bar{R} = 1$), $\alpha = \frac{1}{2}$ and σ_x max = 1.15X. In the cup wall during drawing, $d\varepsilon_y = 0$ and $\alpha = \frac{\bar{R}}{\bar{R}+1}$, which corresponds with the condition for maximum strengthening, whereas in the flange $d\varepsilon_z = 0$ and $\alpha = 1$. Under combined tension-compression some softening occurs from $\bar{R} > 1$. For maximum drawability in ductile metals the wall strength should be as high as possible relative to that of the flange so that the largest reduction can be accomplished before wall failure by necking. The most practicable way of doing this is by control of texture so as to produce a material having a high $\bar{R}$ value, since the wall strength increases and the flange strength decreases with increasing $\bar{R}$.

Whitely[4] has carried out an analysis of the punch load required during drawing for the case of an anisotropic but non-strain hardening material. This load, acting on the base of the cup, is transmitted through the cup wall to the die opening where it then acts in the form of radial tensile stress to cause plastic deformation of material in the flange. Based on an analysis by Hu[5] and applying a correction factor given by Willis[6] to account for frictional forces, the total punch load required to draw a blank of diameter D was shown to be

$$P_r = (1+\eta)\pi.d.t.\sqrt{\frac{\alpha_{33}}{G}}.K.\ln\left(\frac{D}{d}\right) \qquad \text{.....(10)}$$

where α_{33} and G are anisotropic parameters

K is the effective strength

d is the final cup diameter

t is the thickness of the blank

η is a friction parameter

The parameter η is constant for given conditions of geometry and friction, and usually has a value between 0.2 and 0.3. The maximum diameter of blank that can be drawn is limited by the maximum punch load which can be supported by the material forming the wall of the cup. It was further shown that this maximum punch load is given by

$$P_{max} = \pi . d . t . \sqrt{\frac{\alpha_{22}}{G}} . K \qquad \ldots\ldots\ldots\ldots\ldots (11)$$

where α_{22} is another anisotropic parameter. At the critical blank diameter equations (10) and (11) must be equal, so that the limiting drawing ratio is given by

$$\ln \left(\frac{D}{d} \right)_{max} = \frac{1}{(1+\eta)} \sqrt{\frac{\alpha_{22}}{\alpha_{33}}} \qquad \ldots\ldots\ldots\ldots (12)$$

Equation (12) indicates that for given conditions of geometry and lubrication, the limiting drawing ratio is governed only by the anisotropic parameters of the sheet and is independent of the effective strength of the material. Whitely[4] extended his analysis to express the anisotropic parameters α_{22}, α_{33} and G in terms of $\bar{R}$. Assuming a material with only normal anisotropy it was shown that

$$P_r = (1+\eta) . \pi . d . t . \sqrt{\frac{(2+2\bar{R})}{(1+2\bar{R})}} . K . \ln \left(\frac{D}{d} \right) \qquad \ldots\ldots\ldots (13)$$

$$P_{max} = \pi \,.d.t. \sqrt{\frac{(1+\bar{R})^2}{(1+2\bar{R})}} \,.\, K \qquad \ldots\ldots\ldots\ldots\ldots(14)$$

Equating (13) and (14) then gives

$$\ln \left(\frac{D}{d}\right)_{max} = \frac{1}{(1+\eta)} \sqrt{\frac{1+\bar{R}}{2}} \qquad \ldots\ldots\ldots\ldots\ldots(15)$$

Figure 3 shows the corresponding linear relationship derived from equation (15) between $\left(\frac{D}{d}\right)_{max}$ and $\bar{R}$. Rigorously, the analysis applies to what might be best termed pure radial drawing with no bending and unbending around the tool radii. In the flat-bottomed cup drawing of ductile metals, however, this restriction does not seriously limit the implication of the analysis.

Whitely[4] demonstrated the relationship between $\left(\frac{D}{d}\right)_{max}$ and $\bar{R}$ for a series of materials with a range of $\bar{R}$ values from 0.58 to 1.62, and the range was later extended by Lloyd[7] with $\bar{R}$ = 3.8 for titanium. Assuming the experimental accuracy of the drawing ratio to be $\pm$ 0.025, a direct straight line relationship is observed between $\left(\frac{D}{d}\right)_{max}$ and $\bar{R}$. Results obtained by Lilet and Wybo[8,9] and Wright[10] indicate that slightly better correlation with deep drawing tests may be obtained by using R min instead of $\bar{R}$, whereas Atkinson and Maclean[11] found that the drawability of low carbon steels correlated more closely with $\bar{R}$ than with maximum or minimum values.

In practice the linear relationship does not hold for values of $\bar{R}$ approaching zero, and results with $\bar{R}<1$ obtained by Atkinson and

Maclean[11] and Wilson, Sunter and Martin[12] actually fall below the straight line to form a smooth curve between $\bar{R} = 0.5$ and $\bar{R} = 1$.

c) Effect of anisotropy on stretch formability

A pure stretching operation is terminated by plastic instability. The effect of anisotropy on instability in stretch forming has been considered by Keeler and Backofen[13] and by Moore and Wallace[14].

Applying the theories of Hill[1] and Swift[15], Keeler and Backofen[13] considered the general condition of instability for a sheet loaded under plane stress, with the ratio of the intermediate to the largest principal stresses, $\frac{\sigma_2}{\sigma_1}$, = α. Deformation can continue without change in load when

$$\frac{d\bar{\sigma}}{d\bar{\varepsilon}} = \frac{\bar{\sigma}}{S} \qquad \ldots\ldots\ldots\ldots (16)$$

where $\bar{\sigma} = \sigma_1 (1-\alpha+\alpha^2)^{1/2}$ ..... (17)

$$\bar{\varepsilon} = \varepsilon_1 \left[\frac{2(1-\alpha+\alpha^2)^{1/2}}{2-\alpha} \right] \qquad \ldots\ldots\ldots\ldots (18)$$

S is a function of the stress ratio α.

The graphical solution of equation (16) is shown in Figure 4. Two modes of unstable flow are indicated; S_d relates to the beginning of diffuse and S_1 to the beginning of localized necking. Diffuse necking is broadly and symmetrically distributed about the loading directions and is encountered at $\bar{\varepsilon}_d^*$ when

$$S_d = \frac{4(1-\alpha+\alpha^2)^{3/2}}{(1+\alpha)(4-7\alpha+4\alpha^2)} \qquad \ldots\ldots\ldots\ldots (19)$$

Localized necking involves a thin band of flowing material inclined

at an angle θ across the sheet and is encountered at $\bar{\varepsilon}_1^*$ when

$$S_1 = \frac{2(1-\alpha+\alpha^2)^{1/2}}{(1+\alpha)} \qquad \ldots\ldots\ldots\ldots\ldots (20)$$

A necessary condition for localized necking is that no strain is imposed on the deforming material adjacent to the flowing region or that no extension occurs along the trough of the neck. Thus a local neck may be accommodated as long as $d\varepsilon_2 \leqslant 0$.

It was shown[13] that for an isotropic ($\bar{R} = 1$) sheet

$$\frac{d\varepsilon_2}{d\varepsilon_1} = \frac{(2\alpha-1)}{(2-\alpha)} \qquad \ldots\ldots\ldots\ldots\ldots (21)$$

Therefore $d\varepsilon_2 = 0$ is identified with $\alpha = 1/2$ and $S_d = S_1$, so that a neck may form at 90° to the σ_1 axis. With $d\varepsilon_2 < 0$, ($\alpha < 1/2$), θ is $< 90^\circ$ and given by

$$\theta = \arctan \left[\frac{\alpha-2}{2\alpha-1}\right]^{1/2} \qquad \ldots\ldots\ldots\ldots (22)$$

In punch stretching, with a securely clamped sheet, $d\varepsilon_2 > 0$, ($\alpha > 1/2$). There is no direction of zero extension and therefore localized necking cannot occur. The conditions for the onset of both diffuse and localized necking in an isotropic material under plane-stress loading are summarized in Figure 5.

If $\bar{R} > 1$ but there is still rotational symmetry about the sheet normal, $d\varepsilon_2$ is reduced algebraically relative to $d\varepsilon_1$ for a given stress ratio. The result is that $d\varepsilon_2$ does not become greater than 0 until $\alpha > 1/2$. Figure 6 shows the effect of $\bar{R}$ on the limiting stress ratio above which localized necking cannot occur.

In order to suppress localized necking ,operations where $\alpha < 1/2$ require $\bar{R} < 1$. On the other hand, in normal biaxial stretching, $\alpha = 1$ and localized necking is not a problem. In the latter case, high $\bar{R}$ values would be beneficial in increasing ε_d^*, as shown in Figure 7.

Moore and Wallace[14] considered the effect of anisotropy on instability in sheet metal forming for a range of biaxial stress conditions. The treatment was similarly based on Hill's macroscopic theory but it was assumed that fracture occurred by necking in a band perpendicular to the maximum principal stress, as previously postulated by Swift[15]. A further assumption was that the axes of principal stress and strain coincide, a fact which is strictly true only for an isotropic material. For the special case of rotational symmetry about the sheet normal it was shown that the stability condition becomes

$$\frac{d\sigma}{d\varepsilon} = \frac{\sigma}{S}$$

where $$S = \sqrt{\frac{2(2+\bar{R})}{3}} \left\{ \frac{[(1+\bar{R})\alpha^2 - 2\bar{R}\alpha + (1+\bar{R})]^{3/2}}{(1+\bar{R})^2\alpha^3 - (2+\bar{R})\bar{R}\alpha^2 - (2+\bar{R})\bar{R}\alpha + (1+\bar{R})^2} \right\} \quad \ldots\ldots (24)$$

Moore and Wallace[14] actually plotted curves of S for various ratios of the principal strains ε_x and ε_y, and various values of R_x and R_y. It was shown that two materials having the same $\bar{R}$ but with different polar variations of R did not have the same value of S, but for biaxial stretching, polar variations of R did not affect the instability point.

Using the generalised stress strain relationship

$$\sigma = \sigma_o (1+c\varepsilon^n) \qquad \ldots\ldots(25)$$

where σ_o is the initial yield stress

c is an arbitrary constant

n is a fraction <1

which ignores elastic strains, and inserting values of σ_o, c and n which are typical of mild steel, curves were obtained showing the variation of critical strain with the stress ratio, α, for different values of $\bar{R}$. These are shown in Figure 8, which indicates the beneficial effect of increasing $\bar{R}$ in biaxial stretching ($\alpha = 1$), while for uniaxial tension ($\alpha = 0$), $\bar{R}$ should be low. The theory assumes that necking is normal to one of the principal directions and is due to the action of the principal stresses σ_x and σ_y and affected only by the properties R_x and R_y. However, in practice, polar variations of R may be such that the critical conditions are due to R_θ and the stress component σ_θ, where θ does not necessarily define a principal direction.

Results obtained by Mellor[16] on stabilized steels showed that high elongation in uniaxial tension was associated with high $\bar{R}$, which disagrees with the predictions of both theories. However, Wallace[17] has pointed out that the theoretical curves in Figure 8 have a cross-over point close to the uniaxial tension stress system so that with different materials the cross-over point might fall on the other side of the uniaxial line, which would account for Mellor's observations.

For biaxial stretching, both the theory of Keeler and Backofen[13] and that of Moore and Wallace[14] predict the beneficial effect of increasing $\bar{R}$ and receive some support from observations made by Pearce[18]. He found that in sheets of zirconium ($\bar{R}$ = 9.4) and aluminium ($\bar{R}$ = 0.6) having initially similar mechanical properties, and pressed to obtain similar bulge heights, the amount of thickness strain in the polar regions was much greater for aluminium than for zirconium.

2.2.2. Work Hardening Ability

For most materials the true stress vs. true strain curve derived from a simple tensile test can be made to fit equation (25). The coefficient n is a measure of the work hardening ability of the material and is referred to as the work hardening index or the coefficient of work hardening. At least in cubic metals, planar variations of n may be neglected.

a) Effect of n on deep drawability

Keeler and Backofen[19] made an analysis of the drawing limit for an isotropic strain-hardening material. Assuming, as Whitely[1] did, pure radial drawing, the applied stress at any stage of the drawing operation was shown to be

$$\sigma_r = K(\tfrac{1}{2})^n \int_{r_o}^{r_p} \left[\ln \left(B_o^2 - \frac{r_o^2}{r^2} + 1 \right) \right]^n \frac{dr}{r} \quad \ldots\ldots\ldots (26)$$

where B_o = initial blank radius

r_o = radius to outer edge of undrawn flange

r_p = punch or cup radius

r = radius between r_o and r_p

From opposing tendencies due to strain hardening (acting to increase (σ_r) and diminishing reduction (giving a drop in σ_r) as the draw progresses, σ_r passes through a maximum for any ratio of blank to cup diameter and σ_r (max) is obtained by a series of integrations each for a different r_o between B_o and r_p. For given conditions there is a limit when the maximum drawing load becomes equal to the load for pure tensile instability in the stretch formed region at the bottom of the cup wall. Neglecting friction, drawability was found to be related to n as shown in Figure 9.

In Figure 9, the limiting drawing ratio is essentially constant, although the analysis is restricted to materials for which the power law approximation of the true stress-true strain curve is valid. The slight downward trend with n increasing from zero might account for the observations that more heavily prestrained materials (lower n) are found to give slightly deeper cups, other conditions fixed, than softer materials capable of a larger overall amount of strain hardening (larger n)[20].

Results obtained by Swift and Chung[22] for aluminium-killed steels suggested that although high $\bar{R}$ was necessary for an operation involving predominantly die drawing, high n might also be desirable.

b) Effect of n on stretch formability

The limit in stretch forming occurs when instability is reached, and providing that the power law is valid, at instability it can be shown that $n = \varepsilon$. Hence the forming limit for a given stress ratio is raised by increasing n.

Results obtained on aluminium-killed steels showed that good performance in stretch forming tests was obtained with $n > 0.22$ irrespective of the R value[21].

2.2.3. Grain Size

The influence of grain size on formability arises from its effect on the yield stress, elongation and rate of work hardening. The smaller the grain size the higher the yield stress[22] according to the equation

$$\sigma_y = \sigma_i + \sigma_D \, l^{1/2} \, d^{-1/2} \qquad \text{.....(27)}$$

where d is the grain diameter

σ_D is the shear stress to unpin a dislocation from its atmosphere.

σ_i is the shear stress resisting the movement of dislocations across the slip plane after they have been unpinned

l is the distance from piled-up dislocations at the head of the plastic front held up by the boundary to the nearest Frank-Read sources in the next grain.

A smaller grain size would therefore require a higher load to cause deformation.

A larger grain size increases ductility and should therefore increase stretch formability. This could also increase deep drawability because of the increased capacity of material to be stretched formed over the punch nose profile. Alternatively, the lower rate of work hardening associated with an increase in grain size could itself be responsible for either an increase or a decrease in deep drawability according to Figure 9.

The effects of grain size on forming limits are usually only slight or insignificant compared with other factors which influence the inherent formability. Control of grain size in commercial sheets is important mainly because of its effect on surface finish. Surface roughening or "orange peeling" is observed on pressings when the grain size is too large.

2.2.4. Other Tensile Properties

Many industrial pressing operations and certain simulative tests such as round-nosed punch drawing involve the processes of deep drawing and stretch forming taking place simultaneously. Under these conditions the factor ($\bar{R}$ x n) may give better correlation with forming behaviour [21, 23, 24].

For zinc, Derricott and Wright [25] concluded that deep drawability was dependent on the ultimate tensile strength.

2.3. The Development of Sheet Textures in F.C.C. Metals and Alloys

During the plastic deformation of polycrystalline aggregates, individual grains rotate so that certain crystallographic directions become aligned with the principal directions of strain in the metal. The rotation takes place gradually as the deformation proceeds, and the final orientation is approached when slip planes and directions become symmetrically aligned with respect to the direction of working. The preferred orientation or texture produced depends on:-

a) material variables such as the crystal structure, metal, solute content, second phases, initial grain size and initial texture.

b) process variables such as the stress system, amount of deformation, deformation temperature and strain rate.

On annealing preferred orientation may be retained, the actual texture being characteristic of the deformation texture, annealing temperature and time, heating and cooling rates and annealing atmosphere.

Dillamore and Roberts[26] have made a comprehensive review of texture development in metals and alloys generally. For the present we are concerned only with the most important aspects of texture development in sheets of F.C.C. metals and alloys. As regards the development of annealing textures, those formed during primary recrystallisation only are reviewed, since the textures derived by

secondary recrystallisation are generally associated with a grain size which is much too large for a desirable surface finish on pressings (see Section 2.2.3.).

2.3.1. Rolling Textures

The room temperature rolling textures which are observed in F.C.C. metals and alloys are of two general types. All the common pure metals, with the exception of silver, exhibit a texture which can be described as $\{135\}\langle 1\bar{2}1\rangle$. This orientation actually represents the central region of a spread between the orientations $\{110\}\langle \bar{1}12\rangle$ and $\{112\}\langle \bar{1}\bar{1}1\rangle$. Silver and F.C.C. alloys containing certain amounts of solute exhibit a texture described as $\{110\}\langle \bar{1}12\rangle$ with a minor $\{110\}\langle 001\rangle$ component. The $\{135\}\langle 1\bar{2}1\rangle$ texture changes gradually to $\{110\}\langle \bar{1}12\rangle$ as the amount of solute is increased, although equal amounts of different solutes do not have the same effect as regards the extent of transition [27-32].

Depending on the type of texture which is characteristic of a particular metal or alloy rolled at room temperature, transition may also be brought about either by increasing or decreasing the rolling temperature. The $\{110\}\langle \bar{1}12\rangle$ texture changes to $\{123\}\langle 1\bar{2}1\rangle$ as the rolling temperature is increased [33-37]. Conversely, rolling at below room temperature favours a transition from $\{135\}\langle 1\bar{2}1\rangle$ to $\{110\}\langle \bar{1}12\rangle$ [38,39]. In either case the temperature range over which transition occurs is characteristic of the particular metal or alloy.

The effects of alloying and change in temperature are qualitatively additive, in that transition to $\{110\}\langle \bar{1}12\rangle$ by alloying may be counteracted by an increase in temperature [29].

A fundamental factor governing transition in texture is the decrease of stacking fault energy associated with alloying. Smallman and Green[40] related the texture transition to stacking fault energy using copper-aluminium and copper-germanium alloys, while Haessner[41] observed a similar correlation in cobalt-nickel alloys. Smallman and Green[40] concluded that the {110}<$\bar{1}$12> texture is characteristic of any pure metal or alloy with a stacking fault energy of about 35 ergs cm.$^{-2}$ or lower rolled at a temperature below about 0.25 Tm (Tm=absolute melting point). The critical value of stacking fault energy is reached at a smaller solute addition as the atomic misfit and valency difference between the solute and solvent increases. These authors further established that the {110}<$\bar{1}$12> texture can be characteristic of a metal of higher stacking fault energy than 35 ergs cm.$^{-2}$ providing it is rolled at a temperature below about 0.2 Tm. In materials of very low stacking fault energy, the texture tends to be stable at temperatures up to 0.5 Tm.

2.3.2. Theories of Rolling Textures

Current theories regarding the development of the alloy texture and the pure metal texture are due mainly to Wassermann[42], Haessner[43], Smallman and Green[40], and Dillamore and Roberts[44].

Wassermann[42] assumed that all metals first tend to form the pure metal texture, which he described as two limited fibre textures centred on the orientations $\{110\}\langle\bar{1}12\rangle$ + $\{112\}\langle\bar{1}\bar{1}1\rangle$. He showed that mechanical twinning would transform material in the $\{112\}\langle\bar{1}\bar{1}1\rangle$ orientation to $\{255\}\langle\bar{5}11\rangle$, which subsequently rotated by slip processes to $\{110\}\langle001\rangle$. It was argued that the strain accompanying twinning of the $\{110\}\langle\bar{1}12\rangle$ component is less compatible with the overall required strain than for twinning of the $\{112\}\langle\bar{1}\bar{1}1\rangle$ component. Twinning merely limits the spread about the $\{110\}\langle\bar{1}12\rangle$ orientation. The theory is in agreement with the observation that metals of low stacking fault energy may deform by mechanical twinning[45].

Haessner[43] considered that mechanical twinning would aid the formation of the $\{110\}\langle\bar{1}12\rangle$ component and would also cause the formation of a $\{110\}\langle001\rangle$ component. He attributed the pure metal texture to the onset of non-octahedral slip, and for the case of mixed proportions of cubic slip and octahedral slip he suggested the range of orientations

$$\{110\}\langle\bar{1}12\rangle - \{135\}\langle\bar{5}\bar{3}3\rangle - \{112\}\langle\bar{1}\bar{1}1\rangle$$

to explain the pure metal texture. It should be noted that $\{135\}$ does not belong to a $\langle\bar{5}\bar{3}3\rangle$ zone and that the correct orientation to describe the centre of the spread was probably meant to be $\{135\}\langle\bar{2}\bar{1}1\rangle$. Other workers[46,47] have also proposed cubic slip to explain the development of the pure metal texture. Haessner[43] explained the dependence of cubic slip on stacking fault energy by pointing out that the wider the separation of the partials, the less likely will

dislocations dissociated in a {111} plane be able to lie on a {100} plane.

Dillamore and Roberts [44] determined the end point of rotations for all possible initial grain orientations and found that most orientations rotate to {110}<$\bar{1}$12> although some move initially towards {110}<001>. They pointed out that the complete alloy texture could therefore be explained solely on the basis of primary and duplex slip, without invoking twinning, as suggested by Haessner[43] and Wassermann[42]. Smallman and Green[40] and Dillamore and Roberts[44] attributed the formation of the alloy texture to primary and conjugate slip processes, and the subsequent rotation to the pure metal texture to the onset of cross-slip. A reasonable amount of cross-slip could produce a final texture of the form {135}<$\bar{2}\bar{1}$1> or {146}<$\bar{2}\bar{1}$1>, while a very large amount of cross-slip, such as that found in aluminium, would cause a rotation to the texture {112}<$\bar{1}\bar{1}$1>. A correlation of texture and stacking fault energy clearly follows from the dependence of cross-slip on stacking fault energy. The temperature dependence of the texture was explained by the thermal activation of cross-slip.

Haessner[41] dismissed the possibility of cross-slip as a contributory factor to texture development on the grounds that the internal stresses during rolling are generally greater than τ_{III}, the stress at the onset of Stage III work hardening in single crystals, so that cross-slip should always be possible during the rolling of

polycrystalline metals. Dillamore and Roberts[44] disagreed with this hypothesis on the grounds that the amount of cross-slip required to contribute significantly to texture development would be relatively large and would therefore correspond to higher stresses than those required to initiate cross-slip. However, since cubic slip is geometrically equivalent to equal proportions of primary and cross-slip, the observed textures could equally well be explained by the theory of Haessner or that of Dillamore and Roberts.

Recent work by Butler and Green[48] provides evidence for the theories by Wassermann and Haessner regarding the importance of twinning. From results obtained on copper-aluminium alloys they concluded that all alloys, irrespective of stacking fault energy, first undergo primary and duplex slip followed by cross-slip to develop a pure metal texture, but that at higher reductions the alloy texture was formed due to twinning. The lower the stacking fault energy, the lower was the % reduction at which this change occurred, which is consistent with the dependence of twinning on stacking fault energy.

2.3.3. Primary Recrystallisation Textures

Primary recrystallisation textures are largely dependent on the deformation textures, although since different textures may be formed during different stages of annealing, experimental observations do not appear so general as those regarding the rolling textures.

A rolling texture of the type $\{135\}\langle 1\bar{2}1\rangle$ generally recrystallises to the cube texture $\{100\}\langle 001\rangle$. This primary recrystallisation texture has been reported in copper[49-51], aluminium[52,53], nickel[54] and nickel-iron alloys[51,55]. The abundance of the cube texture depends on the annealing conditions and production variables, but generally a pronounced rolling texture is required to obtain it. In copper, after prior deformations of up to 50%, the recrystallisation texture is almost random; after 90% deformation the annealing texture resembles the deformation texture, while higher deformations give a texture consisting of the cube orientation and its twins[49-51]. The cube texture is more perfect and the twin density lower for fine-grained starting material and a high annealing temperature. For aluminium of 99.99% purity, the recrystallisation textures are essentially the same as those of copper, although it is more difficult to produce entirely cube texture[52,53].

The effect of alloying on the recrystallisation texture is related to the effect of alloying on the deformation texture although the amount of solute necessary to completely suppress the cube texture is considerably less than the amount required to cause transition to the alloy rolling texture[27,28]. In 70/30 brass[53] and in silver[56] rolled to 96% reduction at room temperature, the annealing texture is adequately described by the indices $\{225\}\langle 7\bar{3}4\rangle$ or near

$\{113\}\langle\bar{2}\bar{1}1\rangle$. In copper-zinc alloys[53], the $\{225\}\langle73\bar{4}\rangle$ component originates as $\{214\}\langle52\bar{3}\rangle$ in a 3% zinc alloy. With increasing zinc content, it increases in intensity, rotating to $\sim\{427\}\langle42\bar{3}\rangle$ at 6% zinc and then to $\sim\{438\}\langle63\bar{4}\rangle$ at 10% zinc[57]. Other minor components accompany this transition. Similar annealing texture transitions occur in alloys of copper with aluminium[58], tin and germanium[27], and in nickel alloys containing molybdenum or cobalt[54]. The annealing textures of alloys of copper with phosphorus, arsenic and antimony, which are particularly effective in suppressing cube texture, are completely different, the major orientations being $\{227\}\langle77\bar{4}\rangle$ and orientations related to $\{110\}\langle\bar{1}12\rangle$ by a rotation about $\langle110\rangle$[27,28].

2.3.4. Theories of Recrystallisation Textures

Theoretical interpretations of recrystallisation textures are not so widely applicable as the theories regarding deformation textures in F.C.C. metals and alloys. There are two main opposing theories of the mechanisms leading to the development of recrystallisation textures, namely oriented nucleation and oriented growth.

Burgers and Louwerse[59] suggested that the new grains grow from small regions of certain orientations which are already present in the deformed matrix: the orientation of the recrystallised grains is therefore determined by that of the original nuclei. However, in order to explain why recrystallisation textures are generally different from the rolling textures three assumptions are necessary:-

a) that the oriented nuclei are too small to be detected when the rolling texture is determined.

b) that these nuclei are more favourably oriented for recrystallisation than those in the greater part of the matrix.

c) that after polygonisation has taken place within these nuclei, the resultant polygonised nuclei are capable of growth.

Although this approach is able to explain certain observations, such as the retention of the rolling texture in aluminium, it is not widely accepted. Moreover, in copper having a normal pure metal texture, electron microscope examination has shown that the individual crystal orientations describe completely the texture of the bulk material but no evidence was found of cube oriented grains[60]. Nucleation theories can account only for annealing textures whose component orientations are represented in the deformation texture or are related to deformation components by comparatively slight orientations.

Barrett[61] and Beck[62] have suggested that recrystallisation textures are determined by the preferential growth of nuclei with certain orientations. It is supposed that nuclei of many orientations initially form but since the rate of growth of a given nucleus depends on the orientation difference between the matrix and the growing crystal, the nuclei with the fastest growth rates will be those which are bounded by high angle boundaries.

These nuclei, which give rise to the recrystallisation texture, will have orientations that differ from the original by a rotation of approximately 45° about a <111> axis. The theory is well supported by the fact that the recrystallisation textures of many metals and alloys are related to the deformation textures by simple rotational relationships. Burke[63] has pointed out that the theory does not explain why rotations about a full set of crystallographically equivalent <111> axes are rarely found experimentally, instead of a rotation about a particular [111] axis. This indicates that the initial nucleation is not entirely random.

A general criticism of the oriented growth theory is that the growth relationship is not sharp enough to account for the well defined recrystallisation textures which are obtained. However, Dillamore[58] has shown that by considering the restrictions on the growth of a nucleus to form part of the recrystallisation texture, the site at which nucleation occurs and the range of orientations through which the nucleus must grow, the sharpness of the recrystallisation texture can be due to the conflicting conditions of growth into a multicomponent matrix. In his analysis of the relationship between deformation textures and annealing textures in F.C.C. metals the most probable sites for nucleation were assumed to be grain boundaries and deformation boundaries, while the major components of the annealing texture

were considered to arise from nuclei which are capable of growth (a) into the orientations on either side of the boundary, (b) through the spread of these orientations, and (c) into the remaining two out of the four symmetrical components of the deformation texture. For a $\{110\}\langle\bar{1}12\rangle$ deformation texture, the annealing texture orientations are predicted as $\{4\ 9\ 17\}\langle 38\bar{5}\rangle$, $\{490\}\langle 001\rangle$ and $\{112\}\langle\bar{1}10\rangle$. For a deformation texture in the spread between $\{135\}\langle 1\bar{2}1\rangle$ and $\{236\}\langle 73\bar{4}\rangle$ it is predicted that the $\{100\}\langle 001\rangle$ component will be predominant in the annealing texture.

Although the oriented-growth theory is more widely applicable in accounting for the observed textures, oriented nucleation is still a possible mechanism of formation of annealing textures. More generally, when oriented nucleation does occur, there will be further selection from the nuclei during competitive growth[64-66].

2.3.5. Rolling and Annealing Textures in Austenitic Stainless Steels

The development of cold rolling and recrystallisation textures in austenitic stainless steels is particularly interesting because of the possibility of the strain-induced austenite → martensite transformation taking place during rolling and the subsequent formation of a duplex texture. In the absence of this phase transformation the textures are dependent on stacking fault energy and rolling temperature as with normal F.C.C. metals and alloys.

Goodman and Hu[35,36] studied the rolling and annealing textures in a commercial 18/8 chromium/nickel type of steel, the analysed composition of which is given below

Cr	Ni	C	Mn	P	S	Si	N
18.6	9.5	.037	.55	.01	.032	.39	.032

During cold rolling, extensive transformation to martensite (alternatively termed "martensitic ferrite" or more loosely "ferrite" by Goodman and Hu) occurred. They observed that after 90% reduction crystallites of each phase had assumed their stable end orientations. The retained austenite developed a typical F.C.C. alloy texture, viz. $\{110\}\langle\bar{1}12\rangle$ + a minor $\{110\}\langle001\rangle$ component, while the texture of the ferrite consisted of a spread between the main orientations $\{111\}\langle\bar{1}\bar{1}2\rangle$ + $\{112\}\langle1\bar{1}0\rangle$ and a spread towards a minor $\{100\}\langle011\rangle$ component. The amount of ferrite was estimated from pole figure intensities as 70-80%. Annealing for 1h at 600°C increased the intensity of the austenite texture and a new orientation appeared in the austenite near $\{230\}\langle3\bar{2}1\rangle$, while the intensity of the ferrite texture decreased. After 1 min. at 900°C, the new orientation completely disappeared so that the final annealing texture was the same as the austenite rolling texture.

As the rolling temperature was increased so the stability of the austenite increased, with the result that at 200°C no ferrite was formed and the texture was predominantly of the F.C.C. alloy type.

Transition to the pure metal type of texture was effected by rolling in the range 400-800°C. The transition in the annealing texture was similar to that observed in other F.C.C. alloys. Annealing at 900°C of strip rolled to 90% reduction at 200-600°C produced orientations near $\{113\}\langle 33\bar{2}\rangle$, near $\{112\}\langle 53\bar{4}\rangle$ and near $\{123\}\langle 11\bar{1}\rangle$, while strip rolled at 800°C exhibited predominantly cube texture together with $\{122\}\langle \bar{2}\bar{1}2\rangle$ twins and a minor component near $\{530\}\langle 001\rangle$.

2.3.6. Effect of Second Phases on Recrystallisation Textures

Recrystallisation textures, being dependent on nucleation and grain growth phenomena, may sometimes be controlled by the presence of second phase particles.

The relative proportions of cube texture and retained rolling texture in aluminium are markedly dependent on processing variables and also on purity. It is generally agreed that iron is the impurity which has the most effect on annealing textures, but opinions differ as to the role which it plays. Bunk and Esslinger[67] suggested that iron restricts recrystallisation to a cube texture by its effect on the rolling texture, but observations by Blade[68] indicate that small amounts of iron do not affect the rolling texture. A more likely explanation is that the growth of the cube texture is restricted by precipitated particles[68,69,70].

Gokyu, Abe and Veyama[71] observed that recrystallisation textures in aluminium-copper alloys were dependent on the solution treatment prior to cold rolling ,but that the rolling textures remain unaffected. Specimens which had not been solution treated recrystallised to {100}<001> and {113}<33$\bar{2}$ > whereas solution treated specimens recrystallised to {110}<001> and {110}<$\bar{1}$10>. These differences were attributed to the distribution of the precipitate during primary recrystallisation and the suppression of random nucleation around precipitate particles.

Goodman and Hu[36,37] have shown that in an 18.6% chromium 9.5% nickel stainless steel, which was rolled in a temperature range where the austenite was fully stable, the intensity of the cube texture produced on annealing could be influenced by the precipitation of carbide particles. Specimens rolled at 600°C and 800°C indicated that transition to the pure metal type of rolling texture was almost as complete at 600°C as at 800°C. However, on annealing at 900°C, cube texture was formed only in the strip which had been rolled at 800°C. Rolling at 600°C produced a fine dispersion of carbides visible only by electron microscopy whereas rolling at 800°C produced extensive precipitation of large particles which were visible optically. It was concluded that the finely dispersed carbides had impeded the growth of cube oriented grains.

Mee and Sinclair[72] found that during the cold rolling of nickel-2½ volume% thoria orientations of the type {hkl}<001>, and in particular {110}<001>, which originated from the starting texture, were metastable, and that the degree of cold work required for their degeneration was a function of the initial milling and fabrication conditions. Heavy cold rolling produced a F.C.C. pure metal type of texture. A range of recrystallisation texture components was observed, including {100}<001> and its twin orientation {122}<$\bar{2}\bar{1}$2>, {210}<$\bar{1}$21>, {359}<$\bar{3}$01> and {445}<$\bar{1}\bar{2}$,7,4>, the exact nature of the texture being dependent on the particular alloy and on the degree of deformation. For an alloy in which the rolling texture after 91% reduction was described as mainly {110}<001> + {100}<001>, annealing for 1h at 1000°C produced a weak cube component and major orientations near {359}<$\bar{3}$01> and {445}<$\bar{1}\bar{2}$,4,7>. Annealing at 1400°C decreased the proportion of cube component while the other components were strengthened. This alloy possessed a banded structure of thoria particles. In other alloys in which there was no banding, the rolling texture at 93% reduction was described in terms of components near {430}<$\bar{3}$,4,10> and {320}<001>, the former being a normal F.C.C. rolling texture. After annealing at 1000°C the textures contained varying proportions of {100}<001>, {122}<$\bar{2}\bar{1}$2> and {210}<$\bar{1}$21> components. It was suggested that the {210}<$\bar{1}$21> component could be the result of second order twinning or alternatively that the particular size spectrum and dispersion of thoria particles obtained in these alloys had impeded the nucleation and growth of cube oriented grains.

2.4. Relation of Plastic Anisotropy to Crystallographic Texture

Until the last 20 years or so, control of texture in materials intended for fabrication into structural components by press forming was solely with the intention of minimising the tendency to form ears. A low earing tendency is desirable because in order to remove ears from a final pressing, a larger size of blank must be used which necessarily involves extra cost. Also, the wall of the cup is made thinner where the ears occur and this may lead to fracture during the forming operation.

It is now realised, however, that controlled normal anisotropy can be an asset in operations which involve mainly deep drawing. For a given metal or alloy, the ideal situation would be to decide which orientation gives rise to the desired anisotropy and then to choose processing conditions, which would produce the particular orientation. In practice, this is not always possible since the annealing textures characteristic of the metal or alloy may not be associated with the desired form of anisotropy, but some compromise may be possible which would at least give a higher deep drawability than for randomly oriented material.

In this section, experimental and theoretical work relating the strain ratio and ear formation to crystallographic texture are reviewed.

2.4.1. Dependence of R on Tensile Strain and Preferred Orientation

Various experimental results indicate that R sometimes varies with strain. For steel, Lilet and Wybo[73] observed that R values

are scattered below about 7.5-10% elongation, but from 10-25% elongation R decreasesgradually. On the other hand, Wilson and Butler[74] have reported that R increases with strain for both steel and copper sheet, and that the rate of increase depends on the angle between the tensile axis and the rolling direction, and on the initial texture. Continuous measurements of width and thickness by Jegaden, Voinchet and Rocquet[75] indicate that in steel R increases linearly with strain up to maximum load and then decreases, but the validity of the results has been questioned[76] due to the effect of surface irregularities in strip specimens subjected to high strains.

Lankford, Snyder and Bausher[77] have shown that R does not vary with strain at least up to maximum load. Similarly, Whitely[78] has reported that R is constant during straining and that any detectable variation is explained by the inhomogeneity of the specimen.

Randerson[76] concluded that up to 10% elongation the strain in sheet tensile specimens is confined mainly to the length and thickness directions due to constraints imposed by specimen shape, but after work hardening has overcome the constraints, further deformation is accompanied by decreases in both thickness and width directions, i.e. R increases. In this work no explanation was given for occasional high values of R at low strains which decreased with strain. Since other results clearly

indicate that R sometimes decreases with strain, Randerson's explanation seems doubtful.

The above authors failed to realise the effect of texture in controlling the variation, if any, of R with strain and no attempts were made to correlate the tensile results with textures.

For a completely isotropic polycrystalline metal sheet it would be expected that R in any direction would equal one. This has been shown to be the case for extra soft normalised steel[79].

Wilson and Butler[74] have shown that in copper a recrystallisation texture similar to the rolling texture gives values of $R_0^o = 0.77$, $R_{45}^o = 1.31$ and $R_{90}^o = 0.58$. In contrast, for a cube texture R_0^o and R_{90}^o approach unity but $R_{45}^o = 0.33$. Dickson[80] has observed that in copper having an almost random grain orientation but with a small fraction of the grains having orientations near to the rolling texture, R_0^o and R_{90}^o were slightly <1 while R_{45}^o was slightly >1. Up to the limit of uniform elongation R_0^o and R_{90}^o remained constant but R_{45}^o decreased steadily.

In titanium sheet having a texture described as $(0001)\langle 10\bar{1}0\rangle$ with the (0001) planes tilted $\pm 35^o$ towards the transverse direction, Dickson[81] found that $R_0^o = 1.8$, $R_{45}^o = 3.0$ and $R_{90}^o = 3.8$. Up to the limit of uniform elongation R_{90}^o decreased slightly while R_0^o remained constant. R_{45}^o was constant up to 17% plastic strain but between 17% and 19% strain a marked decreased was observed.

For steel, Burns and Heyer[82] considered the distribution of slip directions of ideal orientations with respect to the width and thickness directions of tensile test pieces, and associated high values of $\bar{R}$ with the $\{111\}\langle\bar{1}10\rangle$ component of the texture. Whitely and Wise[83] produced various amounts of the $\{100\}\langle011\rangle$ and $\{111\}\langle\bar{1}10\rangle$ components in steel by varying the amount of cold rolling prior to annealing. They concluded that $\bar{R}$ was dependent on the absence of a week $\{100\}\langle011\rangle$ component rather than on the presence of a strong $\{111\}\langle\bar{1}10\rangle$ component.

2.4.2. Theories of the strain ratio

It is evident that R, being a measure of plastic anisotropy, should be directly related to crystallographic texture. Theories relating R with texture should aim at explaining planar variations and variations with strain as well as the mean value, $\bar{R}$. Most theories ignore the possibility of R varying with strain.

Bourne and Hill[84] produced a theory based on the macroscopic anisotropic properties of the sheet, which indicated that R should be constant as long as the deformation did not produce any pronounced change in the anisotropy of the sheet. However, the theory did not take into account the crystallographic requirements of deformation.

Burns and Heyer[85] suggested an approach for B.C.C. metals and found some correlation between predicted $\bar{R}$ values and experimental measurements. They assumed that the width and thickness strains,

ε_w and ε_t, resulting from a shear strain, S, in a particular direction are given by

$$\varepsilon_w = S.\cos\lambda_w \qquad \text{.....(28)}$$

$$\varepsilon_t = S.\cos\lambda_t \qquad \text{.....(29)}$$

where λ_w and λ_t are the angles between the slip direction and the width and thickness directions respectively. This assumption is incorrect since it assumes that the relationship between the lateral strains is principally dependent on the slip direction, and furthermore no attempt was made by Burns and Heyer to account for the varying amounts of slip on different systems within a grain. Elias, Heyer and Smith[86] later adopted this analysis for a rapid graphical prediction of $\bar{R}$ from {111} pole figures. Slip directions were projected onto a plane normal to the tension axis, R being given by the tangent of the angle between the thickness axis and a line joining the projection of the slip direction to the tension axis. This implies that for a given slip rotation, there is no variation of R with strain as the slip direction moves towards the tension axis along a line of constant R. The method was applied to pole figures either by determining R for the pole peaks or by determining an average value, weighted in favour of the regions of high pole density. Although qualitative agreement was obtained with experimental results, predicted values were too low when $\bar{R}$ was >1 and too high when $\bar{R}$ was <1. The approach appeared to be reasonable for B.C.C. metals because of the large number of slip directions.

The Elias, Heyer and Smith method has been applied with qualitative success to predict R values in titanium[76,81], copper, brass and zinc[76]. Randerson[76] found that for copper and brass two values were often predicted only one of which agreed favourably with the experimental value, while for zinc the experimental values agreed with those predicted for the $\{11\bar{2}2\}\langle\bar{1}\bar{1}23\rangle$ slip system of maximum resolved shear stress. For titanium, both Randerson[76] and Dickson[81] found that R values agreed with those predicted from $\langle 11\bar{2}0\rangle$ slip directions, although Dickson considered only the $\{10\bar{1}0\}\langle\bar{1}\bar{1}20\rangle$ systems of maximum resolved shear stress.

The correct relations for resolving crystallographic shear strains into linear strains are given by

$$\varepsilon_w = S.\cos\lambda_w.\cos\phi_w \qquad \ldots\ldots\ldots\ldots(30)$$

$$\varepsilon_t = S.\cos\lambda_t.\cos\phi_t \qquad \ldots\ldots\ldots\ldots(31)$$

where ϕ_w and ϕ_t are the angles between the slip plane normal and the width and thickness directions respectively.

Pearce and Natarajan[87] compared experimental R values in aluminium-magnesium alloys and values obtained by the above relations. The agreement obtained was only qualitative and their analysis was limited by the deduction of textures from inverse pole figures.

Vieth and Whitely[88] carried out an analysis, based on equations (30) and (31), of the influence of crystallographic orientation on plastic anisotropy in sheet steel. The sheet structure was assumed to be a single crystal stressed uniaxially in tension. The strain was attributed to

slip produced by one or more operating systems that are favourably oriented with respect to the direction of applied stress, and the operating system was assumed to be the one having the highest critical resolved shear stress. Predicted R values were calculated for various orientations in the unit stereographic triangle. It was predicted that all orientations along the <111> zone between {011} and {112} should have infinite R values in many test directions in the plane of the sheet regardless of the assumptions made for the slip mechanisms, whereas all orientations close to {001} have low average R values. Vieth and Whitely concluded that the level and variation of R values is determined by the crystal orientation rather than by the slip mechanism involved, although experimental R values determined on single crystals agreed more frequently with the assumption that the slip plane was simply the plane of maximum resolved shear stress in a <111> zone rather than {110}, {112} or {123}. No attempt was made to account for the restraints on the crystal that occur in polycrystalline material and the R values were measured at 10% strain only so that possible variations with strain were ignored.

Hosford and Backofen[3] devised a method for predicting quantitatively the effects of textureon the plastic properties of F.C.C. metals. The theory can also be applied to B.C.C. metals deforming by {110}<111> slip. They applied the analysis developed by Taylor[89] and later modified by Bishop and Hill[90,91]

for calculating the tensile (or compressive) stress-strain curves of randomly oriented polycrystals from the stress-strain curves of single crystals. To identify the operative slip systems, Taylor assumed that only those would be active which gave the minimum value of $M = \frac{dy}{d\varepsilon_x}$, where d_y is the sum of the incremental shear strains on all of the active slip systems needed to produce an increment of tensile strain $d\varepsilon_x$. Minimum M values were obtained for a number of orientations in the unit stereographic triangle and the average value was found to be $\bar{M} = 3.06$. The tensile stress and strain and the shear stress and strain for a single crystal are related by the equation

$$\frac{\sigma_x}{\tau} = \frac{d_y}{d\varepsilon_x} = M = \frac{1}{\cos\lambda\cos\phi} \qquad \ldots\ldots\ldots(32)$$

where σ_x = stress required for a given grain to flow with axial symmetry.

$d\varepsilon_x$ = increment of tensile strain

τ = shear stress

d_y = increment of shear strain

Thus, the σ_x vs ε_x curve for a randomly oriented polycrystal was obtained from the τ vs. y curve for a single crystal of the same material by using $\bar{M} = 3.06$ and by neglecting changes in $\bar{M}$ from lattice rotation.

Hosford and Backofen established the orientation dependence of M for axially symmetric flow over the full stereographic triangle. Assuming rotational symmetry about the sheet normal the M values indicated that components with <111> or <110> normal to the sheet would increase the yield strength in simple tension, simple compression or in balanced biaxial tension. It was remarked that the same textures would strengthen a sheet even if the principal tensile stresses were unbalanced. The analysis was broadened to take into account planar anisotropy by incorporating the strain ratio (R) in a parameter

$$r = \frac{d\varepsilon_y}{d\varepsilon_y + d\varepsilon_z} = \frac{R}{R+1} \qquad \ldots\ldots\ldots(33)$$

By assuming different values of r and calculating the corresponding values of $M = \frac{d_y}{d\varepsilon_x}$, an M vs. r plot was obtained. Minimum values of M represent the least slip with which the strain increment $d\varepsilon_x$ could be produced and therefore correspond to the expected behaviour. The values of M and r at the minimum identify the relative strength $\frac{\sigma x}{\bar{T}}$ and the strain ratio $R = \frac{r}{(1-r)}$. For a $\{110\}\langle\bar{1}12\rangle$ texture it was predicted that $R_0o = 1$ but it was impossible to predict a single value of $R_{90}o$. For a $\{111\}\langle\bar{1}10\rangle$ texture R_0o was predicted as infinity. Hosford and Backofen commented that small amounts of other textural components would probably create a minimum for the $\{110\}\langle\bar{1}12\rangle$ texture in the transverse direction and move the minimum to finite R values in the rolling direction for the $\{111\}\langle\bar{1}10\rangle$ texture. In fact it was demonstrated that because of the shape of the M vs r curve for randomly oriented material, the presence of some randomly oriented grains in a textured sheet would always move R towards unity.

By averaging curves for various components, M vs r curves were obtained for rotationally symmetric textures with {100}, {110} or {111} planes in the sheet. It was predicted that pure {111} or {110} textures should give infinite R values, but small amounts of other components such as {100} would preclude this possibility. Hosford and Backofen showed that the effect of a {100} component in depressing R would balance the elevating effect of 4 to 5 times as much {111} component. This provides a concise theoretical explanation of the observations of Whitely and Wise[83] concerning textures and related R values in steel sheets.

The analysis of Hosford and Backofen has not been widely applied to predict strain ratios, possibly because of its complexity. A major objection is that in some instances a range of values are predicted, rather than a particular value. However, Hosford and Backofen[3] proposed a slightly different correlation of anisotropy and texture in the form of the ratio of plane strain strengths, β, given by

$$\beta = \frac{\sigma_x \ (d\varepsilon_y=0)}{\sigma_x \ (d\varepsilon_z=0)} = \frac{M(r=0)}{M(r=1)} = \frac{M(r=0)}{M(r=1)} \quad \ldots\ldots\ldots(34)$$

Thus, instead of determining the entire M vs r curve, only the values of M(r=0) and M(r=1) are required. β is related to R by the equation

$$\beta = \sqrt{\frac{R+1}{2}} \quad \ldots\ldots\ldots(35)$$

By calculating values of β for rotationally symmetric textures it was predicted that sheet normals near <111> are desirable for high drawability and those near <100> are undesirable.

None of the previous theories considers in any detail variations of R with strain. Also, the agreement between predicted and experimentally determined R values is only approximate, the basic difficulties being the present inability to completely define crystallographically a preferred orientation and the problem of accounting for the interaction between deforming grains in a polycrystalline aggregate. Dickson[81] has suggested an approach which is able to predict qualitatively variations of R with strain. For a specimen having an ideal preferred orientation it is argued that R may change fairly abruptly as the predominant mode of deformation changes. On the other hand, when there is a low degree of preferred orientation, the changeover from one deformation mechanism to another takes place in different grains at different overall strains, with the result that R may change continuously with strain. Results obtained on titanium give some support for this theory. A marked decrease in R_{45}° between 17% and 19% strain was correlated with a predicted change in the main mode of deformation from primary slip on $\{10\bar{1}0\}\langle\bar{1}\bar{1}20\rangle$ systems to duplex slip on $\{10\bar{1}3\}\langle\bar{1}\bar{1}20\rangle$ systems.

2.4.3. Dependence of Earing on Texture

The pattern and degree of earing depends upon which texture is predominant.

In brass, Wilson and Brick[92] found that a $\{110\}\langle\bar{1}12\rangle$ secondary recrystallisation texture produced four ears at 45° to the rolling direction, while changes in the details of this texture produced ears at 0° and 60° to the rolling direction. A $\{113\}\langle\bar{2}\bar{1}1\rangle$ primary recrystallisation texture obtained by low temperature annealing was associated with low 45° earing.

The cube texture in copper is associated with ears at 0° and 90° to the rolling direction, while a retained rolling texture produces 45° earing [50,93]. Baldwin[50] observed an approximately linear relationship between the height of the 0° and 90° ears and the proportion of grains having the cube texture. Yen[93] has shown that a mixture of the rolling and annealing textures balances the two earing tendencies. Increasing the final annealing temperature tends to change the earing from 45° to 90° as the proportion of cube texture increases, while at very high annealing temperatures, the height of the 90° ears diminishes and the earing reverts back to the 45° type. Similar effects have been found in aluminium[94,95].

In titanium sheet having a texture described as $(0001)\langle10\bar{1}0\rangle$ with the (0001) plane tilted $\pm$ 35° towards the transverse direction, ears occur at 45° to the rolling direction[80,96].

2.4.4. Theories of Earing

A concise theory of earing must be able to explain observed relationships between textures and ear formation and also the relative heights of ears and troughs around the cup periphery. Of the theories available to date, only that due to Tucker[97] is able to fulfil these requirements and even then this theory only applies rigorously to F.C.C. single crystals. No attempts have yet been made to take into account the complexity of deformation in polycrystals.

Wilson and Brick[92] observed that the ear positions in brass correspond in direction with low peripheral concentrations of {111} poles and the troughs with high peripheral concentrations. Based on this they offered a qualitative explanation for the different earing patterns of cube textured copper and annealed brass having a $\{110\}\langle\bar{1}12\rangle$ texture. Roberts[98] has explained the observations as coincidence rather than a fundamental fact.

Bourne and Hill[84] suggested an approach based on macroscopic properties to predict the behaviour of a sheet under the stresses of a deep drawing operation. They concluded that 45° and 90° earing were the only types possible, which is incorrect when earing patterns of single crystals are considered [97]. Moreover, their approach does not account for the crystallographic requirements of deformation.

Tucker[97] produced a theory of earing in F.C.C. single crystals which gave very concise agreement with observed earing patterns in single crystals of aluminium. Four basic assumptions were made:-

a) that the total radial strain is equivalent to that which would be obtained if the radial and circumferential stresses were equal in magnitude at all points in the blank and the stress normal to the blank were zero (i.e. a condition of plain strain).

b) that at any point deformation occurs on the $\{111\}\langle\bar{1}10\rangle$ system of highest resolved shear stress.

c) that the orientation is constant over the blank, i.e. a single crystal. Orientation changes occurring during drawing were ignored as far as the shear stress was concerned but were taken into account in resolving strains.

d) that the shear stress-shear strain relationship was parabolic.

The first assumption (a) is not valid when the results of Chung and Swift[99] are considered. They showed that for a drawing ratio of 2, the ratio of the radial stress to the circumferential stress varies from 0 at the rim of the blank to 2.3 just before the rim of the die. Tucker[97] remarked, however, that the predicted deformation is not very sensitive to the relative magnitudes of the principal stresses.

In Tucker's analysis, at any point the resolved shear stress on a particular slip system is given by

$$\tau = \sigma (ad-be) \qquad \ldots\ldots\ldots\ldots (36)$$

where σ = numerical value of the compressive and tensile stresses.

abc = direction cosines of {111} plane relative to the directions of principal stress.

def = direction cosines of <110> direction relative to the directions of principal stress.

The direction cosines are expressed in terms of θ, the angle between the radius of the blank passing through the point and an arbitrary reference direction lying in the plane of the sheet. The resolved shear stress was calculated for 12 possible slip systems in terms of θ, and from these results, the range of values of θ over which any particular slip system or systems had the maximum resolved shear stress was determined. The shear strain was taken as the square root of the shear stress. The radial strain was calculated from the shear strain by the relationship

$$L = \sqrt{(1+2\gamma \left| \cos \phi . \cos \lambda \right| + \gamma^2 \cos^2 \phi)} \quad \ldots\ldots\ldots (37)$$

where L = final length of an element in the radial direction which was initially of unit length

γ = shear strain

ϕ = angle between slip plane normal and radial direction

λ = angle between slip direction and radial direction

Because absolute values of γ are not known, relative values of L cannot be calculated precisely. Two limiting cases may be recognised,

however. If γ is small

$$L \sim 1 + \gamma \mid \cos \phi . \cos \lambda \mid \quad \ldots\ldots\ldots (38)$$

which is the actual strain in the radial direction without reorientation. This would be expected since if γ is small, the orientation change is small.

If γ is large

$$L \sim 1 + \gamma \mid \cos \phi \mid \quad \ldots\ldots\ldots (39)$$

Tucker considered that γ would be large in normal deep drawing and assumed that the relative radial strains could be obtained by multiplying the shear strain by $\mid \cos \phi \mid$.

The analysis predicts a strain discontinuity at θ values representing a change from one slip system to another since in general $\mid \cos \phi_1 \mid \neq \mid \cos \phi_2 \mid$ even though the resolved shear stresses will be equal on the two systems. Such discontinuities did not appear in experimental curves of cup height. Tucker explained this by postulating that additional slip systems would be operating at such points and surface markings observed at positions corresponding to predicted strain discontinuities provided some evidence for this. These lines which have also been observed by Baldwin et al[100] and Zaat[101] were not vertical, which indicated that the relative circumferential strain is not constant up the cup wall.

In the experimental earing curves, Tucker[97] found that troughs occurred where <111> directions lie in the plane of the sheet, thus confirming the observations of Wilson and Brick[92].

Tucker[97] concluded that the predicted profiles were not very sensitive to assumptions made in the theory. No account was taken of the possible operation of conjugate slip systems.

Vieth and Whitely[88] applied the Tucker analysis to predict radial strains in single crystals of mild steel. No correlation was made with experimental earing profiles but it was predicted that ears and troughs should occur at the same angular position calculated for the maximum and minimum values of the strain ratio, respectively. A {111} orientation was associated with the least amount of earing.

2.5. Future Possibilities of Texture Control in Commercial F.C.C. Metals and Alloys

The desired characteristic of sheet for deep drawing purposes is a high resistance to thinning under the action of tensile stresses in the plane of the sheet. This resistance to thinning must be obtained in a condition which also gives adequate stretch formability. In cubic metals, maximum resistance to thinning would be achieved with a {111} fibre texture, i.e. with {111} planes parallel to the rolling plane and no preferred direction along the rolling direction. Sheet with such a texture would have a high value of the mean strain ratio, $\bar{R}$, and a zero value for ΔR, the variation of R in the plane of the sheet. These would be associated respectively with a high limiting drawing ratio and minimum earing tendency.

The production of F.C.C. metals with the correct texture for high through-thickness strength has not yet been achieved and from theoretical considerations, it seems unlikely that a {111} primary recrystallisation texture would be formed from the whole range of deformation textures developed in pure F.C.C. metals and F.C.C. solid solution alloys, although Mee and Sinclair[72] have observed the orientation $\{445\}\langle\bar{1}\bar{2}\ 4\ 7\rangle$, which is near to $\{111\}\langle\bar{1}\bar{1}2\rangle$, as a component in the annealing texture of Ni-2½ vol.% thoria. The presence of this component was due to the influence of thoria particles on the deformation texture and/or to their influence on the recrystallisation texture.

Future possibilities of texture control in commercial F.C.C. metals and alloys lie in defining the role played by impurities and second phases on the formation of textures. In metastable alloys, such as certain austenitic stainless steels, the occurrence of strain-induced phase transformation during rolling leads to the possibility of forming rolling texture orientations characteristic of a different crystal structure and these orientations may subsequently give rise to orientations on annealing which are not characteristic of F.C.C. metals and alloys.

3. PRESENT WORK

The object of the present work was to attempt to analyse the factors controlling the inherent formability of austenitic stainless steels, with particular interest in the effect of preferred orientation and the possibility of improving formability via texture control. The textures of immediate interest are those developed by cold rolling and annealing, since, from the work of Goodman and Hu[36,37] hot rolling would merely promote the development of the cube texture on annealing, which is associated with a very low value of R_{45^o}[74] and consequently a low resistance to thinning during deep drawing, and a high degree of earing[50,93].

In a previous study by Summerton[102], attempts were made to improve the formability of austenitic stainless steels by control of composition and surface finish, but no account was taken of the possible effects of texture and no attempt was made to ensure that texture variations were not present throughout the alloys examined. The actual variations observed in deep drawability approached the limit of experimental accuracy in determining the critical blank diameter, and the improvements claimed were of no commercial significance.

In the present work, in order to eliminate variations in formability due to different impurity contents and differences in surface finish, the alloys used were laboratory made 18/10, 18/12 and 18/14 chromium/nickel steels of relatively high purity, and careful control was exercised over the surface finish of sheets used for

tensile and press forming tests. Also, in order to make a reliable assessment of the effects, if any, of preferred orientation, the tensile and press forming properties were compared in sheet processed to obtain (a) an essentially random grain orientation, and (b) a strong primary recrystallisation texture.

4. EXPERIMENTAL TECHNIQUES

4.1. Casting

50 lb. ingots of 18/10, 18/12 and 18/14 chromium/nickel steels were made from high purity (>99.9%) base elements by vacuum melting in a 100 lb. capacity basic lined electric arc furnace.

The initial charge of electro iron, nickel pellets and graphite was melted under 100 mm pressure of argon and the furnace was evacuated when the charge was beginning to melt. Thermic chromium was added to the clear melt. Melting under argon was necessary so that deoxidation by carbon was suppressed until the charge was actually melting, and the chromium was not added initially since it would have partly prevented this reaction. When the chromium had completely dissolved, the furnace was evacuated to 1μ and the melt was allowed to solidify under vacuum in order to expel dissolved gases. The alloy was remelted under vacuum and argon was admitted up to 100 mm pressure while a sample was taken for carbon analysis. The waiting time for the analysis result was about 10 minutes. A calculated amount of nickel oxide was then added in order to remove excess carbon. The argon pressure was increased to 500mm and a small quantity of calcium silicide was added to complete deoxidation and purification. This relatively high argon pressure was necessary in order to avoid complete loss of the calcium before it could react with the melt.

The alloys were cast at 1600°C into large end up mild steel chill moulds, 4 in. in diameter. The analysed compositions of the ingots are given in Table I. Surface defects were removed from the outside and bottom of the ingots by machining.

4.2. Forging

The ingots were annealed for 2h at 1100°C, in order to effect homogenisation of the cast structure, prior to forging down to 4½ in. wide x $^{5}/_{8}$in. thick slab on a 15 cwt. pneumatic hammer. During the forging operation, two intermediate preheats of 15 minutes were used.

The ingot heads, which had been used to grip the workpieces, were cut off and the forged slabs were cut into 8 in. lengths. These were annealed for 1h at 1050°C in order to remove any cold work which might have accumulated during the final stages of forging. They were then machined in order to remove surface cracks and the machining marks were removed by grinding on grade 100 silicon carbide paper.

4.3. Rolling

Cold rolling of the annealed slabs was carried out on a 2-high mill having 18 in. diameter rolls. Two basic schedules were adopted to obtain sheet 0.036 in. thick.

The first was aimed at minimising the retention of preferred orientation on annealing and consisted of using cold reductions $\geq$ 30% with intermediate and final annealing in air for ½h at 1050°C. Sheet was also prepared having subsequent cold reductions of up to 15%.

The second was aimed at retaining a strong preferred orientation after annealing and consisted of cold rolling to 93% reduction and annealing at temperatures in the range 500-1000°C.

Surface scale produced during annealing was removed by pickling in a boiling solution of 5% HNO_3/30% HCl/65% water followed by abrading with silicon carbide paper. Consistency of surface finish was achieved by final grinding to a 400 grade finish.

4.4. Determination of Pole Figures

Quantitative pole figures were determined by the Schulz X-ray reflection method using a Siemens texture goniometer in conjunction with a G.E.C. XRD5, X-ray set. In the Schulz method, the specimen undergoes two step-wise rotations simultaneously, one being about an axis normal to the rolling plane (α rotation), and the other being about an axis lying in the plane of the sheet (β rotation). The diffracted radiation was monitored continuously with an argon Geiger-Mueller counter and recorded on a chart to indicate the variation in diffracted intensity (proportional to the density of {hkl} planes reflecting) with specimen rotation. Since the rotations of the specimen were calibrated with the chart speed, the intensity contours on pole figures were readily plotted from charts of diffracted intensity vs. specimen rotation.

The Schulz method is only accurate for up to 70° of β rotation. Above this angle, defocussing occurs, ~~the incident or diffracted beam is cut off by the specimen~~, so that the peripheral regions of the pole figure cannot be determined accurately. However, this was not a disadvantage in the present work because the important features of nearly all the textures

were contained in this area of the pole figure. Additionally, in plotting the intensity contours for $\beta > 70^{\circ}$ an attempt was made to allow for the decrease in intensity by assuming it to follow a theoretical curve[103]. By correcting the intensity levels in this manner, contours may be plotted with reasonable accuracy for β values between 70° and 80°-85°.

Specimen preparation included grinding to grade 400 silicon carbide paper followed by etching for 1 minute in a boiling solution of 5% HNO_3/30% HCl/65% water.

For specimens which consisted of austenite and martensite, separate {200} pole figures were determined for each phase. In the absence of martensite, either $\{111\}_{\gamma}$ or $\{200\}_{\gamma}$ pole figures were determined. The intensity levels on all pole figures have been labelled in arbitrary units. The random levels, obtained by integration, are indicated.

4.5. Tensile and Press Forming Tests

As a consequence of the texture determinations, it was decided to investigate the tensile and press forming properties of material

a) having a nominally random grain orientation.

b) as (a) but subsequently temper rolled to reductions of up to 15%.

c) having a strong preferred orientation after annealing.

For (c), the selected annealing treatments after 93% cold reduction were ½h at 800°C, ½h at 900°C or 1h at 1000°C. The treatment at 1000°C is regarded as a full anneal and those at 800°C and 900°C as temper anneals.

Strip tensile specimens were taken at 0°, 45° and 90° to the rolling direction. The specimens were 4 in. long with a 1 in. gauge length and a $\frac{1}{4}$ in. gauge width. Except for temper rolled material, machining of the test specimens was carried out before the final annealing treatment, so as to avoid the presence of machining stresses in the annealed specimens. The tests were carried out on a Hounsfield tensometer using a constant strain rate of approximately 11% $min.^{-1}$. Load-extension curves were plotted manually, and from these the following properties were evaluated;-
U.T.S., Limit of Proportionality, total elongation, limit of uniform elongation, and the rate of work hardening. Strain ratios were calculated from measurements of the gauge length and width after various strains in the plastic range from about 5% up to the limit of uniform elongation. Assuming constancy of volume in the gauge length, R is given by equation (2), i.e.

$$R = \frac{\ln\left(\frac{w_o}{w_x}\right)}{\ln\left(\frac{l_x w_x}{l_o w_o}\right)}$$

Deep drawability was assessed by measuring the critical blank diameter using a 33 mm diameter flat-nosed punch, a blank holding load of 1500 Kg and 0.002 in. thick polythene sheet as lubricant between the blank and the die. Earing profiles were measured on cups drawn at the critical blank diameter, the % earing being given by

$$\frac{2(a-b)}{(a+b)} \times 100\% \qquad \text{.....(40)}$$

where a is the average peak height

b is the average trough height

Stretch formability was assessed by measuring the depth of a cup at maximum load formed by using a 20 mm diameter round-nosed punch, a blank holding load of 1500 Kg and polythene sheet as lubricant between the punch nose and the blank.

4.6 Phase Analysis by X-ray Diffraction

In order to identify the type of martensite which is formed in these steels during cold rolling, Debye-Scherrer powder patterns or automatically recorded diffraction patterns were obtained for selected specimens using CoK_α radiation. The amount of martensite was estimated by comparing the integrated intensities of different diffraction lines of each phase.

4.7 Optical Metallography

Selected specimens were mounted and polished to $\frac{1}{4}\ \mu$ diamond and etched electrolytically in a saturated solution of oxalic acid for 10-15 secs. at 15 volts. The specimens were examined on a Vickers Projection Microscope. With the exception of temper rolled material, grain sizes were measured for all conditions used for deep drawing and stretch forming tests.

5. RESULTS

5.1. Metallographic Examination

In samples consisting of austenite and martensite (the presence of the martensite being revealed by testing with a magnet and by X-ray diffraction), differentation of the two phases by etching was unsuccessful, probably because of the severe distortion of the metal.

Carbide precipitation was observed in samples annealed in the range 700-800°C, but no marked differences occurred between the three steels. No detailed study of the nature of the precipitation was attempted.

The measured grain sizes in the conditions used for tensile and press forming tests are shown in Table 2. In all cases a larger grain size occurred after the treatment used to develop a random grain orientation than after 93% cold rolling + 1h at 1000°C. Temper annealing of 93% cold rolled material resulted in a marked reduction in grain size.

5.2. Phase Analysis

All diffraction patterns showed the presence of γ (F.C.C.) or $\gamma + \alpha'$ (B.C.C.), the lattice parameters of the phases in the 18/10 alloy being $a_\gamma = 3.591 \pm .001$ Å and $a_{\alpha'} = 2.87 \pm .01$ Å. The value for the austenite was obtained from filings which were stress relieved by annealing in argon for 4h at 800°C, while the value for the martensite was obtained from a sample which had been cold rolled to 93% reduction and annealed for ½h at 500°C.

In samples which had been cold rolled to 93% reduction prior to annealing, including tensile specimens prepared from sheet having 93% reduction + anneal, quantitative estimation of the amount of martensite formed during tensile tests was made difficult by the presence of marked preferred orientation. Data obtained from these specimens were considered to be unreliable because widely differing results were obtained when comparing different pairs of integrated line intensities.

However, in tensile specimens taken from sheet processed to produce a random grain orientation, subsequent tensile elongations up to 50% did not affect the reliability of relative intensity measurements. This is shown by the following results for a specimen strained to 50% plastic elongation. The ratio of the volume fractions of the two phases is given by

$$\frac{C_\gamma}{C\alpha'} = \frac{I_\gamma R\alpha'}{I\alpha' R_\gamma}$$

where C_γ and $C\alpha'$ are the volume fractions

I_γ and $I\alpha'$ are the integrated line intensities

R_γ and $R\alpha'$ are factors of proportionality which depend on the Bragg angle θ, {hkl} and the phase itself.

Diffraction Line	Integrated Intensity	R factor	% Martensite
111_γ	279	90.96	54.3
$110_{\alpha'}$	440	120.8	
200_γ	176	36.45	54.0
$200_{\alpha'}$	186	14.98	
200_γ	176	36.45	47.4
$211_{\alpha'}$	136	30.87	

5.3. Development of Randomly Oriented Material

Figures 10-15 show that for all the steels alternate 30% cold reductions with intermediate and final annealing for ½h at 1050°C developed an essentially random grain orientation, but after subsequent cold reductions of 15% some preferred orientation had developed. After 15% reduction the 18/10 steel had started to transform to martensite.

5.4. Cold Rolling and Annealing Textures

5.4.1. 18/10 Chromium/Nickel Steel

The 18/10 steel started to transform to martensite after reductions ~15% and was strongly magnetic after 93% reduction. Figure 16 shows that the texture of the α' martensite consisted of two principal components, $\{111\}\langle 11\bar{2}\rangle$ and $\{112\}\langle \bar{1}10\rangle$, with a spread towards $\{001\}\langle 110\rangle$. Figure 17 shows that the texture of the remaining untransformed austenite was of the F.C.C. alloy type, i.e. $\{110\}\langle \bar{1}12\rangle$ + a minor $\{110\}\langle 001\rangle$ component. ~~The amount of austenite was estimated as ~20-30%~~.

On annealing at 400, 500 or 600°C no new orientations appeared in the martensite. The steel remained magnetic for annealing treatments up to ½h at 600°C, but was completely austenitic after annealing for ½h at 700°C.

After ½h at 500°C, new orientations appeared in the austenite near $\{230\}\langle 3\bar{2}1\rangle$ and in a spread in the region of $\{112\}\langle 31\bar{2}\rangle$ (Figure 18). The remainder of the texture consisted of a spread between $\{110\}\langle \bar{1}12\rangle$ and $\{110\}\langle 001\rangle$ and it was apparent that the absolute

intensity of the {200} reflection in this region (3.5 x random) was greater than the intensity of the same region in Figure 17 (2 x random). After 1/2 h at 600°C (Figure 19) the intensity in the {110}<001> region had not changed significantly, whereas the intensity in the {230}<3$\bar{2}$1> region had increased from 2.8 x random after 1/2 h at 500°C (Figure 18) to 4 x random after 1/2 h at 600°C (Figure 19). After 1/2 h at 700°C (Figures 20 and 21) the texture became sharper near {110}<$\bar{1}$12> and the existence of a further component near {230}<3$\bar{2}$,13> was necessary in order to explain the spread of intensity near {110}<$\bar{1}$12>. As the annealing temperature was increased to 800°C the intensity of the ~{230}<3$\bar{2}$,13> orientation increased at the expense of the {110}<$\bar{1}$12> component (Figures 22 and 23) and after 1/2 h at 900°C (Figures 24 and 25), or 1h at 1000°C, the texture was reasonably described by two types of orientations, one being near {230}<3$\bar{2}$1> and containing {430}<$\bar{3}$40>, the other being near {230}<3$\bar{2}$,13> and containing {430}<001>. It was estimated from {200} pole figures that the relative amount of the ~{230}<3$\bar{2}$1> component increased from approximately 60% after 1/2 h at 800°C, 900°C at 1000°C to approximately 75% after 1h at 1000°C.

5.4.2 18/12 Chromium/Nickel Steel

The 18/12 steel started to transform to martensite after reductions ~20%, but after 93% reduction was only moderately magnetic compared with the 18/10 steel. The austenite exhibited a typical F.C.C. alloy type of texture (Figure 26), while the texture of the ferrite consisted of two main orientations, {111}<11$\bar{2}$> and {112}<$\bar{1}$10> (Figure 27).

After 3 minutes at 600°C (Figure 28) the steel was only weakly magnetic and the austenite texture was the same as the rolling texture. After 15 minutes the steel was non-magnetic and the texture became sharper (Figure 29), while after ½h a new orientation appeared near $\{113\}\langle\bar{2}\bar{1}1\rangle$ (Figure 30). With increasing degree of anneal the ~$\{113\}\langle\bar{2}\bar{1}1\rangle$ component became sharper and its intensity increased at the expense of that of the $\{110\}\langle\bar{1}12\rangle$ component (Figures 31-33).

5.4.3. 18/14 Chromium/Nickel Steel

The 18/14 steel only started to become magnetic after ~80% reduction and even after 93% reduction was only weakly magnetic compared with the 18/10 and 18/12 steels. The amount of martensite formed after 93% reduction was too small (probably ~10% or less) for its texture to be determined. The cold rolling and annealing textures of the austenite (Figures 34-37) were similar to those in the 18/12 steel.

5.5. Tensile Tests

During tensile tests on annealed or temper rolled (up to 15% reduction) sheet, only the 18/10 steel partly transformed to martensite.

5.5.1. Randomly oriented or temper rolled material

Data obtained from the tensile tests on randomly oriented or temper rolled material are shown in Figures 38-45. Although no rigorous analysis was made of the true stress-true strain relationships, it was evident from log (true stress) vs. log (true strain) plots that a simple parabolic relationship did not completely define the true stress-

true strain curves, especially for the 18/10 steel. The measured values of n therefore represent the average rate of work hardening during the tests. The U.T.S., Limit of Proportionality, % elongation and rate of work hardening did not vary significantly with the direction of testing, and the values shown in Figures 38-40 are the mean of values obtained at 0°, 45° and 90° to the rolling direction, weighted in favour of the value at 45° to the rolling direction. The strain ratios shown in Figures 41-43 are the average of several values between ~5% plastic strain and the limit of uniform elongation. The mean strain ratio obtained from each average value in the 0°, 45° and 90° directions is defined by equation (3), i.e.

$$\bar{R} = \tfrac{1}{4} (R_{0^{\circ}} + 2R_{45^{\circ}} + R_{90^{\circ}})$$

The parameter ΔR, used as a measure of planar anisotropy, is defined as

$$\Delta R = \tfrac{1}{2} (R_{0^{\circ}} + R_{90^{\circ}} - 2R_{45^{\circ}}) \quad \text{.....(40)}$$

Figure 38 shows that the U.T.S. and Limit of Proportionality were increased by cold rolling, while Figure 39 shows that the total and uniform elongations were reduced. In the fully annealed condition, the 18/10 steel had a higher uniform elongation than the 18/12 or 18/14 steels, but after ~5% cold reduction the situation was reversed. The total elongation behaved similarly. Figure 40 shows that cold rolling lowered the rate of work hardening, and reduced the initial difference which occurred between the rate of work hardening of the 18/10 steel and that of the 18/12 or 18/14 steels.

For the annealed sheets, the strain ratio, R, was slightly less than 1 and varied slightly with the direction of testing (Figures 41-44). Cold rolling caused the planar variations to become more marked, especially for the 18/10 steel. In the annealed condition, the mean strain ratio, $\bar{R}$, varied only slightly with composition, but with increasing cold work $\bar{R}$ decreased for the 18/10 and 18/14 steels yet remained almost unchanged for the 18/12 steel (Figure 45).

5.5.2. Material having primary recrystallisation textures

Data obtained from the tensile tests on material having strong primary recrystallisation textures are shown in Figures 46-53. The results are presented in a similar manner to those on randomly oriented or temper rolled material. After annealing for ½h at 900°C or 1h at 1000°C, the 18/10 steel had a higher uniform elongation (Figure 47) and a higher rate of work hardening (Figure 48) than the 18/12 or 18/14 steels. The values for all the textured steels were slightly lower than for the randomly oriented material.

In all three steels, the textures were associated with marked planar anisotropy (Figures 49-51). As the annealing temperature was increased, the 18/10 steel exhibited a marked increase in the value of $R_{90}°$ while $R_0°$ and $R_{45}°$ remained substantially constant. On the other hand, the 18/12 and 18/14 steels behaved differently, with $R_{45}° > R_0° > R_{90}°$ after temper annealing or after full annealing. The numerical value of ΔR was much greater for the 18/12 and 18/14 steels (Figure 52). Figure 53 shows that the texture in the 18/10 steel

was associated with a $\bar{R}$ value slightly greater than that for the texture in 18/12 or 18/14 steels. For all the steels, $\bar{R}$ was only slightly greater than the value obtained for randomly oriented material.

5.5.3. Effect of plastic strain on R values

Tables 3(a), 3(b) and 3(c) summarise the effect of plastic strain on the R values at 0°, 45° and 90° to the rolling direction. In all cases, the values were measured at 5 or 6 strains from about 5% up to the limit of uniform elongation. Most of the values remained constant during straining, but since only single tests were carried out, the observations may not be reproducible.

5.6. Press Formability Tests

The results of the press forming tests are shown in Figures 54-57. During these tests only the 18/10 steel became magnetic.

Figures 54 and 55 indicate that the critical blank diameters achieved in deep drawing tests were not significantly affected by the differences in composition, by the presence of strong primary recrystallisation textures, by cold reductions of up to 12.5% or by temper annealing instead of full annealing. In all cases failure occurred in the zone which is stretch formed over the punch radius. In the randomly oriented condition, all three steels exhibited a similar earing tendency. For the 18/10 steel subsequent cold reductions of up to 12.5% developed ears at 0° and 90° to the rolling direction. The amount of earing associated with the recrystallisation texture in the 18/10 steel was the same as that in randomly oriented material, whereas the texture in 18/12 and 18/14

steels was associated with a much larger amount of earing. For all the steels less earing occurred after temper annealing than after full annealing. The texture in the 18/10 steel was associated with ear formation mainly in the rolling direction, with a lower set of ears at 60° to the rolling direction, whereas the texture in 18/12 or 18/14 steels was associated with 45° earing.

Figures 56 and 57 indicate that in the fully annealed conditions, stretch formability decreased with increasing nickel content. Post-annealing cold reductions of up to 12.5% or temper annealing lowered the stretch formability. For reductions greater than about 5%, the 18/10 steel had a lower stretch formability than the 18/12 or 18/14 steels. A similar changeover was starting to occur with temper annealing in Figure 57, where, after annealing for ½ h at 800°C, the 18/14 steel had the highest stretch formability.

In both deep drawing and stretch forming tests no surface roughening occurred on material cold rolled to 93% reduction and annealed for ½h at 800°C, but pronounced "orange peeling" was observed on fully annealed material.

6. DISCUSSION

6.1. Cold Rolling and Annealing Textures in 18/10, 18/12 and 18/14 Chromium/Nickel Steels

In metastable austenitic steels, increasing degree of cold work continuously raises the M_S temperature until a limiting value is reached which depends on the alloy composition. Transformation to martensite can occur as long as the M_S temperature is continuously raised above the deformation temperature. In relatively pure steels of the type 18% chromium 10-14% nickel α' martensite is formed, and providing the carbon content is sufficiently low, the martensite is effectively B.C.C. (In this respect Goodman and Hu[36,37] appropriately used the term "martensitic ferrite".)

The martensite formed at any instant is related to its parent austenite by established orientation relationships. Both the Kurdjumov-Sachs and the Nishyama relationships have been observed in iron-nickel alloys,[104] the former being

$(111)_\gamma \,||\, (110)_{\alpha'}$ and $[1\bar{1}0]_\gamma \,||\, [1\bar{1}1]_{\alpha'}$

and the latter being

$(111)_\gamma \,||\, (110)_{\alpha'}$ and $[\bar{2}11]_\gamma \,||\, [1\bar{1}0]_{\alpha'}$

However, during cold rolling, where the orientation of the austenite and also that of the martensite which has already been formed is continuously changing, new martensite regions will be unlikely to have the same orientation as martensite formed at a much earlier stage during rolling. Similarly, the preferred orientations developed by the two phases would be unlikely to be related by a Kurdjumov-Sachs or by a Nishyama relationship unless by coincidence. A possible exception to this is discussed with respect to martensite formation in the 18/14 steel.

The pole figures obtained for the 18/10 and 18/12 steels show that both phases develop their characteristic preferred orientation during cold rolling to heavy reductions. The orientations $\{111\}\langle 11\bar{2}\rangle$, $\{112\}\langle \bar{1}10\rangle$ and $\{001\}\langle 110\rangle$, which are the main components of the martensite texture, have been generally observed in B.C.C. metals after heavy reductions[26]. In fact, Barrett and Levenson[104] observed that single crystals of these orientations are stable after quite heavy deformation. However, in B.C.C. metals generally, the $\{112\}\langle \bar{1}10\rangle$ component has always been found to occur but the $\{111\}\langle 11\bar{2}\rangle$ component occurs in some cases only[26]. Also, the main component of the B.C.C. texture is usually $\{001\}\langle 110\rangle$, which was not observed in the cold rolling texture of the 18/12 steel. Results obtained by Bennewitz[105] on a low-carbon steel and a 3% silicon steel, and suggestions by Dillamore and Roberts[44] indicate that the texture in B.C.C. metals arises from the development and subsequent breaking up of the $\{112\}\langle \bar{1}10\rangle$ component. Bennewitz[105] found that an initial orientation $\{100\}\langle 011\rangle$ rotates to $\{112\}\langle \bar{1}10\rangle$ whereas $\{110\}\langle 001\rangle$ rotates to $\{111\}\langle 11\bar{2}\rangle$ and then to $\{112\}\langle \bar{1}10\rangle$. In either case the $\{112\}\langle \bar{1}10\rangle$ component then rotates to $\{001\}\langle 110\rangle$ or $\{111\}\langle \bar{1}10\rangle$.

The absence of the $\{001\}\langle 110\rangle$ component in an 18/12 steel may be explained by the following argument. In this steel, until the limiting M_S value is reached, a larger amount of deformation is necessary in order to obtain the same increase in M_S or the same extent of transformation as in an 18/10 steel. Thus, the same grain

rotations of the martensite take place at higher rolling reductions than those in an 18/10 steel, with the result that, according to the previous mechanism, the $\{112\}\langle\bar{1}10\rangle$ component does not rotate to $\{001\}\langle110\rangle$, at least up to 93% reduction.

Martensite which is formed at high rolling reductions (>80%) from austenite having a strong $\{110\}\langle\bar{1}12\rangle$ type of texture will itself have a preferred orientation which is related to that of the austenite by the crystallographic relationships of the transformation. In the 18/14 alloy, which was weakly magnetic after 93% reduction, the martensite would be expected to have a preferred orientation near $\{111\}\langle\bar{1}\bar{1}2\rangle$ assuming a Kurdjumov-Sachs relationship or near $\{001\}\langle011\rangle$ assuming a Nishyama relationship.

The cold rolling texture orientations observed in the 18/10 steel are the same as those observed by Goodman and Hu[36,37] in a commercial steel having a similar composition. They found that annealing for 1h at 600°C increased the intensity of the $\{110\}\langle\bar{1}12\rangle$ component and a new orientation appeared near $\{230\}\langle3\bar{2}1\rangle$, while the intensity of the ferrite texture decreased. At higher annealing temperatures, this new orientation disappeared leaving a $\{110\}\langle\bar{1}12\rangle$ texture. These authors concluded that the transformation of $\alpha' \longrightarrow \gamma$ was by the growth of crystallites of retained austenite, but they explained the presence of the orientation near $\{230\}\langle3\bar{2}1\rangle$ by stating that it could be related to the $\{111\}\langle11\bar{2}\rangle_{\alpha'}$ component of the rolling

texture by a Kurdjumov-Sachs relationship and was therefore derived from $\{111\}\langle 11\bar{2}\rangle_{\alpha'}$ by a reverse martensite transformation. However, it is unreasonable to assume that only one component of the ferrite rolling texture should transform to austenite by a reverse martensitic process, and furthermore the two orientations are not exactly related.

In the present work the increase in intensity of the $\sim\{230\}\langle 3\bar{2},13\rangle$ and $\sim\{230\}\langle 32\bar{1}\rangle$ orientations was associated with a decrease in the intensity of $\{110\}\langle\bar{1}12\rangle$ and a reduction in the spread towards $\{112\}\langle 31\bar{2}\rangle$. Orientations near $\{110\}\langle\bar{1}12\rangle$ and $\{112\}\langle 31\bar{2}\rangle$ are related to orientations near $\{230\}\langle 3\bar{2},13\rangle$ and $\{230\}\langle 32\bar{1}\rangle$ respectively by approximately 25° rotations about common $\langle 111\rangle$ axes. However, since these orientations are merely simple descriptions of the texture, there will be many grains which have much larger ($\sim 40^{\circ}$) rotational relationships. It is therefore suggested that the latter orientations originate from the former by an oriented growth process, in accordance with previous theories[58,61,62].

The $\{110\}\langle\bar{1}12\rangle$ and $\sim\{112\}\langle 31\bar{2}\rangle$ orientations were observed in the austenite after annealing for ½h at 500°C, at which temperature they could not be a result of recrystallisation. The $\{110\}\langle\bar{1}12\rangle$ component could be the standard F.C.C. alloy rolling texture, but the spread in the region of $\{112\}\langle 31\bar{2}\rangle$ is an orientation entirely foreign to the austenite or martensite rolling textures. Also the intensity of the ~~$\{200\}_{\gamma}$ reflection~~ $\{110\}\langle\bar{1}12\rangle$ component was much higher after annealing for ½h at 500°C than after cold rolling, possibly indicating that the amount of

austenite had increased on annealing. This suggests that some of the orientations after annealing for ½h at 500°C arise from the martensite. A more rational approach than that adopted by Goodman and Hu[36,37] is therefore to assume that all the orientations in the martensite give rise to corresponding orientations in the austenite according to the crystallographic relationships of the transformation. The $\sim\{112\}\langle 31\bar{2}\rangle_\gamma$ and $\{110\}\langle\bar{1}12\rangle_\gamma$ orientations are related to $\sim\{112\}\langle\bar{1}10\rangle_{\alpha'}$ and $\{111\}\langle 11\bar{2}\rangle_{\alpha'}$ orientations respectively by a Kurdjumov-Sachs relationship, so that they could have been derived from the latter by a reverse martensitic process. Orientations in the martensite rolling texture which lie in the spread between $\{112\}\langle\bar{1}10\rangle$ and $\{001\}\langle 110\rangle$ probably contribute towards the wide orientation spread in Figures 18-20. During recrystallisation such components are assumed to be largely absorbed by the growth of $\sim\{230\}\langle 3\bar{2}1\rangle$ and $\sim\{230\}\langle 3\bar{2}13\rangle$ orientations.

Applying the same explanation to the observations of Goodman and Hu[36,37] merely requires that in the alloy which they examined there must be some additional factor which is capable of suppressing reorientation of the $\{110\}\langle\bar{1}12\rangle$ component during recrystallisation, such that this component is capable of growth and eventually absorbs the $\{230\}\langle 3\bar{2}1\rangle$ component. The difference between the annealing textures observed in the present work and those observed by Goodman and Hu may be attributed to differences in composition between the alloys examined.

In steels which are rolled in a temperature range where the austenite is stable, typical F.C.C. rolling textures are obtained. The 18/14 steel rolled at room temperature approximates to this since only a relatively small amount of martensite was formed in this alloy after 93% reduction. Since the stacking fault energy of an 18/14 steel is ~15 ergs cm^{-2},[106-108] this observation is in agreement with the well-stablished dependence of the room temperature rolling texture on stacking fault energy[40,41]. Decreasing the nickel content to 10% lowers the stacking fault energy to ~10 ergs cm^{-2}, so that the alloy type of texture would still be expected to occur in the austenite of 18/10 or 18/12 alloys rolled at room temperature.

The orientation ~$\{113\}\langle\bar{2}\bar{1}1\rangle$, observed as the annealing texture of the 18/12 and 18/14 steels, is related to $\{110\}\langle\bar{1}12\rangle$ by approximately 40° rotation about a common <111> axis, so that recrystallisation in these steels may be explained by an oriented growth process. The $\{113\}\langle\bar{2}\bar{1}1\rangle$ recrystallisation texture has also been observed in other F.C.C. alloys[53,56].

6.2. Correlation of Plastic Anisotropy and Preferred Orientation

6.2.1. Randomly oriented or temper rolled material

In 18/10, 18/12 and 18/14 chromium/nickel steels the $\gamma \longrightarrow \alpha'$ transformation is accompanied by an increase in volume of ~2.1% (as calculated from the lattice parameters). Since the method of determining R from measurements of the gauge length and width relies

on the absence of volume changes, the validity of R values measured in the presence of the $\gamma \rightarrow \alpha'$ transformation must be questioned. However, after 50% elongation the amount of martensite formed was only ~50%, corresponding to a volume increase ~1%, and from the analysis given in the Appendix, the maximum error in R as a result of the transformation is considered to be ~5%.

In the absence of phase transformation the accuracy of R measurements was limited partly by the relatively small specimen size (especially the relatively small gauge width) and even though measurements for individual tests were averaged over four places in the gauge length, specimen end effects may have introduced additional errors. Minor texture variations and inhomogeneity throughout the processed sheets may have introduced errors which probably gave rise to the anomalous variations of R with strain, which are indicated in Table 3. Although no detailed analysis of the practical errors was attempted, a guide to the total error involved was obtained from the variations of R with strain. It was arbitrarily assumed that R was constant if the experimental values did not deviate by more than $\pm$ 5%. In fact, for most of the variations labelled constant in Table 3, the results fell within an error band of $\pm$ 2%. It is therefore considered that the error in R as a result of the volume change is only of the same order as the experimental error, and that the results obtained for the 18/10 steel are quite valid. However, the results for all the steels may be discussed more rationally by allowing for an error ~ $\pm$ 5%.

For a completely randomly oriented polycrystalline metal, the theoretical values of R and ΔR are, respectively, one and zero. In 18/10, 18/12 or 18/14 chromium/nickel steels the use of 30% cold reductions with intermediate and final annealing for $\frac{1}{2}$h at 1050°C produces sheet which approximates to an isotropic material (Figures 10, 12 and 14). Subsequent cold rolling prior to testing would be expected to develop a preferred orientation which is characteristic of the particular alloy. Figures 11, 13 and 15 clearly indicate the presence of some preferred orientation after 15% cold reduction, but this is probably a surface effect arising from the relatively inhomogeneous nature of the deformation which results from small rolling reductions.

After 15% cold rolling, in the 18/10 and 18/14 steels $R_{90^o} > R_{0^o} \simeq R_{45^o}$ (Figures 41 and 43), whereas for the 18/12 steel there is no significant difference between the R values (Figure 42). Also, after 15% cold reduction, ΔR for the 18/10 and 18/14 steels is higher than for the 18/12 steels. These results for the 18/12 steel may therefore be anomalous, since for all the steels the main deformation mechanisms in the austenite would be expected to be primary and duplex slip on $\{111\}\langle\bar{1}10\rangle_\gamma$ systems to develop a weak $\{110\}\ \langle\bar{1}12\rangle$ austenite texture. Furthermore, after 15% reduction the 18/10 steel exhibited marked earing behaviour at 0° and 90° to the rolling direction, whereas in the 18/12 and 18/14 steels the amount of earing does not increase for reductions <15%. The relative magnitude of the R values for the 18/10 steel does not correlate exactly with the relative heights of ears, since if this were so the earing would have been more pronounced at 90°, instead of being equal at 0° and 90°.

6.2.2 Material having primary recrystallisation textures

In the 18/10 steel, the increase in R_{90}^{o} with increasing degree of anneal is associated with a change in the principal components of the recrystallisation texture i.e. after annealing for ½h at 800°C, ~{230} <3$\bar{2}$1> , ~{230} <3$\bar{2}$,13> and {110} <$\bar{1}$12> components are associated with $R_{0}^{o} \triangleq R_{45}^{o} > R_{90}^{o}$ whereas after 1h at 1000°C, ~ {230} <3$\bar{2}$1> and ~{230} <3$\bar{2}$,13> components are associated with $R_{90}^{o} > R_{0}^{o} \triangleq R_{45}^{o}$. Also the amount of the {230} <3$\bar{2}$1> component changes from approximately 60% after ½h at 800°C to 75% after 1h at 1000°C. Both textures are associated with a relatively low value of ΔR and the same earing behaviour, the ears forming mainly at 0° and also at 60° to the rolling direction. The apparently anomalous earing behaviour in the 18/10 steel is possibly due to the $\gamma \rightarrow \alpha'$ transformation taking place during deep drawing, and the subsequent deformation of a two-phase matrix under a complex stress system.

By contrast, the ~{113} <$\bar{2}\bar{1}$1> texture which occurs in the 18/12 and 18/14 steels is associated with $R_{45}^{o} > R_{0}^{o} > R_{90}^{o}$, a higher numerical value of ΔR than the 18/10 steel and a correspondingly larger amount of earing, the ears occurring at 45° to the rolling direction.

6.3 Correlation of Tensile and Press Forming Properties

In the randomly oriented condition, the slightly lower critical blank diameter of the 18/10 steel coincides with a very high rate of work hardening compared with the rate of work hardening of the 18/12 and 18/14 steels. The predicted effect of such an increase in n on the drawing limit according to the analysis of Keeler and Backofen[19] is shown in Table 4. Although the analysis predicts much higher critical blank diameters than were actually observed, an important feature is that the 18/10 steel would be expected to have a higher critical blank diameter than the 18/12 or 18/14 steels. Their analysis clearly cannot apply in this case, presumably because of the fact that these alloys, especially the 18/10 steel, do not precisely obey a parabolic true stress-true strain relationship.

For all three steels having strong primary recrystallisation textures, the reported increases in $\bar{R}$ compared with randomly oriented material do not cause any marked improvement in deep drawability,

although there is a slight increase in the critical blank diameter of the 18/10 steel. Table 5 shows the predicted behaviour from Whitely's analysis of the effect of anisotropy on the drawing limit. For randomly oriented material the predicted critical blank diameters are in good agreement with the determined values, ~~so that~~ The slightly lower drawability of the 18/10 steel in this condition could be explained by slight differences in ~~planar~~ anisotropy. For the textured condition, however, the predicted values are much higher than the determined values. This is possibly because the $\bar{R}$ values for textured material, calculated from R_0^o, R_{45}^o and R_{90}^o, may not accurately define the degree of normal anisotropy. Further, correlation of the drawing limit with $\bar{R}$ by the Whitely analysis is usually only successful for variations in $\bar{R}$ which are much larger than those reported in the present work.

The differences in stretch formability between the 18/10 steel and the 18/12 or 18/14 steels correlate reasonably well with differences in the extent of uniform elongation. From the theories of Keeler and Backofen[13] and Moore and Wallace[14] the observed variations in $\bar{R}$ would not be expected to cause any marked variation in the extent of uniform elongation and hence stretch formability. Moreover, these theories can only strictly be applied to a situation where $\bar{R}$ varies but n remains constant, since they do not take into account the combined effects of anisotropy and the rate of work

hardening. In the fully annealed condition, the slightly low stretch formability of all the steels in the presence of preferred orientation is related to small differences in the rate of work hardening and in the extent of uniform elongation, which arise from different rolling and annealing schedules, rather than to the presence of the preferred orientation itself.

7. CONCLUSIONS

7.1. During cold rolling to 93% reduction, 18/10 chromium/nickel steel undergoes extensive transformation to α' martensite. The texture of the martensite consists of two main orientations, $\{111\}\langle 11\bar{2}\rangle$ and $\{112\}\langle \bar{1}10\rangle$, with a spread towards $\{001\}\langle 110\rangle$. The texture of the untransformed austenite is of the type $\{110\}\langle \bar{1}12\rangle$. On annealing, orientations near $\{110\}\langle \bar{1}12\rangle$ and in the region of $\{112\}\langle 31\bar{2}\rangle$ are initially present in the austenite. These orientations subsequently recrystallise to $\sim\{230\}\langle 32\bar{1}3\rangle$ and $\sim\{230\}\langle 32\bar{1}\rangle$ components, respectively.

7.2. In an 18/12 chromium/nickel steel, less martensite is formed and the main component of the texture is the $\{110\}\langle \bar{1}12\rangle$ austenite orientation. In the martensite, only the $\{111\}\langle 11\bar{2}\rangle$and $\{112\}\langle \bar{1}10\rangle$ orientations are observed. On annealing, the texture changes to $\sim\{113\}\langle \bar{2}\bar{1}1\rangle$.

7.3. In an 18/14 chromium/nickel steel only a very small amount of martensite is formed compared with 18/10 and 18/12 steels. The texture of the austenite is again of the type $\{110\}\langle \bar{1}12\rangle$ and this changes on annealing to $\sim\{113\}\langle \bar{2}\bar{1}1\rangle$.

7.4. In 18/10, 18/12 and 18/14 chromium/nickel steels, sheet having an essentially random grain orientation can be produced by using cold reductions $\geq$30% with intermediate and final annealing for $\frac{1}{2}$h at 1050°C. Mean strain ratios of 0.92 to 0.94 are obtained.

7.5. Further cold reduction up to 15% prior to testing decreases the rate of work hardening, reducing the initial difference which occurs between 18/10 and 18/12 or 18/14 steels, and develops a low degree of preferred orientation which is associated with an increase in planar anisotropy.

7.6. The primary recrystallisation textures in these steels are associated with marked planar variations in the strain ratio, R, and a mean strain ratio, $\bar{R}$, only slightly greater than that in randomly oriented material. The processing schedules used lead to a decrease in the rate of work hardening and in the extent of uniform elongation compared with randomly oriented material. The magnitude of the decrease depends upon the final anneal.

7.7. The presence of the primary recrystallisation textures has no significant effect on the deep drawability. Moreover, the amount of earing associated with the texture in 18/10 steel is the same as that in randomly oriented material (~3%), whereas the texture in 18/12 and 18/14 steels is associated with a much larger amount of earing (6-8%)

7.8. In the fully annealed condition, stretch formability, which decreases with increasing nickel content , is not significantly affected by the presence of strong preferred orientation.

7.9. Neither temper annealing (instead of full annealing) nor cold reductions of up to 12.5% have any marked effect on deep drawability, but both treatments lower the stretch formability.

APPENDIX

Effect of $\gamma \rightarrow \alpha'$ transformation on the accuracy of R measurements.

The strain ratio, R, is defined as

$$R = \frac{\ln\left(\frac{Wo}{Wx}\right)}{\ln\left(\frac{to}{tx}\right)} \qquad \ldots\ldots\ldots\ldots\ldots (1)$$

where Wo and Wx are, respectively, initial and final gauge width,

to and tx are, respectively, initial and final gauge thickness.

Assuming constant volume conditions in the gauge length, equation (1) may be rewritten as

$$R = \frac{\ln\left(\frac{Wo}{Wx}\right)}{\ln\left(\frac{lxWx}{loWo}\right)} \qquad \ldots\ldots\ldots\ldots\ldots (2)$$

where lo and lx are, respectively, initial and final gauge length.

If a phase change during deformation produces a fractional volume expansion ΔV, equation (2) will give only an apparent value of the strain ratio, the real value being given by equation (1) or by

$$R(\text{real}) = \frac{\ln\left(\frac{Wo}{Wx}\right)}{\ln\left\{\frac{lxWx}{(1+\Delta V)loWo}\right\}} \qquad \ldots\ldots\ldots\ldots\ldots (3)$$

The fractional error, E, in the measured strain ratio (R(apparent)) will be

$$E = \frac{R(\text{real}) - R(\text{apparent})}{R(\text{apparent})}$$

$$= \frac{\ln\,(1 + \Delta V)}{\ln\left(\frac{to}{tx}\right)} \qquad \ldots\ldots\ldots\ldots\ldots\ldots (4)$$

Hence E is a function of the volume expansion, i.e. the amount of martensite present, and of the amount of deformation, $(\frac{to}{tx})$

However, the amount of martensite itself depends on the amount of deformation. This can be taken into account by assuming that ΔV is a linear function of the true strain i.e.

$$\Delta V = k.\ln(\frac{to}{tx}) + C \quad \ldots\ldots\ldots\ldots\ldots (5)$$

where k and C are constants.

More generally, transformation will not occur until a critical value of strain, $(\frac{to}{tc})$, is reached

i.e. $\Delta V = 0$, when $(\frac{to}{tx}) = (\frac{to}{tc})$

$\therefore$ $0 = k.\ln(\frac{to}{tc}) + C$

i.e. $C = -k.\ln(\frac{to}{tc})$

$\therefore$ $\Delta V = k.\ln(\frac{to}{tx}) - k.\ln(\frac{to}{tc})$ ..... (6)

$= k.\ln(\frac{tc}{tx})$ ..... (7)

Equations (4) and (6) give

$$E = \frac{\ln\{1 + k.\ln(\frac{tc}{tx})\}}{\ln(\frac{to}{tx})} \quad \ldots\ldots\ldots\ldots (8)$$

The only limitation of this analysis is the assumption made in equation (5) which is considered acceptable since two important deductions can be made from the analysis, both of which agree with practical expectations:-

(a) from equation (4), $E = 0$ when $\Delta V = 0$

(b) from equation (8), $E = 0$ when $tc = tx$

At any strain the maximum amount of martensite which could be formed, and hence the maximum error in R would occur when $tc = to$ Under these conditions

$$\Delta V = k.\ln\left(\frac{to}{tx}\right) \quad \ldots\ldots\ldots\ldots \quad (9)$$

and $$E = \frac{k.\ln(1 + \Delta V)}{\Delta V} \quad \ldots\ldots\ldots \quad (10)$$

$$= k, \text{ since } \Delta V \text{ is small}$$

i.e. E would be constant and invariant of strain.

More generally, when $tc < to$, equation (8) can be rewritten as

$$E = \frac{k.\ln\left(\frac{tc}{tx}\right)}{\ln\left(\frac{to}{tx}\right)} \quad \ldots\ldots\ldots\ldots \quad (11)$$

$$= k\left\{1 - \frac{K}{\ln\left(\frac{to}{tx}\right)}\right\} \quad \ldots\ldots\ldots \quad (12)$$

where $K = \ln\left(\frac{to}{tc}\right) = \text{constant}$

i.e. E increases as $\left(\frac{to}{tx}\right)$ increases.

The highest uniform elongation at which R was measured in the 18/10 steel was 50%, and since the R values were close to 1, the corresponding value of $(\frac{to}{tx})$ would be $\triangleq 1.25$. Also, at this elongation, 50% martensite was present, which would correspond to a volume increase of 1.05% (i.e. $\Delta V = 0.0105$). Hence the maximum error in the strain ratio measurements as a result of the $\gamma \rightarrow \alpha'$ transformation

$$\triangleq \frac{\ln (1.0105)}{\ln (1.25)} = .047$$

i.e. 4.7%

ACKNOWLEDGEMENTS

The author wishes to thank Mr. D. Green, The University of Aston in Birmingham, and Drs. W.I. Mitchell and D.J. Burr, International Nickel Limited, for their encouragement and helpful suggestions during the course of this work.

Permission given by International Nickel Limited, to attend lectures at the University of Aston in Birmingham and to submit this work for a higher degree, is gratefully acknowledged.

REFERENCES

1. R. Hill — "Mathematical Theory of Plasticity" Oxford University Press, London (1950) 315.
2. R. Hill — Proc. Roy. Soc. A 193 (1948) 281
3. W.F. Hosford and W.A. Backofen — Proc. 9th Sagamore Army Materials Research Conference Syracuse University Press (Aug. 1962) 257.
4. R.L. Whitely — Trans. A.S.M. 52 (1960) 154.
5. L.W. Hu — J. Appl. Mechanics 23 (1956) 444.
6. J. Willis — "Deep Drawing". Butterworth Publications Limited, London (1954) 28.
7. D.H. Lloyd — Sheet Metal Ind. 39 (1962) 82.
8. L. Lilet and M.Wybo — Sheet Metal Ind. 41 (1964) 783.
9. L. Lilet — Sheet Metal Ind. 43 (1966) 949.
10. J.C. Wright — Sheet Metal Ind. 39 (1962) 887.
11. M. Atkinson and I.M.Maclean — I.D.D.R.G. Colloquium London (1964).
12. D.V. Wilson B.J. Sunter and D.W. Martin — Sheet Metal Ind. 43 (1966) 465.
13. S.P. Keeler and W.A.Backofen — Trans. A.S.M. 56(1963) 25.
14. G.G. Moore and J.F. Wallace — J. Inst. Metals 93 (1964) 33.
15. H.W. Swift — J. Mech. Phys. Solids 1 (1952) 1.
16. P.B. Mellor — J. Inst. Metals Discussion 93 (1965) 486.
17. J.F. Wallace — J. Inst. Metals Discussion 93 (1965) 486.
18. R. Pearce — J. Inst. Metals Discussion 93 (1965) 486.

19.	S.P. Keeler and W.A. Backofen	Trans. A.S.M. Discussion 52(1960) 166.
20.	H.W.Swift and S.Y. Chung	Proc. Inst. Mech. Eng. 165 (1951) 199.
21.		A.S.T.M. Special Technical Publication No. 390 (September 1965).
22.	R.E. Smallman	"Modern Physical Metallurgy" Butterworths, London (1963).
23.	P. Wacquez	J. Inst. Metals Discussion 93(1965) 486.
24.	W.T. Lankford, S.C. Snyder and J.A. Bauscher	Trans. A.S.M. 49 (1950) 1197.
25.	R.T. Derricott and J.C. Wright	Sheet Metal Ind. 43 (1966) 845.
26.	I.L. Dillamore and W.T. Roberts	Met. Reviews 10(1965) 271.
27.	Y.C. Liu and R.H. Richman	Trans. Met. Soc. A.I.M.E. 218 (1960) 688.
28.	R.H. Richman and Y.C. Liu	Trans. Met. Soc. A.I.M.E. 221(1961) 720.
29.	R.E. Smallman	J. Inst. Metals 84 (1955-56)10.
30.	A. Merlini and P.A. Beck	Trans. Amer. Min. Met. Eng. 203 (1955) 395.
31.	M. Hatherley	J. Aust. Inst. Metals 8(1963) 140.
32.	F. Haessner	Z. Metallkunde 53 (1962) 403.
33.	H. Hu and R.S. Cline	J. Appl. Physics 32 (1961) 760.
34.	H. Hu R.S. Cline and S.R. Goodman	J. Appl. Physics 32 (1961) 1392.

35. H. Hu and S.R. Goodman — Trans. Met. Soc A.I.M.E. 227 (1963) 1454

36. S.R. Goodman and H. Hu — Trans. Met. Soc. A.I.M.E. 230(1964) 1413.

37. S.R. Goodman and H. Hu — Trans. Met. Soc. A.I.M.E. 233 (1965) 103.

38. H. Mueller — Österr Akad. Wiss. Math-Naturw 7(1958) 117.

39. H. Hu and S.R. Goodman — Trans. Met. Soc. A.I.M.E. 227 (1963) 627.

40. R.E. Smallman and D. Green — Acta Met. 12 (1964) 145.

41. F. Haessner — Zeit. Metallkunde 53 (1962) 403.

42. G. Wassermann — Zeit. Metallkunde 54 (1963) 61.

43. F. Haessner — Zeit. Metallkunde 54 (1963) 98.

44. I.L. Dillamore and W.T.Roberts — Acta Met. 12 (1964) 281.

45. P.R. Thornton and T.E.Mitchell — Phil. Mag. 7(1962) 371.

46. E.A. Calnan — J. Inst. Metals 84 (1955-56) 503.

47. T.Ll.Richards and S.F.Pugh — J. Inst. Metals 88(1959-60) 399.

48. E.Butler and D. Green — University of Aston in Birmingham (1966) To be published.

49. M. Cook and T.Ll.Richards — J. Inst. Metals 66(1940) 1.

50. W.M. Baldwin — Trans. A.I.M.E. 166(1946) 591.

51. E. Schmid and H. Thomas — Zeit. Physik 130 (1951) 293.

52. T.Ll. Richards and S.F. Pugh — J. Inst. Metals 88(1959-60) 399.

53. P. Beck and H. Hu — J. Inst. Metals 4(1952) 83.

54. K. Detert, P. Dorsch, H. Migge — Zeit. Metallkunde 54(1963) 263.

55. W.E. Seymour and D. Harker — Trans. A.I.M.M.E. 188(1950) 1001.

56. H. Hu, R.S.Cline and S.R.Goodman — Trans. Met. Soc. A.I.M.E. 224 (1962) 96.

57. A. Merlini and P.A. Beck — Trans. AIM.M.E. 203 (1955) 395.

58. I.L. Dillamore — Acta Met. 12 (1964) 1005.

59. W.G. Burgers and P.C. Louwerse — Zeit. Physik 67 (1931) 607.

60. F. Haessner, U. Jakubowski and M. Wilkens — Physika Status Solidi. 7 (1964) 701.

61. C.S. Barrett — Trans. A.I.M.E. 137 (1950) 128.

62. P.A. Beck — Trans. A.I.M.E. 191 (1951) 475.

63. J.E. Burke — J. Metals 4 (1952) 263.

64. P.A. Beck — Advances in Physics 3 (1954) 245.

65. C.G. Dunn — Acta Met. 1 (1953) 163.

66. J.E. Burke — Trans. A.I.M.M.E. 194 (1952) 263.

67. W. Bunk and P. Esslinger — Z. Metallkunde 50 (1959) 278.

68. J.C. Blade — J. Inst. Metals 90 (1961-2) 374.

69. T. Amitani — Nippon Kinzoku Gakkai-Si 24 (1960) 765.

70. F. Haessner, G. Masing and H.P. Stuwe — Z. Metallkunke 47 (1956) 743.

71. I. Gokyu, H. Abe and N. Veyama — Nippon Kinzoku Gakkai-Si 29(1965) 515.

72. P.B. Mee and R.A. Sinclair — J. Inst. Metals 94(1966) 319.

73. L. Lilet and M. Wybo — Sheet Metal Industries 41 (1964) 783.

74. D.V. Wilson and R.D. Butler — J. Inst. Metals 90 (1961-2) 473.

75. G. Jegaden, J. Voinchet and P. Rocquet — Mem. Sci. Rev. Metall. 59(1952) 273.

76. K. Randerson — M.Sc. Thesis University of Birmingham (1963).

77. W.T. Lankford, S.C. Snyder and J.A. Bauscher — Trans. A.S.M. 42 (1951) 1197.

78. R.L. Whitely — I.D.D.R.G. Colloquium (1962).

79. C. Crussard, R. Porney, D. Lajeunesse and M. Angeli — Rev. Metal. 58 (1961) 183.

80. M.J. Dickson — B.Sc. Thesis University of Aston in Birmingham (1965).

81. M.J. Dickson — To be published

82. R.S. Burns and R.H. Heyer — Proc. Int. Symp. on Annealing of Low Carbon Steel Cleveland (1957).

83. R.L. Whitely and D.E.Wise — Flat Rolled Products III.Interscience Publishers-NY (1962) 47.

84. L. Bourne and R.Hill — Phil. Mag. 41(1950) 671.

85. R.S. Burns and R.H.Heyer — Sheet Metal Industries 35(1958) 261.

86. J.A. Elias, R.H. Heyer and J.A.Smith — Trans. Met. Soc. A.I.M.E. 224(1962) 678.

87. R. Pearce and K.R. Natarajan — I.D.D.R.G. Colloquium London June 1964

88. R.W. Vieth and R.L. Whitely — I.D.D.R.G. Colloquium London June 1964.

89. G.I. Taylor — J. Inst. Metals 62(1938) 307.

90. J.F.W. Bishop and R. Hill — Phil. Mag. 42(1951) 414.

91. J.F.W. Bishop and R. Hill — Phil. Mag. 42(1951) 1298.

92. F.H. Wilson and R.M. Brick — Trans. A.I.M.E. 161(1945) 173.

93. M.K. Yen — Trans. A.I.M.E. 166(1949) 59.

94. R. Chevingny — Revue de l'Aluminium 153(1949) 79.

95. K.T. Aust and F.R. Morral — J. Metals 5(1953) 431.

96. I.M. Maclean — M.Sc. Thesis. University of Birmingham (1962).

97. G.E.G. Tucker — Acta Met. 9(1961) 275.

98. W.T. Roberts — Sheet Metal Industries 39 (1962) 855.

99. S.Y. Chung and H.W. Swift — Proc. Inst. Mech. Engrs. 165(1951) 199.

100. W.M. Baldwin, T.S. Howald and A.W.Ross — Trans. Met. Soc. A.I.M.E. 166(1946)86.

101. J.A. Zaat — Sheet Metal Industries 34 (1957) 737.

102.	J.M. Summerton	International Nickel Limited, Private Communication.
103.		Texture Goniometer, Siemens und Halske, Aktiengesellschaft, Wernerwek fur Messtechnick.
104.	C.S. Barrett	"The Structure of Metals" McGraw-Hill, New York (1952).
105.	J. Bennewitz	Arch. Eisenhuttenwesen 33(1962) 392.
106.	P.R. Swann	Corrosion 19 (1963) 102.
107.	D.L. Douglass et al	2nd International Conference on Corrosion. New York (1963).
108.	D. Dulieu and J. Nutting	J. Iron and Steel Inst. Special Report No. 86 (1964) 140.

TABLE 1

COMPOSITIONS OF STEELS (Wt.%)

Nominal		Analysed											
Cr	Ni	Cr	Ni	C	Co	Mo	Al	Si	Mn	Cu	Nb	N	Fe
18	10	18.2	10.0	.026	<.05	<.01	.04	<.2	<.1	<.1	<.01	.012	bal
18	12	18.0	11.9	.032	<.1	<.1	.065	<.2	<.2	<.1	<.1	.010	bal
18	14	18.3	14.0	.017	<.05	<.01	.06	<.2	<.1	<.1	<.01	.011	bal

TABLE 2

GRAIN SIZES OF SHEETS USED FOR PRESS FORMING TESTS

Steel	Treatment	Nature of grain orientation	Average grain diameter, mm
18/10	Cold rolled to 93% reduction + ½h at 800°C (temper anneal)	preferred	<.01
	" " " " " + ½h at 900°C (temper anneal)	"	.02
	" " " " " + 1h at 1000°C (full anneal)	"	.033
	30% cold reductions with intermediate and final annealing for ½h at 1050°C (full anneal)	random	.055
18/12	Cold rolled to 93% reduction + ½h at 800°C (temper anneal)	preferred	<.01
	" " " " " + ½h at 900°C (temper anneal)	"	.014
	" " " " " + 1h at 1000°C (full anneal)	"	.02
	30% cold reductions with intermediate and final annealing for ½h at 1050°C (full anneal)	random	.028
18/14	Cold rolled to 93% reduction + ½h at 800°C (temper anneal)	preferred	.01
	" " " " " + ½h at 900°C (temper anneal)	"	.02
	" " " " " + 1h at 1000°C (full anneal)	"	.036
	30% cold reductions with intermediate and final annealing for ½h at 1050°C (full anneal)	random	.045

TABLE 3(a)

EFFECT OF PLASTIC STRAIN ON R VALUES FOR THE 18% CHROMIUM 10% NICKEL STEEL

Condition	R_0°	R_{45}°	R_{90}°
Random	constant	slight decrease	constant
Random + 5% CR	slight increase	constant	<20% decreases >20% constant
Random + 10% CR	constant	slight increase	slight decrease
Random + 15% CR	constant	<10% decreases >10% constant	constant
93% CR+½h at 800°C AC	constant	constant	constant
93% CR+½h at 900°C AC	constant	constant	constant
93% CR+1h at 1000°C AC	constant	<20% constant >20%<25% decreases >25% constant	<25% constant >25% decreases

TABLE 3(b)

EFFECT OF PLASTIC STRAIN ON R VALUES FOR THE 18% CHROMIUM 12% NICKEL STEEL

Condition	R_0°	R_{45}°	R_{90}°
Random	constant	constant	constant
Random + 5% CR	<25% increases >25% constant	constant	constant
Random + 10% CR	<20% increases >20% constant	<20% decreases >20% constant	<20% decreases >20% constant
Random + 15% Cr	slight increase	constant	constant
93% CR+½h at 800°C AC	constant	constant	constant
93% CR+½h at 900°C AC	constant	constant	constant
93% CR+1h at 1000°C AC	constant	constant	constant

TABLE 3(c)

EFFECT OF PLASTIC STRAIN ON R VALUES FOR THE 18% CHROMIUM 14% NICKEL STEEL

Condition	R_{0°	R_{45°	R_{90°
Random	constant	constant	constant
Random + 5% CR	<20% increases >20% constant	constant	constant
Random + 10% Cr	constant	slight increase	slight decrease
Random + 15% CR	marked increase	constant	constant
93% CR+½h at 800°C AC	constant	<20% decreases >20% constant	constant
93% CR+½h at 900°C AC	constant	constant	constant
93% CR +1h at 1000°C AC	<15% increases >15% constant	constant	constant

TABLE 4

EFFECT OF THE RATE OF WORK HARDENING ON DEEP DRAWABILITY OF 18/10, 18/12 AND 18/14 CHROMIUM/NICKEL STEELS

Steel	Work hardening index, n	Predicted $D_{(max)}$ from Figure 9 using d = 33 mm	Measured critical blank diameter
18/10	0.75	83.8 mm	71 mm
18/12) 18/14)	0.54	80.5 mm	72 mm

TABLE 5

EFFECT OF ANISOTROPY ON DEEP DRAWABILITY OF 18/10,18/12 AND 18/14 CHROMIUM/NICKEL STEELS

Steel	Condition	$\bar{R}$	Predicted $D_{(max)}$ from equation (15) using η = .25 and d = 33mm	Measured critical blank diameter
18/10	Random	0.94	72.5 mm	71 mm
	93% CR + 1h 1000°C AC	1.06	74.3 mm	72 mm
18/12	Random	0.92	72.3 mm	72 mm
	93% CR + 1h 1000°C AC	1.02	73.9 mm	72 mm
18/14	Random	0.94	72.5 mm	72 mm
	93% CR + 1h 1000°C AC	0.96	73.2 mm	72 mm

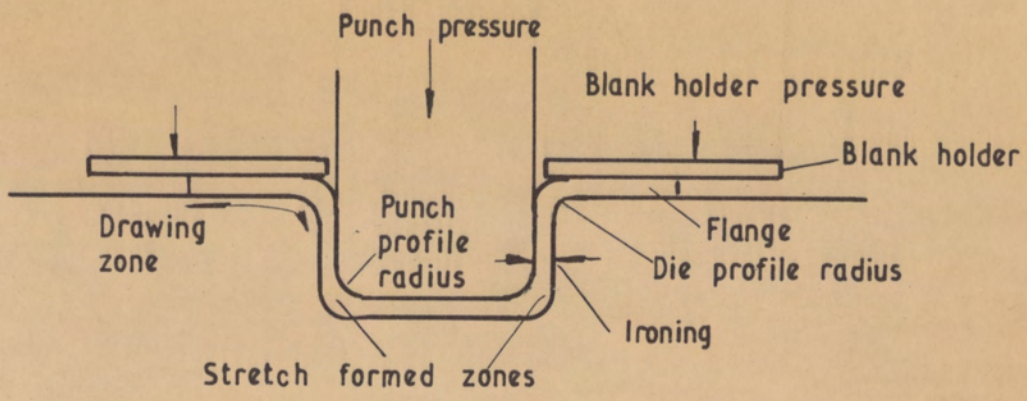

Figure 1(a) Diagrammatic representation of simple cup drawing.

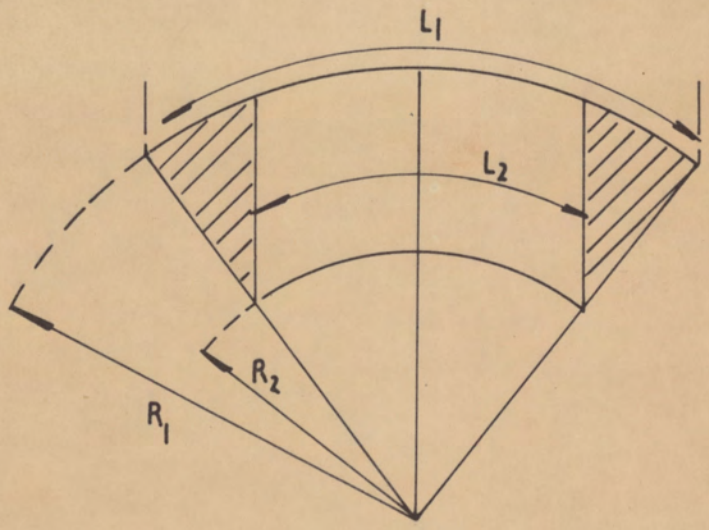

Figure 1(b) Sector from a round blank prior to drawing.

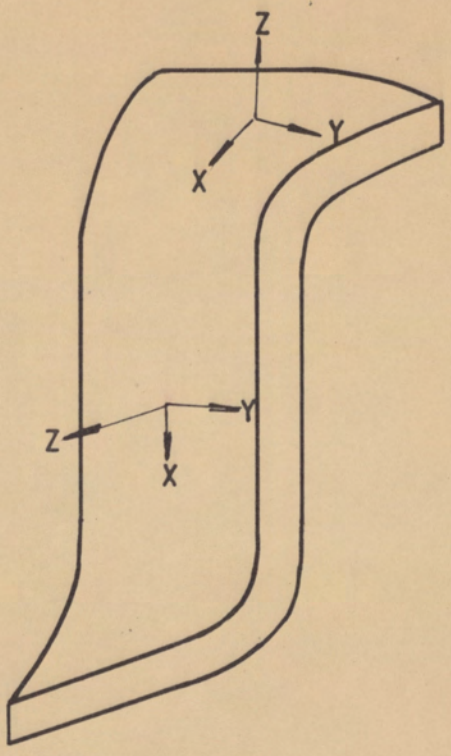

Figure 1(c) Directions of principal stresses in a partly drawn cup.

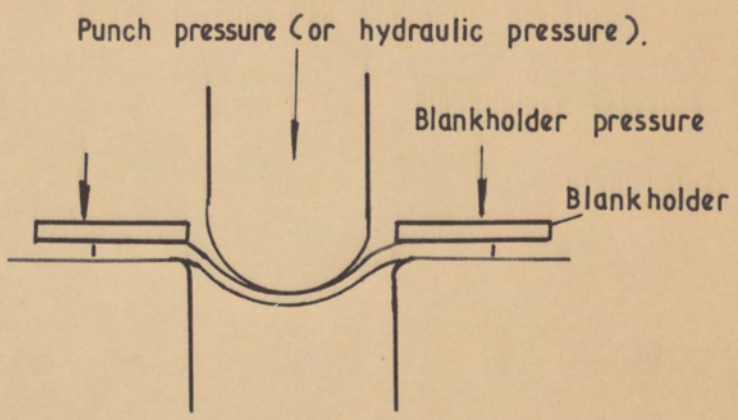

Figure 2 Diagrammatic representation of simple cup stretching.

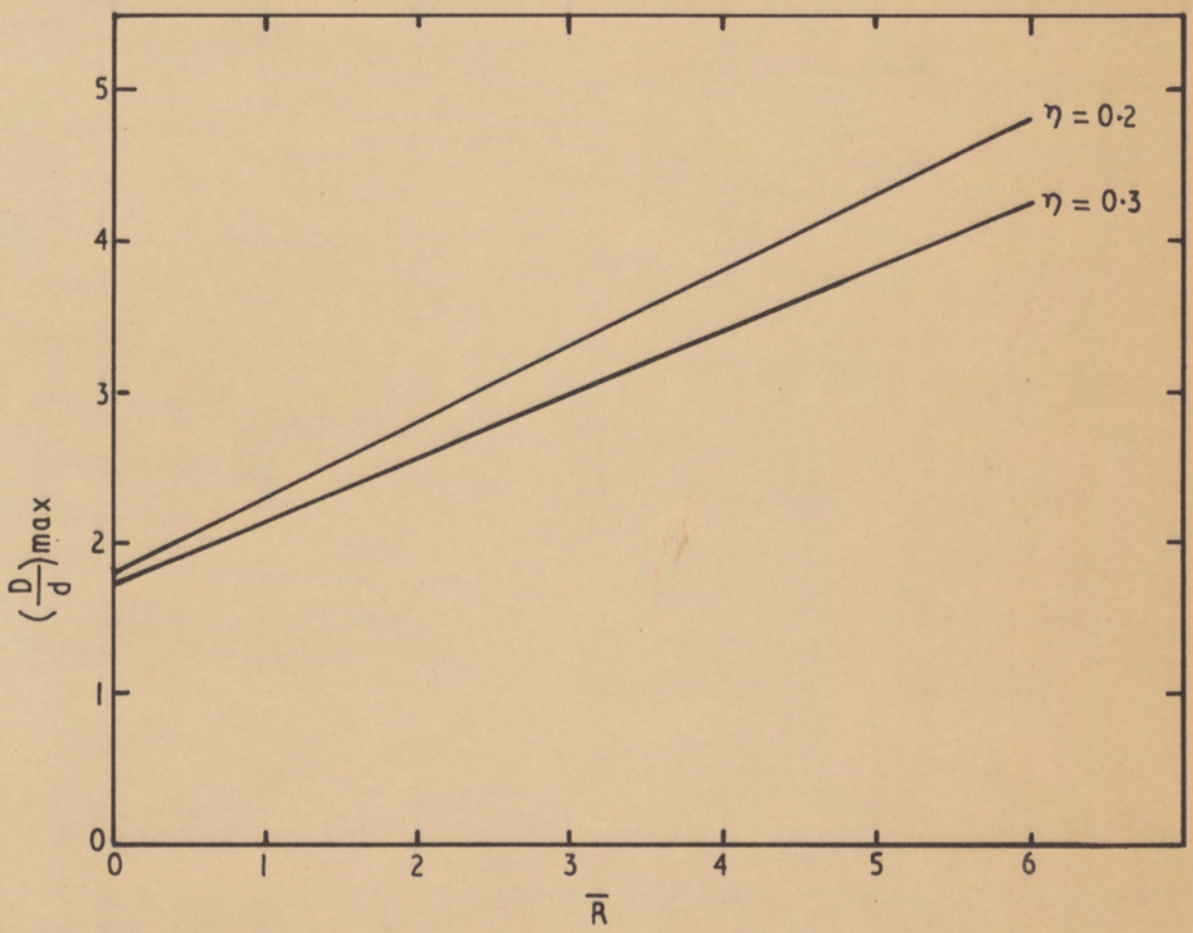

Figure 3 Relationship between $(\frac{D}{d})_{max}$ and $\overline{R}$, from equation (15).

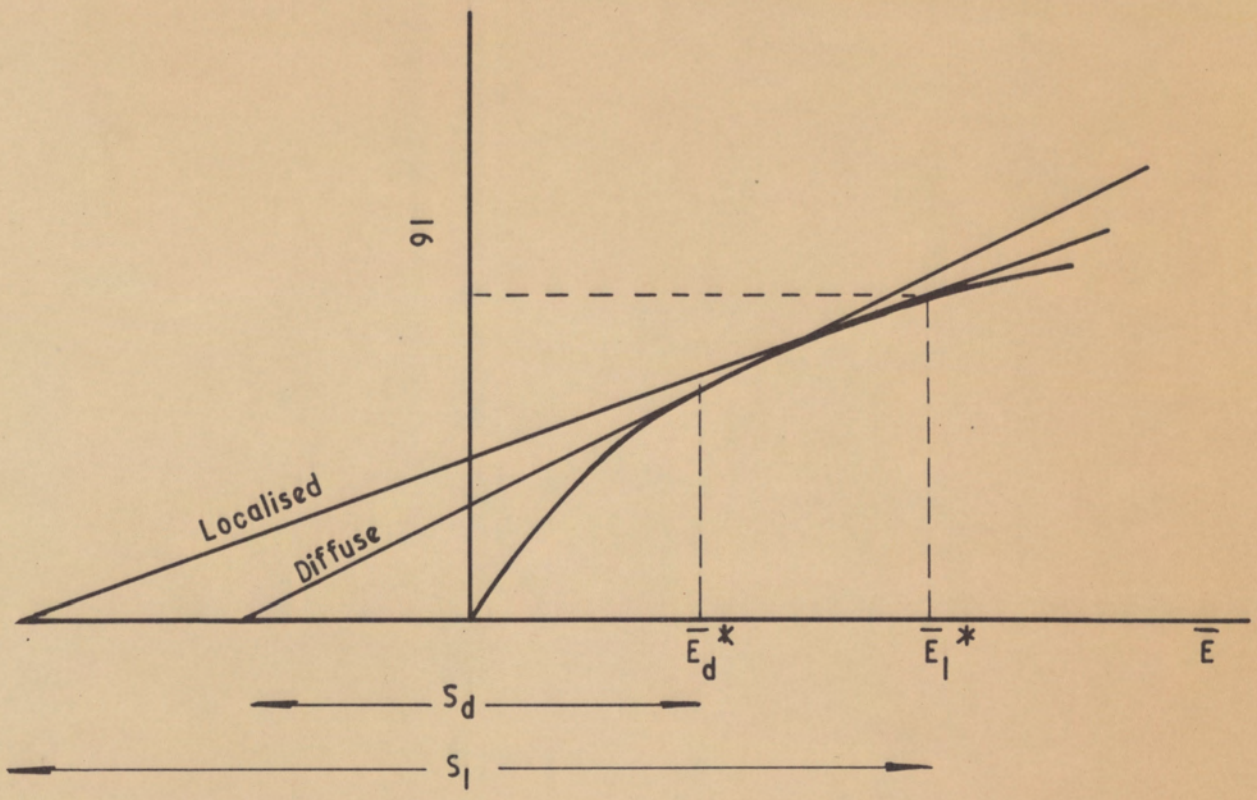

Figure 4 Graphical solution of equation (16). After Keeler and Backofen (13).

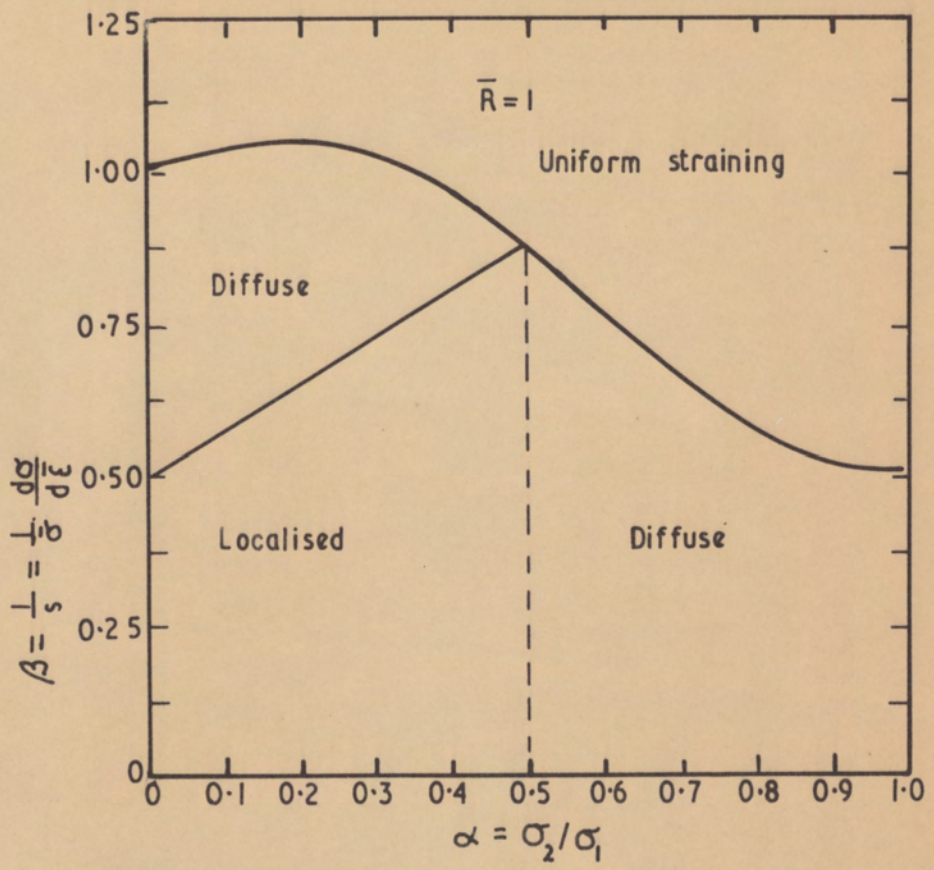

Figure 5 Conditions for the onset of diffuse and localised necking in an isotropic material under plane stress loading. After Keeler and Backofen (13).

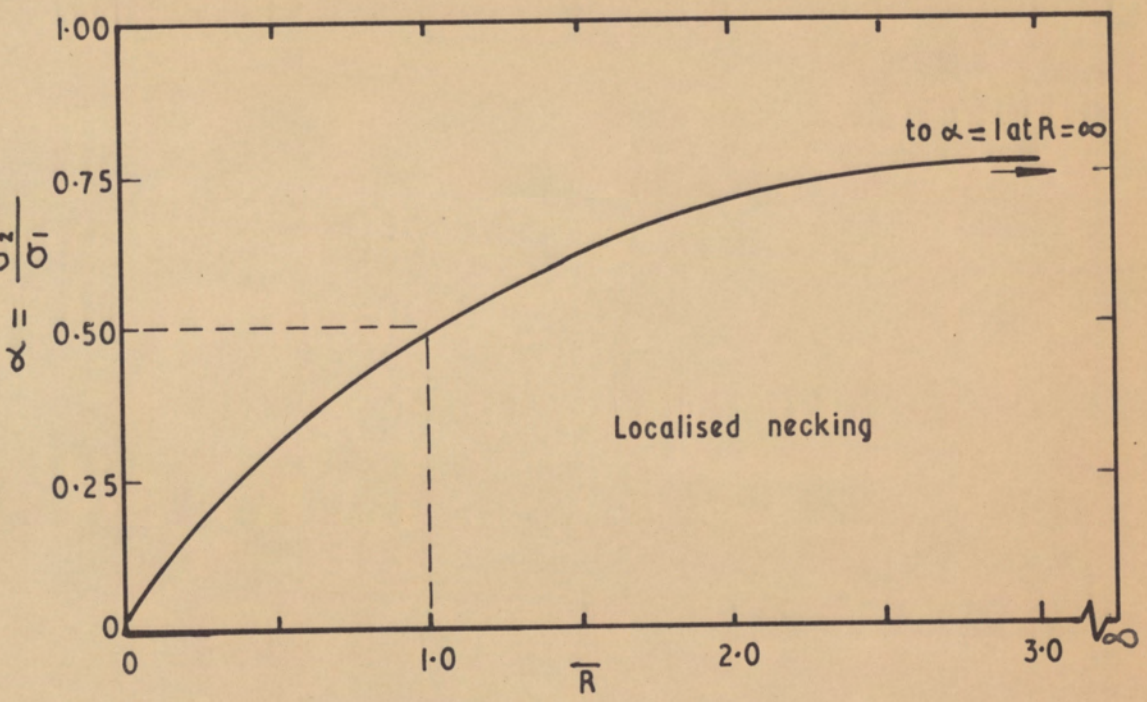

Figure 6. Effect of $\bar{R}$ on the limiting stress ratio after which localised necking cannot occur. After Keeler and Backofen. (13).

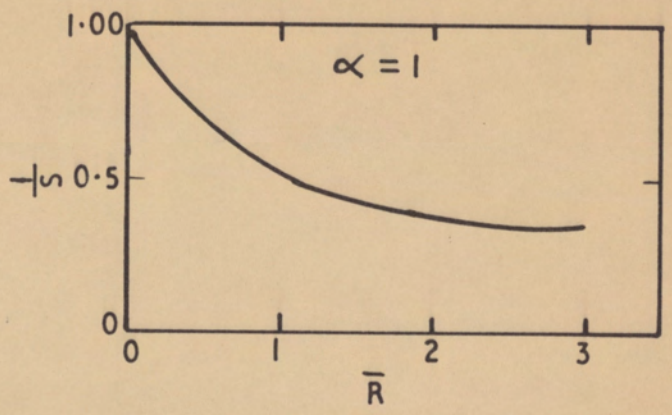

Figure 7 Effect of $\bar{R}$ on $\frac{1}{S}$. After Keeler and Backofen (13).

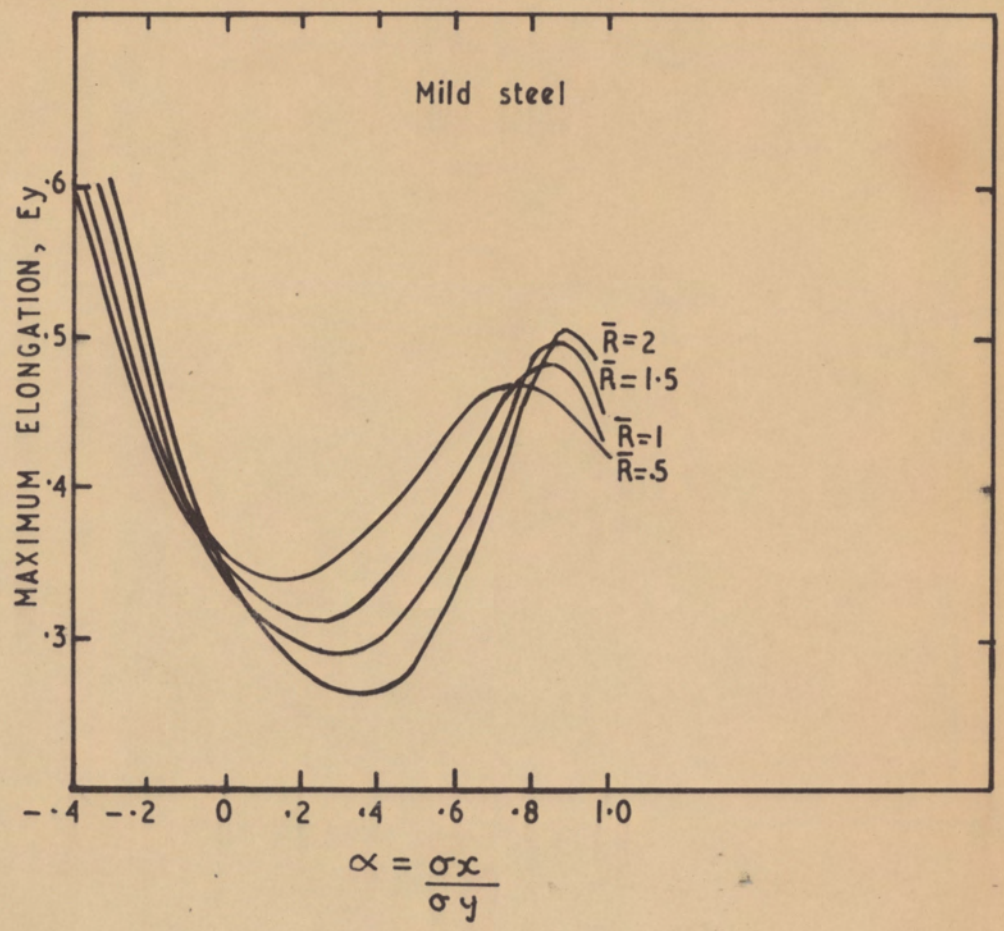

Figure 8. Variation of critical strain with α for different values of $\bar{R}$. After Moore and Wallace.

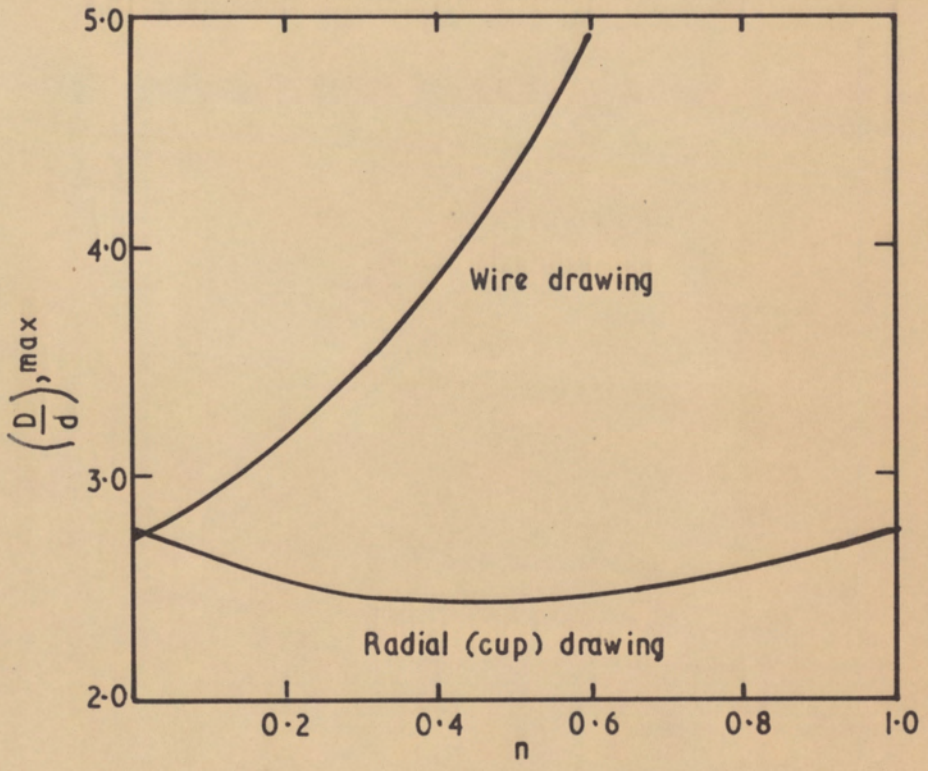

Figure 9 Effect of work hardening on $\left(\frac{D}{d}\right)$ max.

After Keeler and Backofen (19).

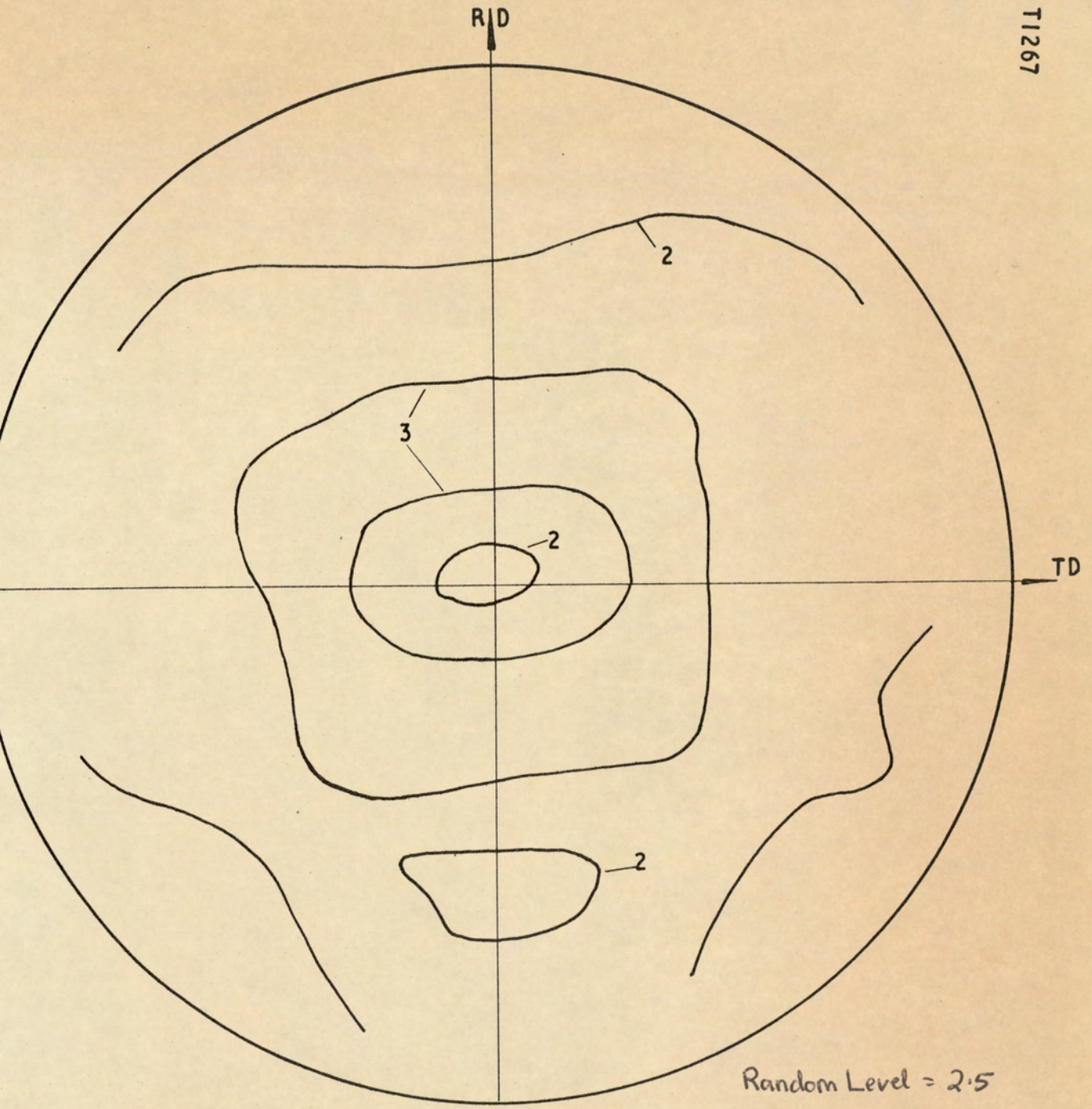

T1267

Figure 10 $\{111\}_{\gamma}$ pole figure of 18% Cr-10% Ni steel rolled from ~ 5/8 in to ·036 in using 30% cold reductions with intermediate and final annealing for 1/2 h at 1050°C A.C.

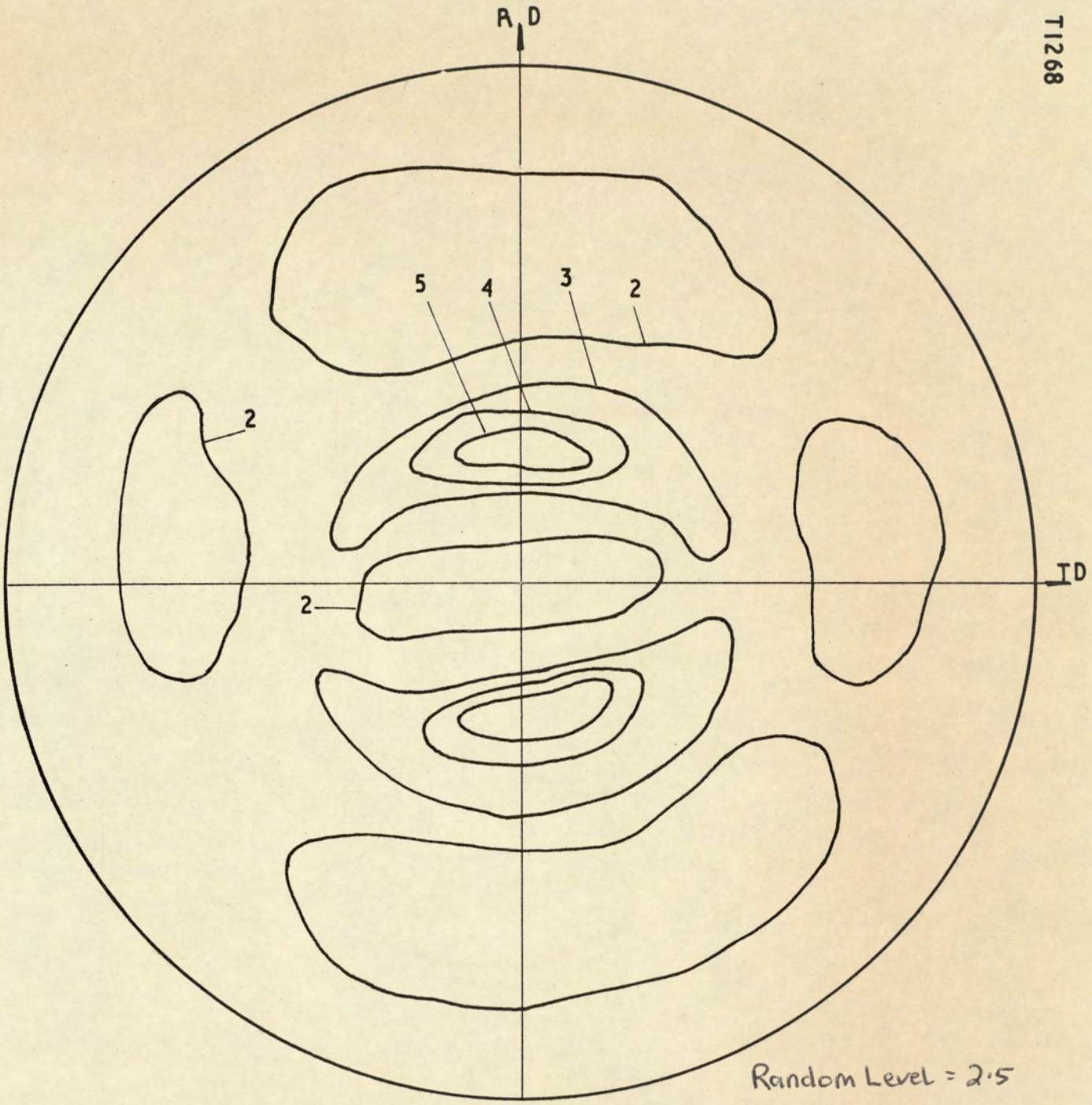

Figure 11 $\{111\}_\gamma$ pole figure of 18% Cr - 10% Ni steel rolled from ~ 5/8 in to ·036 in using 30% cold reductions with intermediate and final annealing for ½ h at 1050° C. A.C. Final cold reduction 15%.

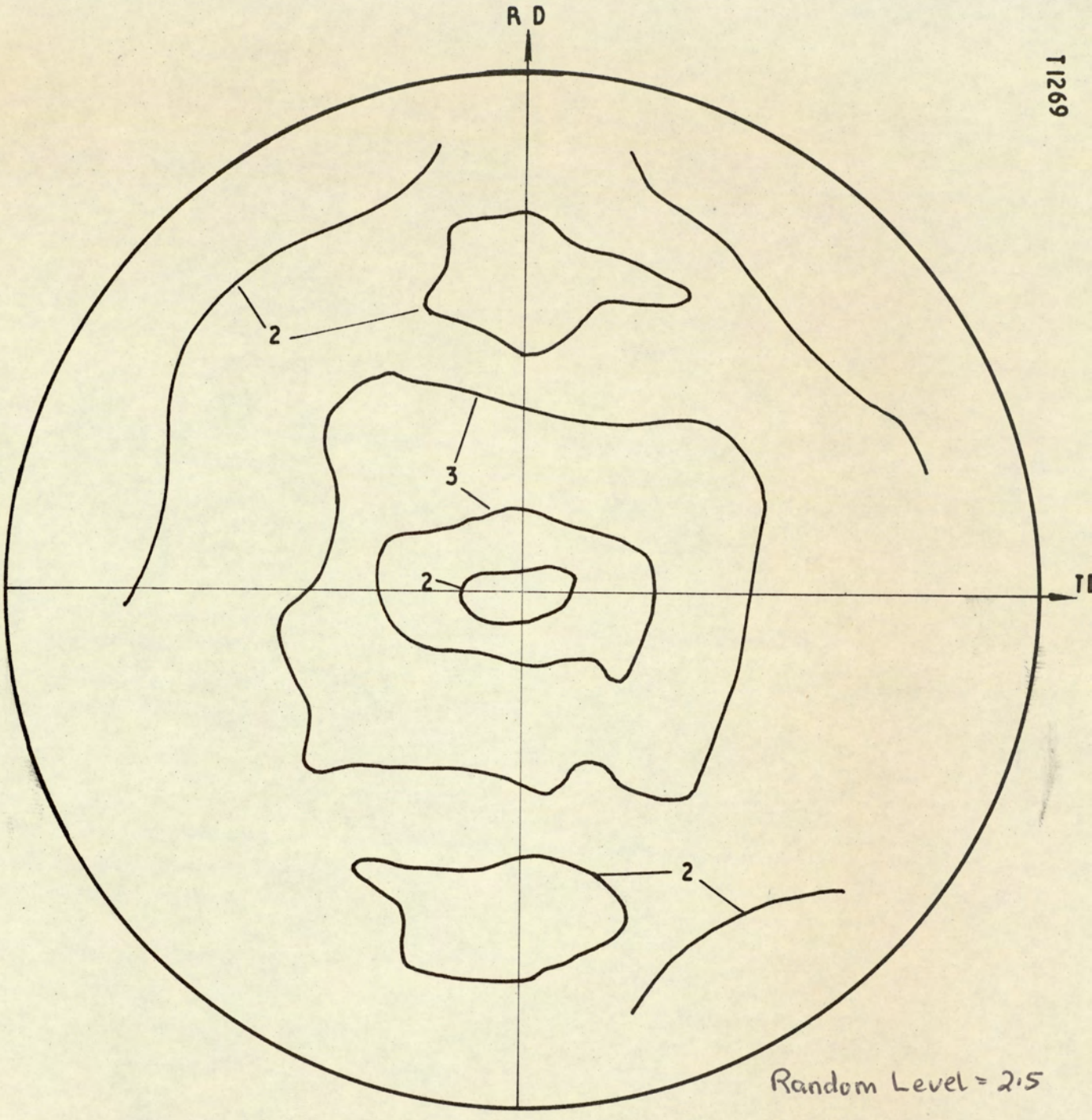

Figure 12 $\{111\}_\gamma$ pole figure of 18% Cr - 12% Ni steel rolled from ~ 5/8 in to ·036 in. using 30% cold reductions with intermediate and final annealing for 1/2 h at 1050°C A.C.

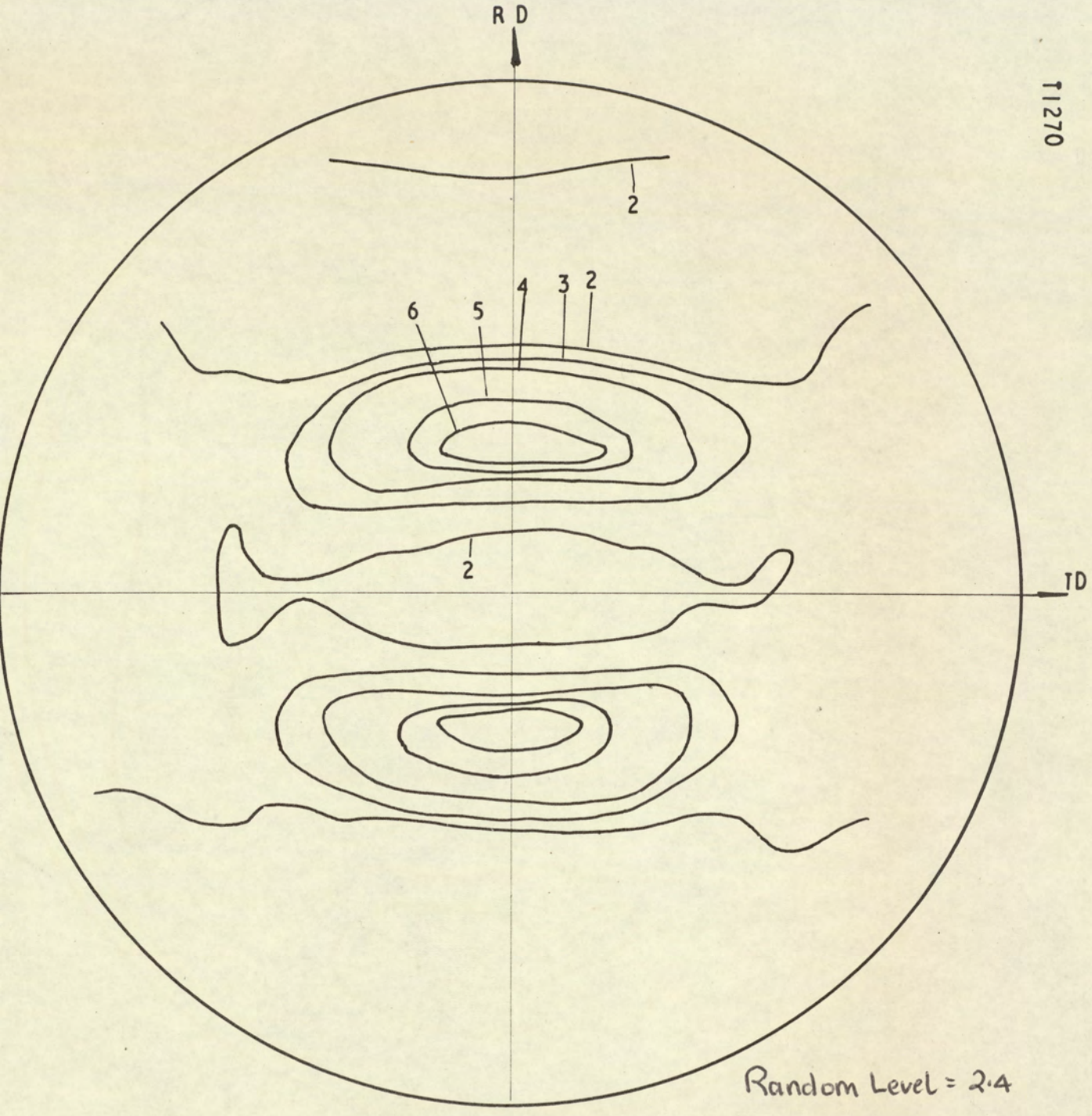

Figure 13 $\{111\}_\gamma$ pole figure of 18% Cr-12% Ni steel rolled from ~ 5/8 in to ·036 in. using 30% cold reductions with intermediate and final annealing for ½ h at 1050°C. A.C. Final cold reduction 15%.

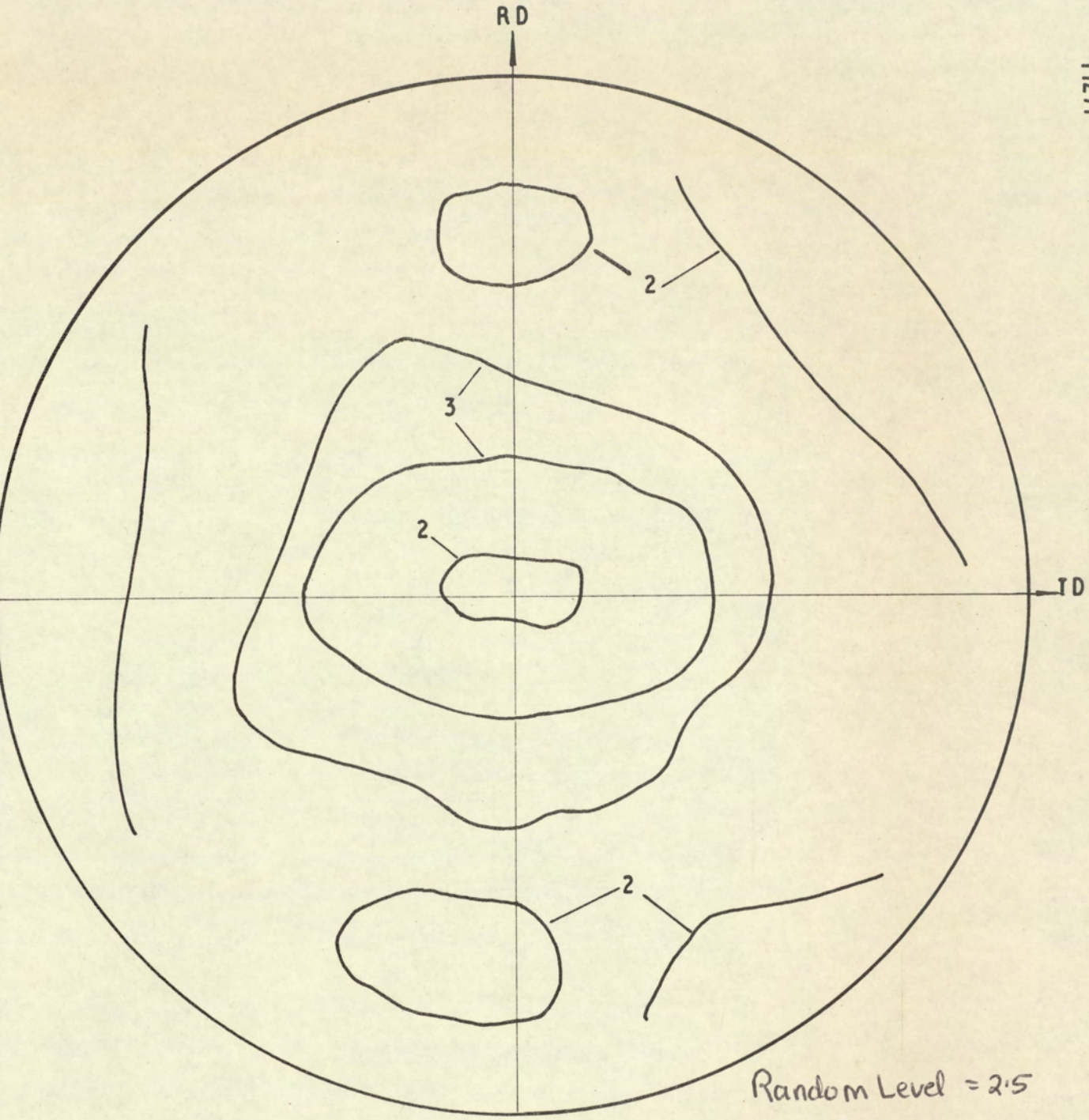

Figure 14 {111}γ pole figure of 18%Cr-14%Ni steel rolled from ~ 5/8 in to ·036 in using 30% cold reductions with intermediate and final annealing for ½ h at 1050°C. A.C.

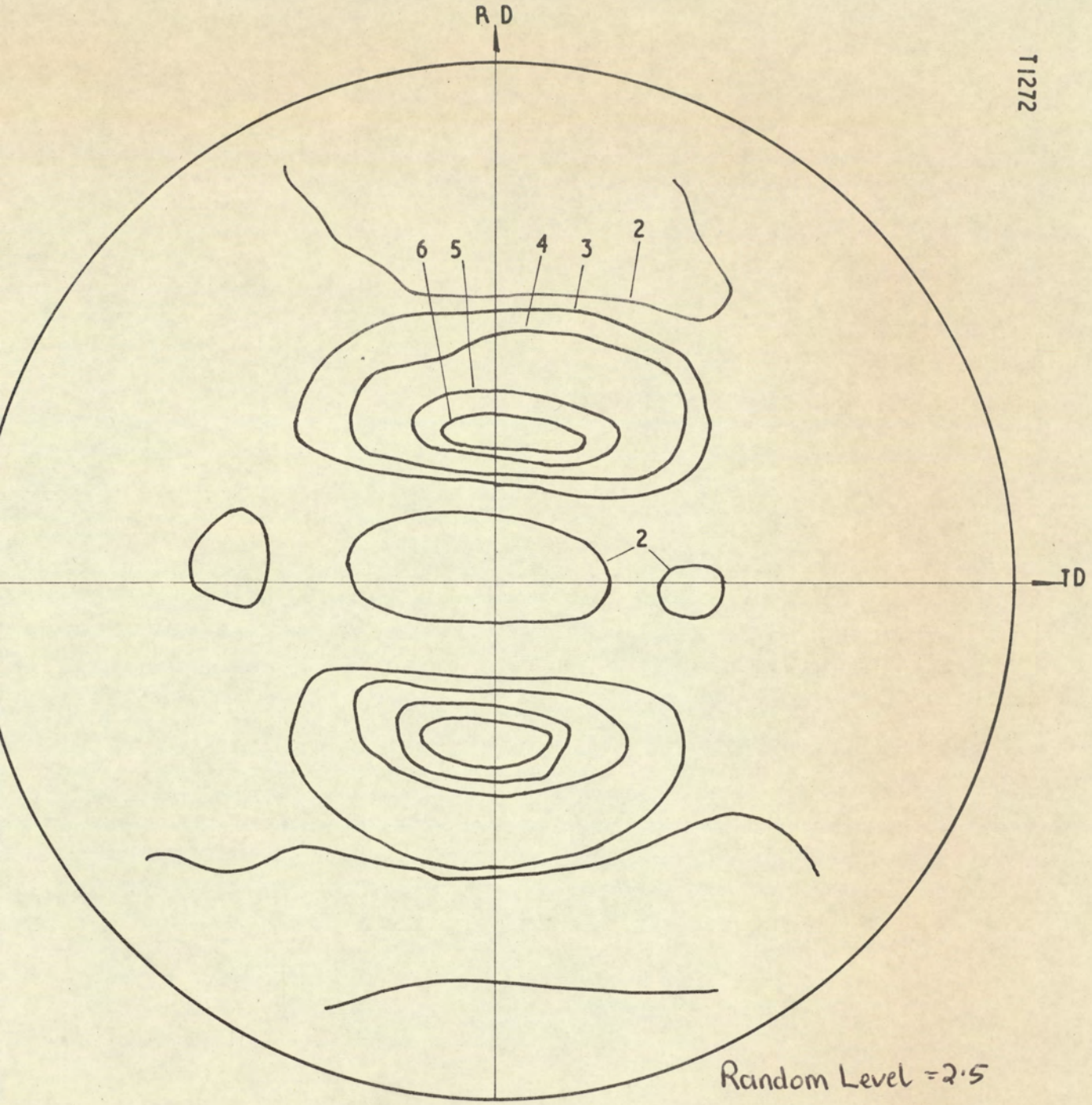

Figure 15 $\{111\}_\gamma$ pole figure of 18% Cr-14% Ni steel rolled from ~ 5/8 in to ·036 in. using 30% cold reductions with intermediate and final annealing for ½ h at 1050°C A.C. Final cold reduction 15%.

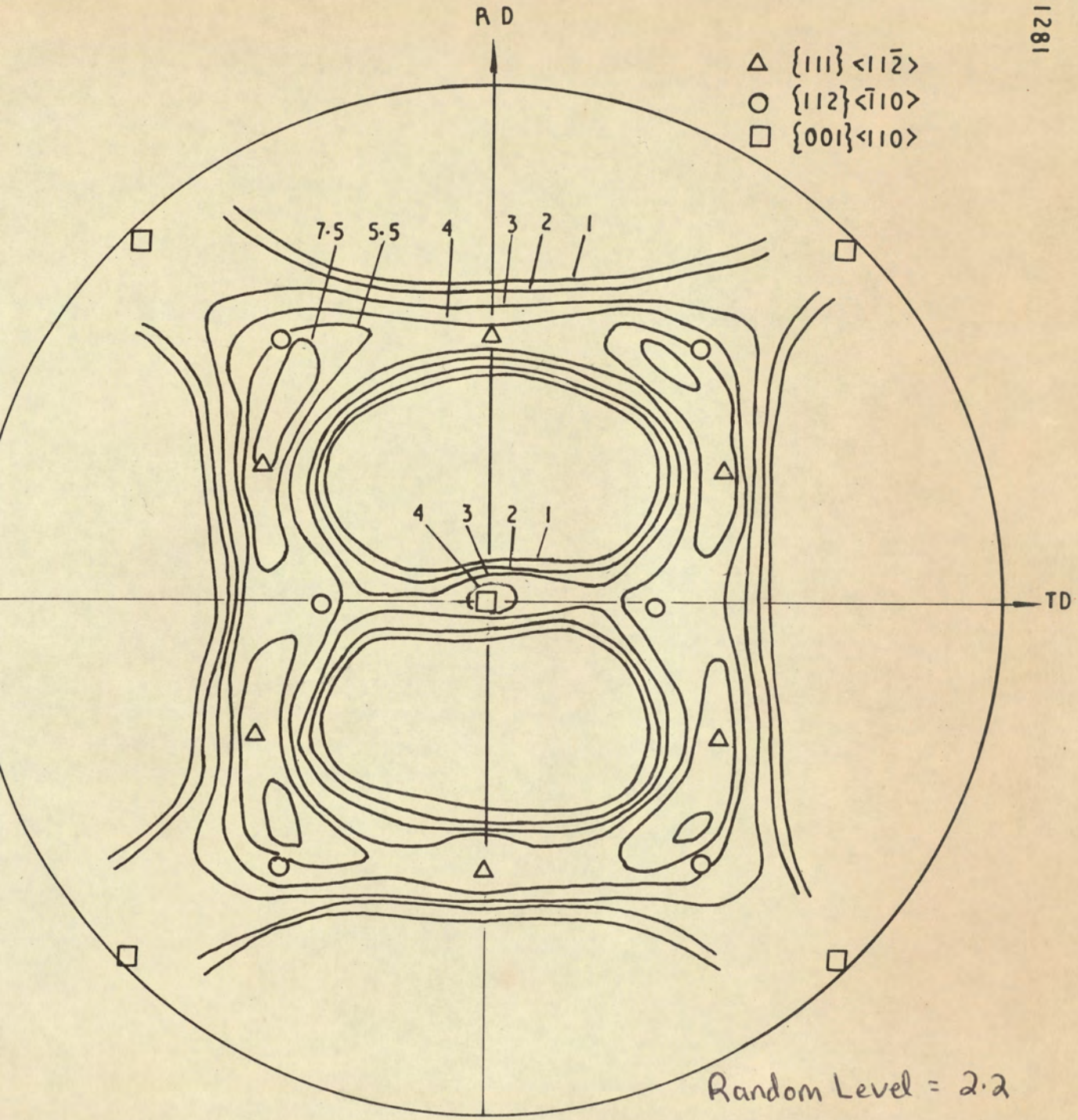

Figure 16 {200} α pole figure of 18% Cr – 10% Ni steel cold rolled to 93% reduction.

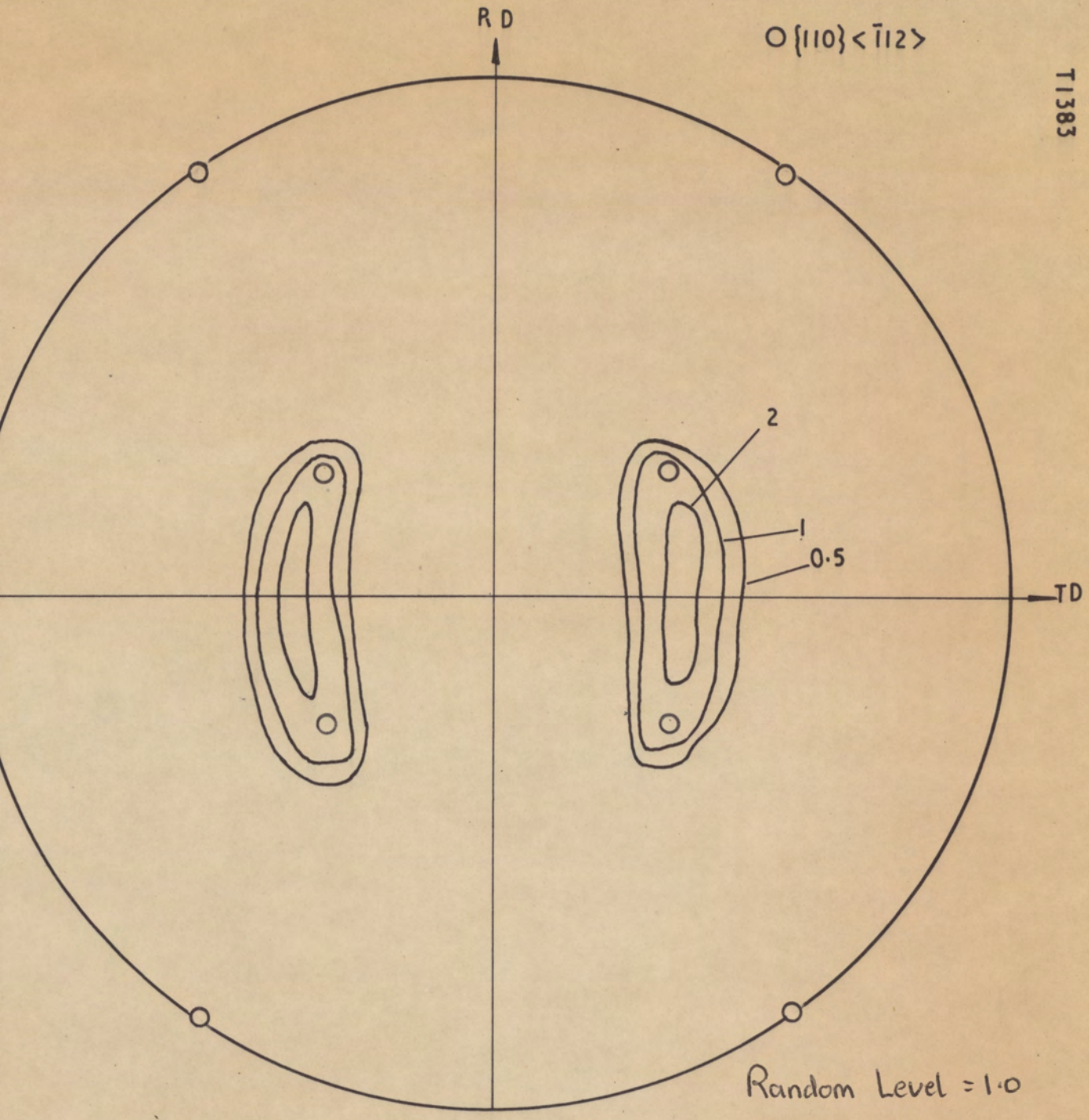

Figure 17 $\{200\}_\gamma$ pole figure of 18% Cr-10% Ni steel cold rolled to 93% reduction.

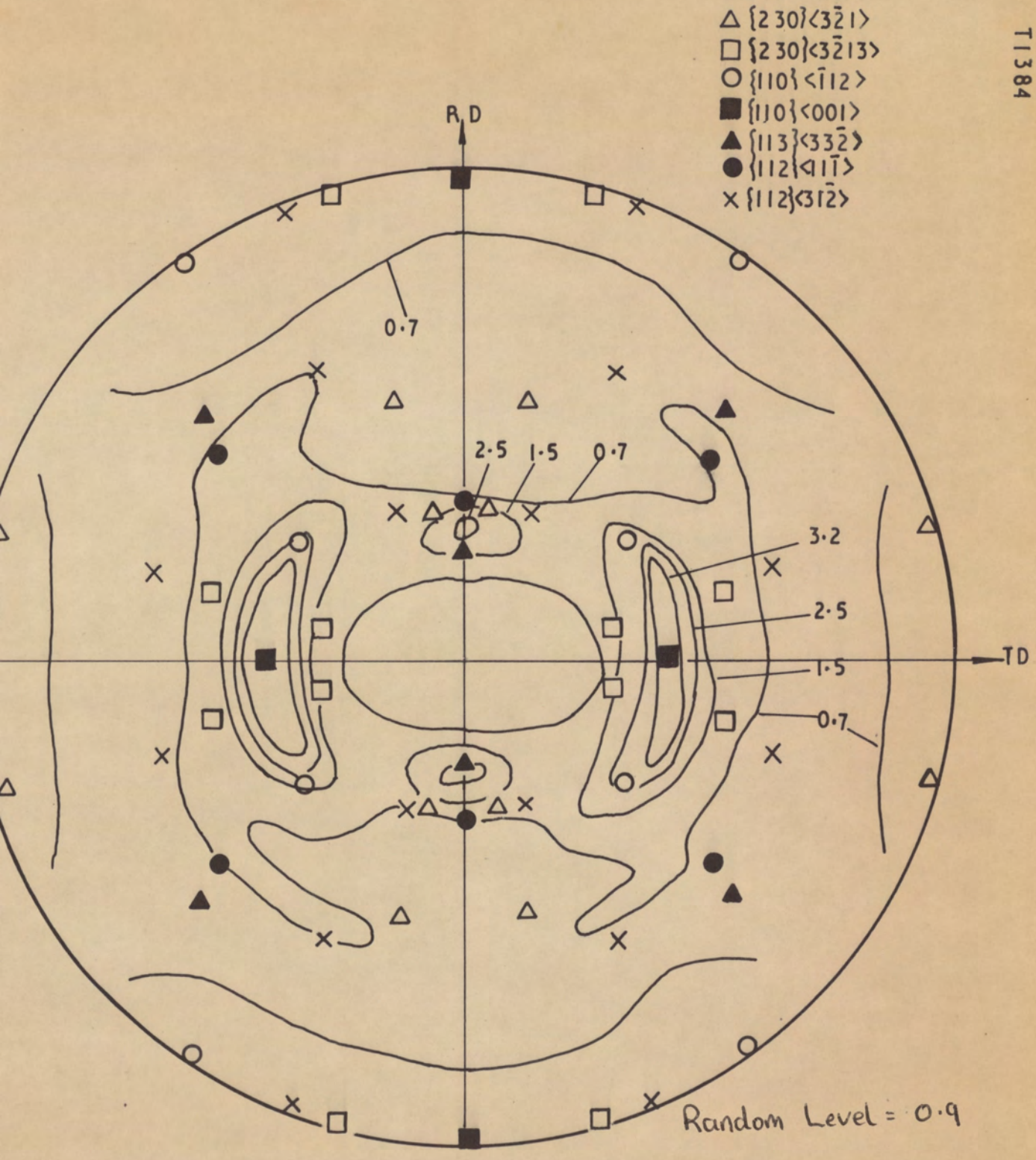

Figure 18 $\{200\}_{\gamma}$ pole figure of 18% Cr-10% Ni steel cold rolled to 93% reduction + ½h 500°C A.C.

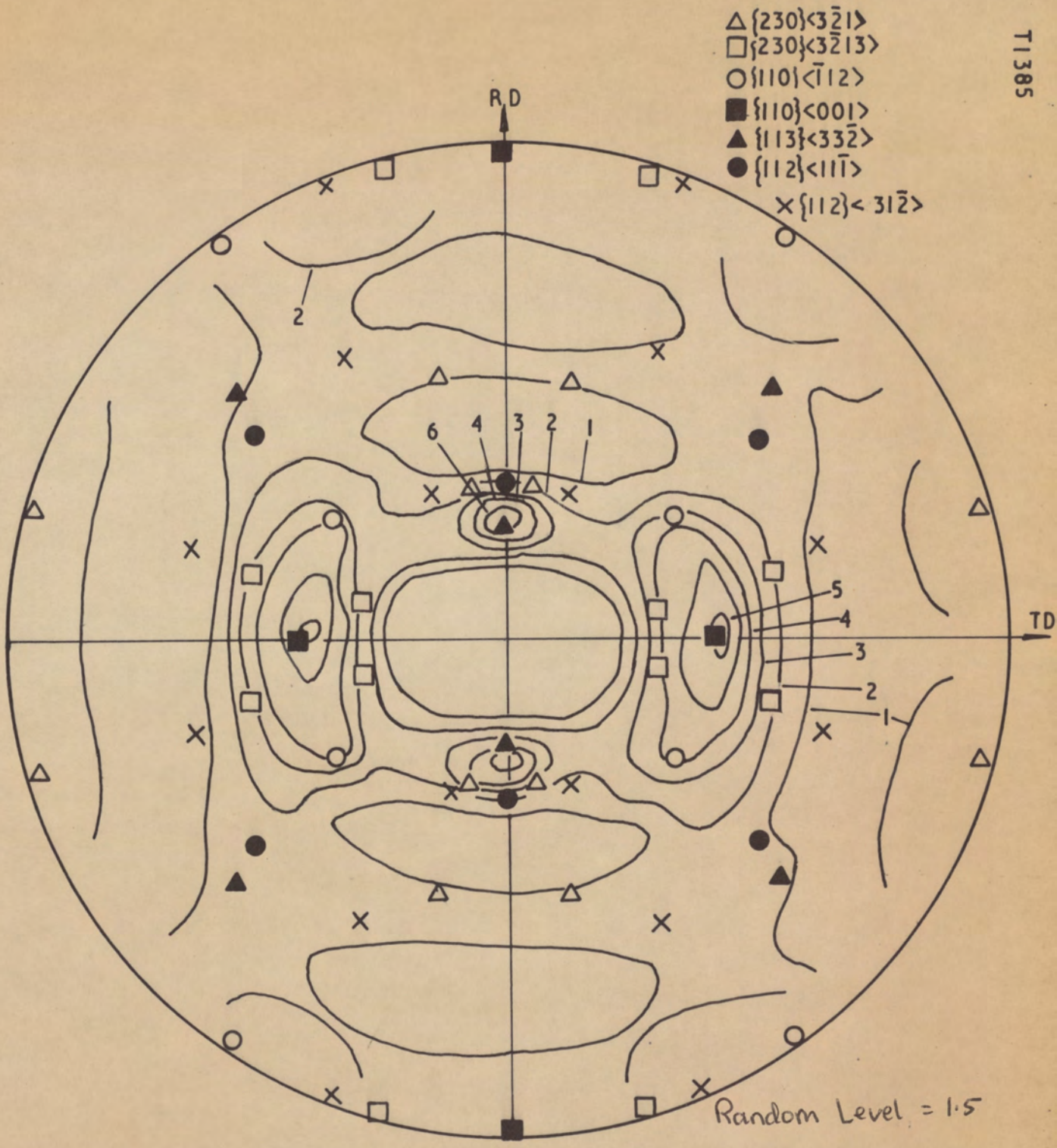

Figure 19 $\{200\}_{\gamma}$ pole figure of 18% Cr-10% Ni steel cold rolled to 93% reduction + ½ h at 600°C. A.C.

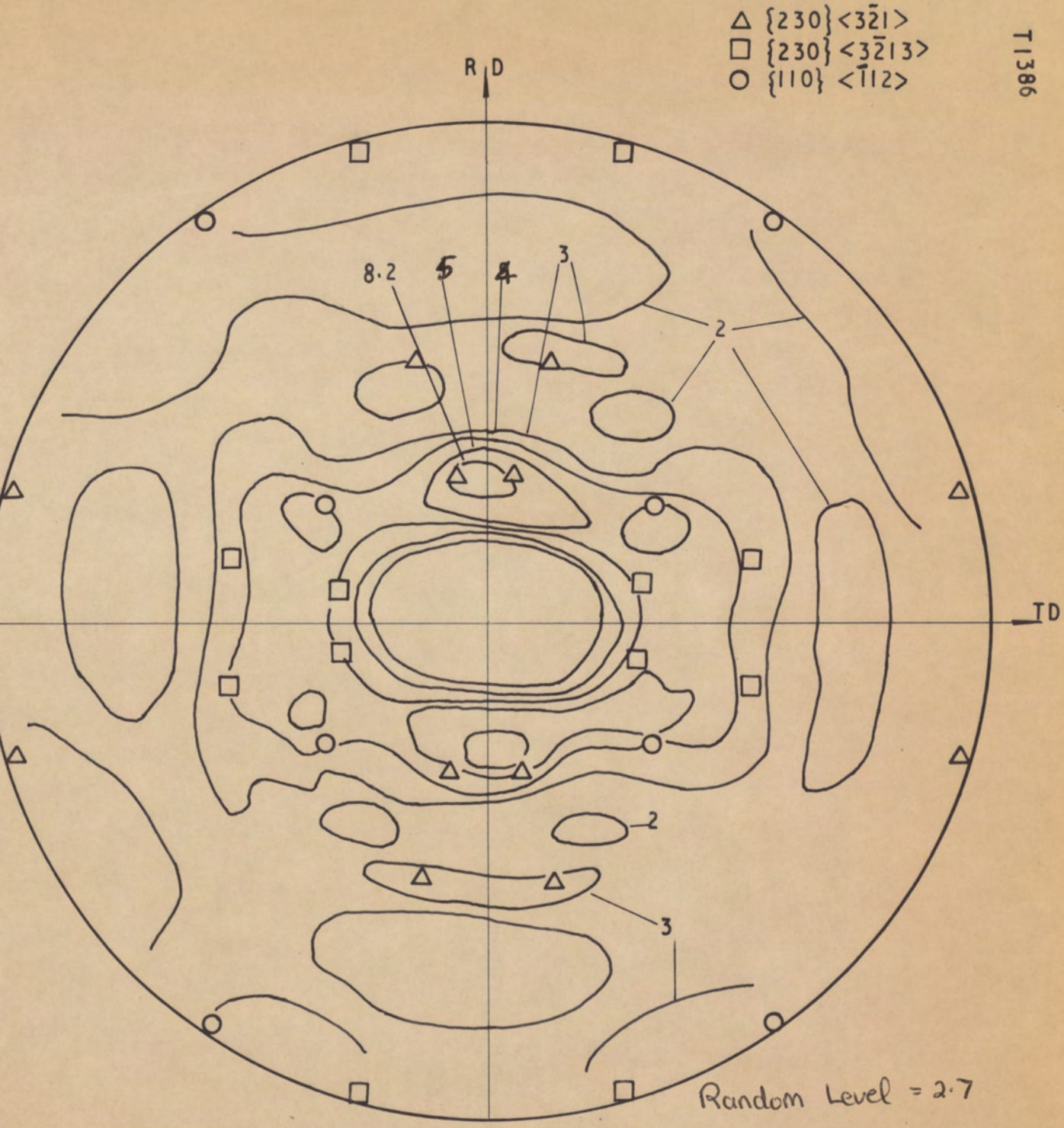

Figure 20 {200}γ pole figure of 18% Cr–10% Ni steel cold rolled to 93% reduction + ½ h at 700° C A.C.

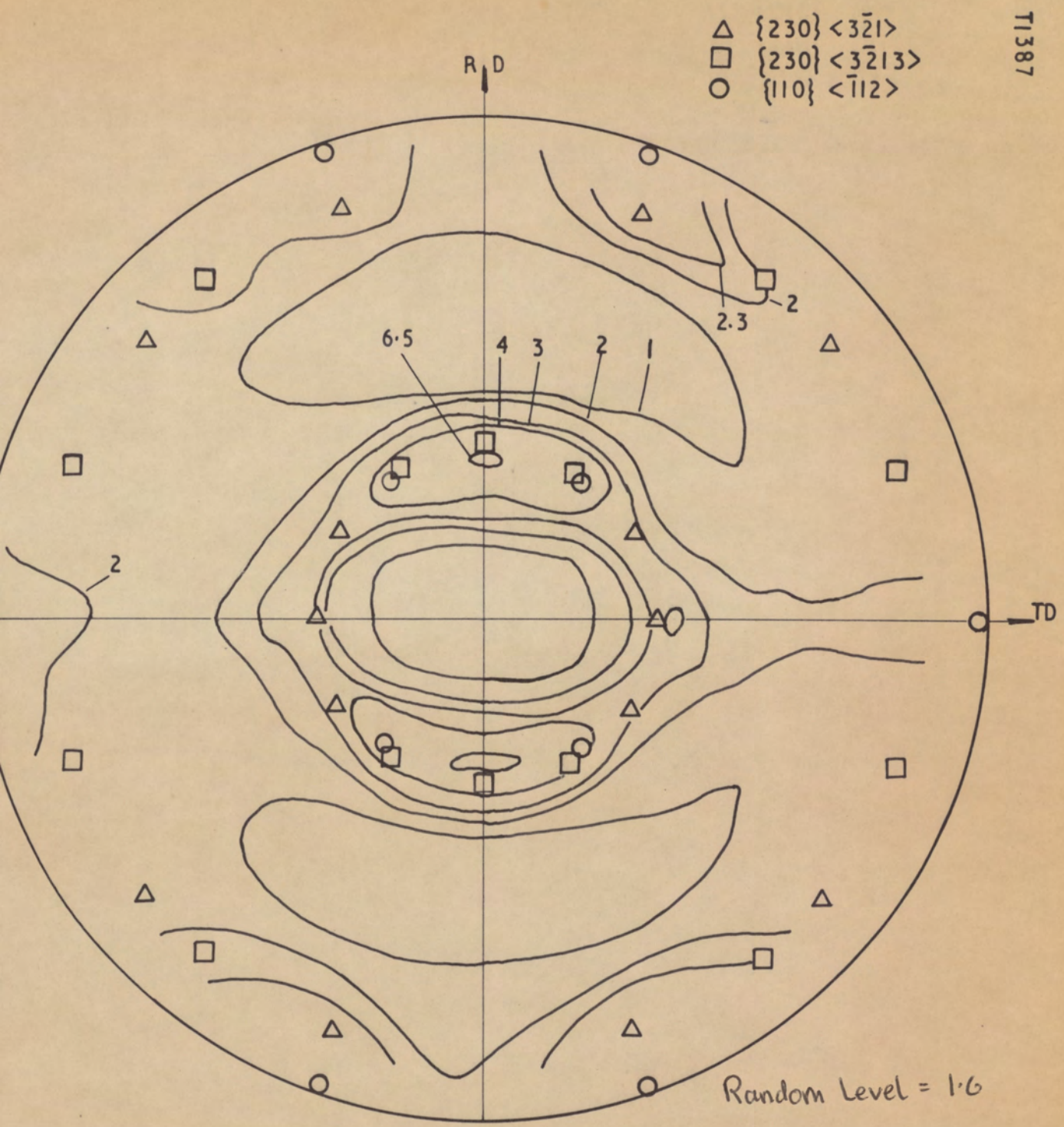

Figure 21 $\{111\}_{\gamma}$ pole figure of 18% Cr-10% Ni steel cold rolled to 93% reduction + ½ h at 700° C A.C.

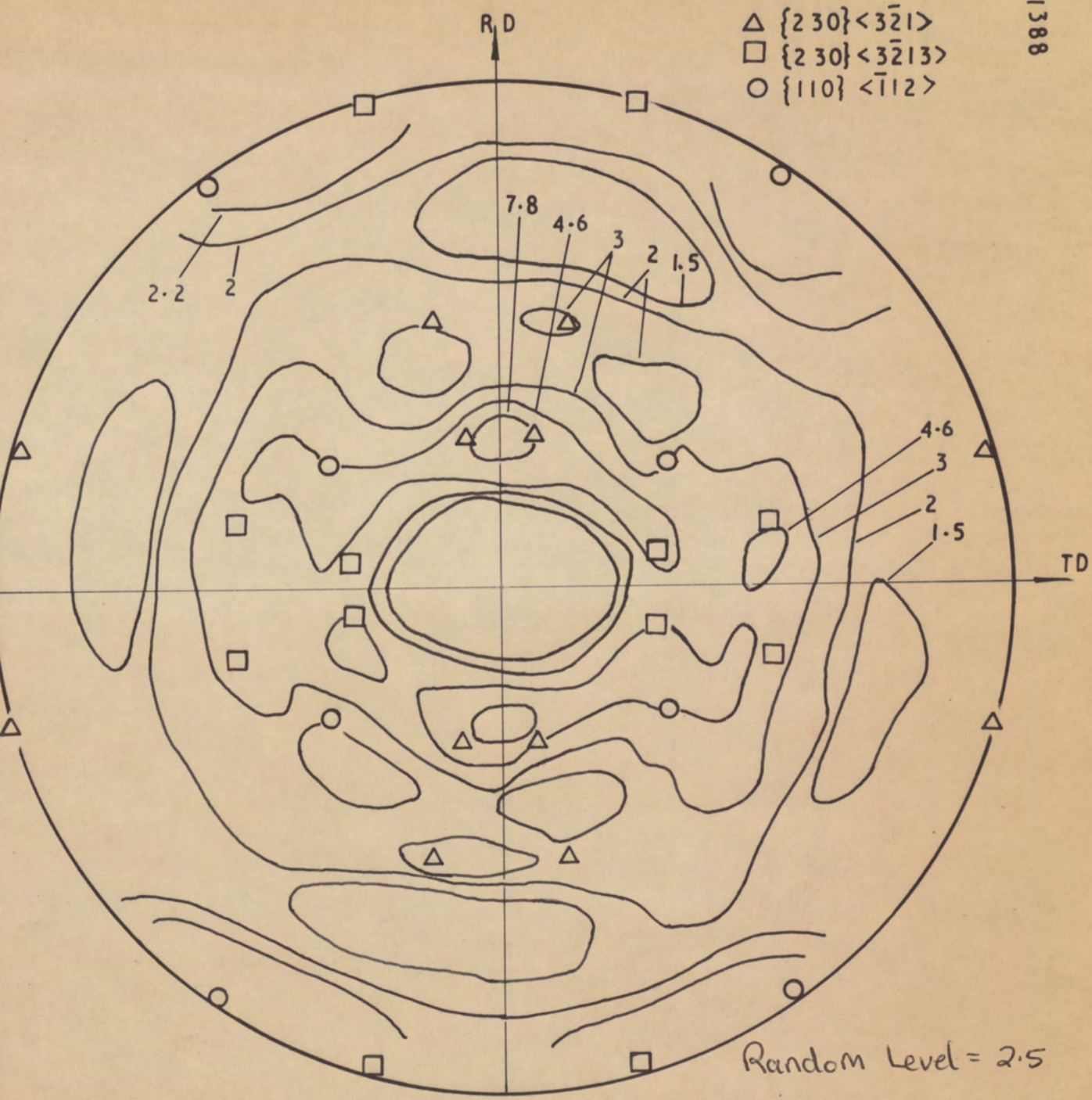

Figure 22 {200}γ pole figure of 18% Cr 10% Ni steel cold rolled to 93% reduction + ½ h at 800°C A.C.

T1389

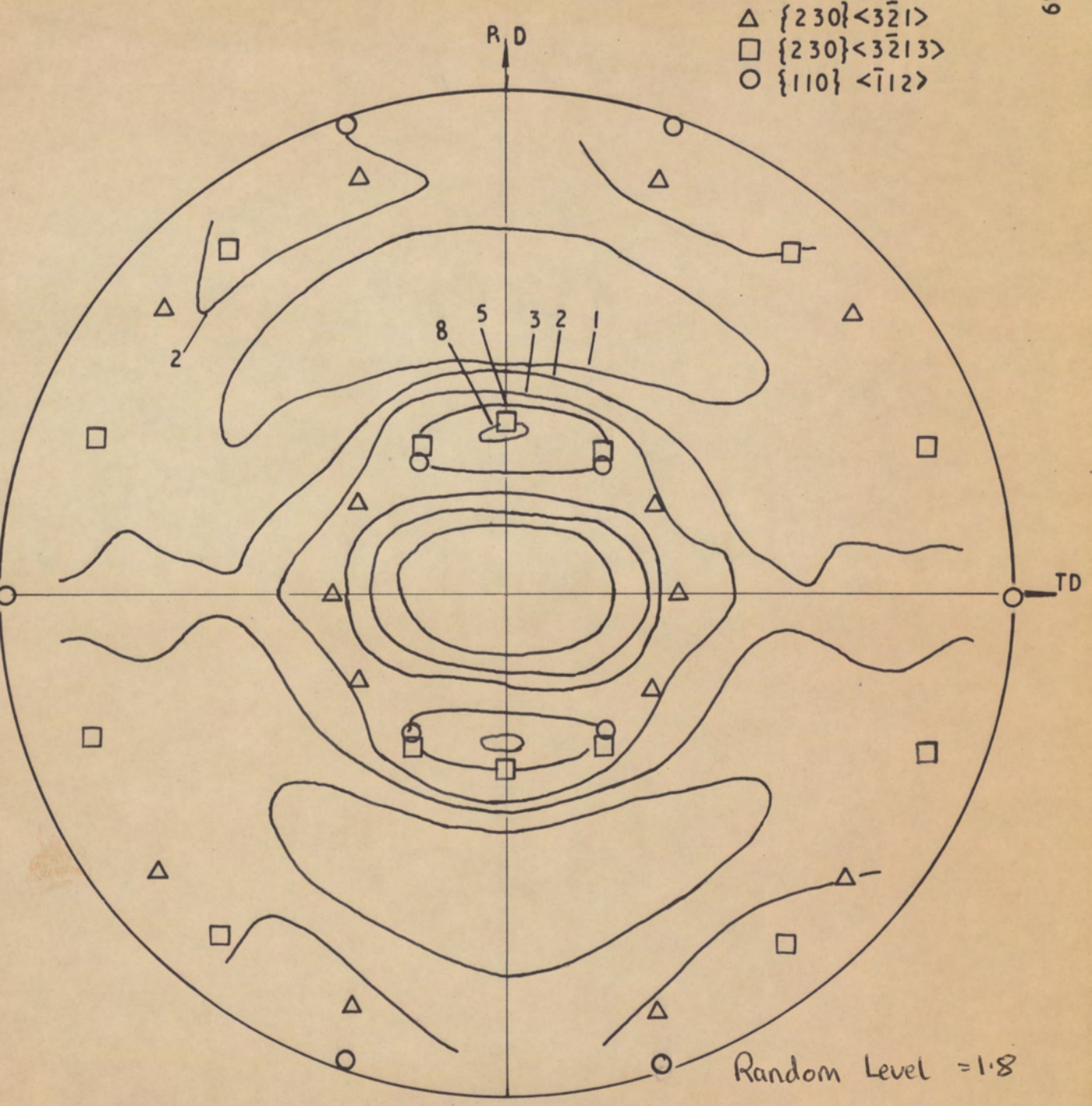

Figure 23 $\{111\}_{\gamma}$ pole figure of 18% Cr-10% Ni steel cold rolled to 93% reduction + ½ h at 800°C A.C.

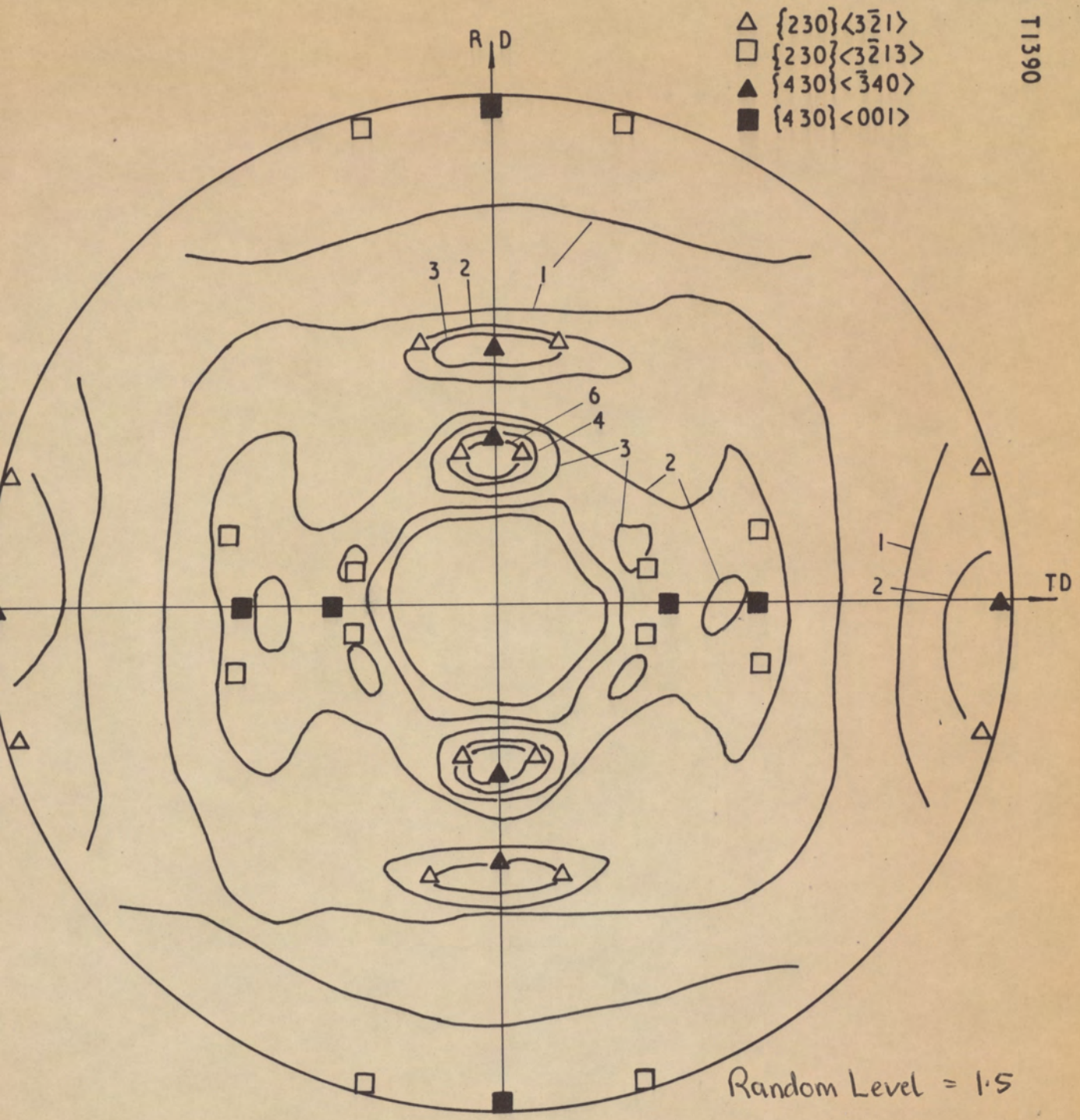

Figure 24 {200} γ pole figure of 18% Cr – 10% Ni steel cold rolled to 93% reduction + ½ h at 900° C. A.C.

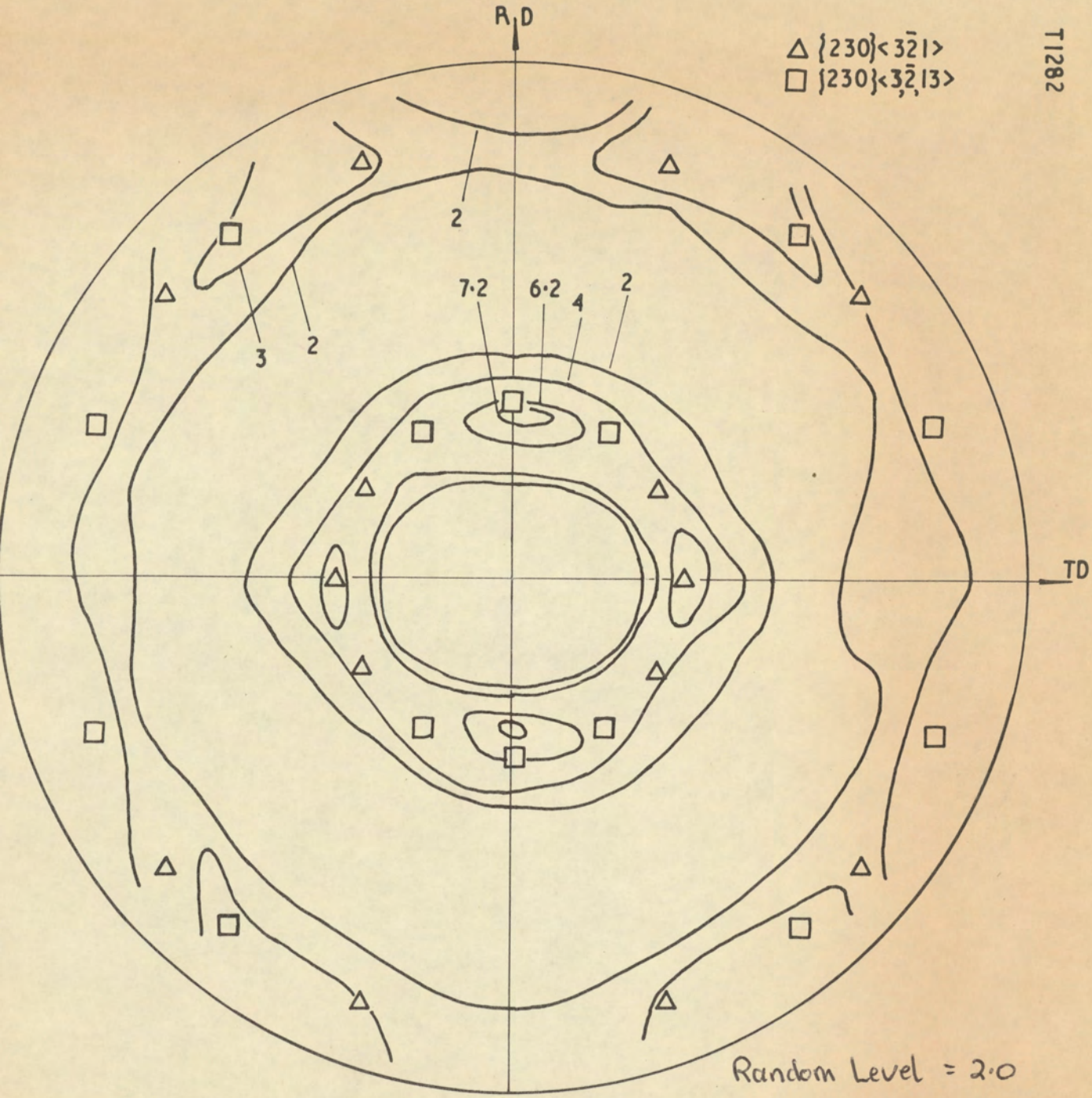

Figure 25 $\{111\}_{\gamma}$ pole figure of 18% Cr-10% Ni steel cold rolled to 93% reduction + ½h at 900°C, A.C.

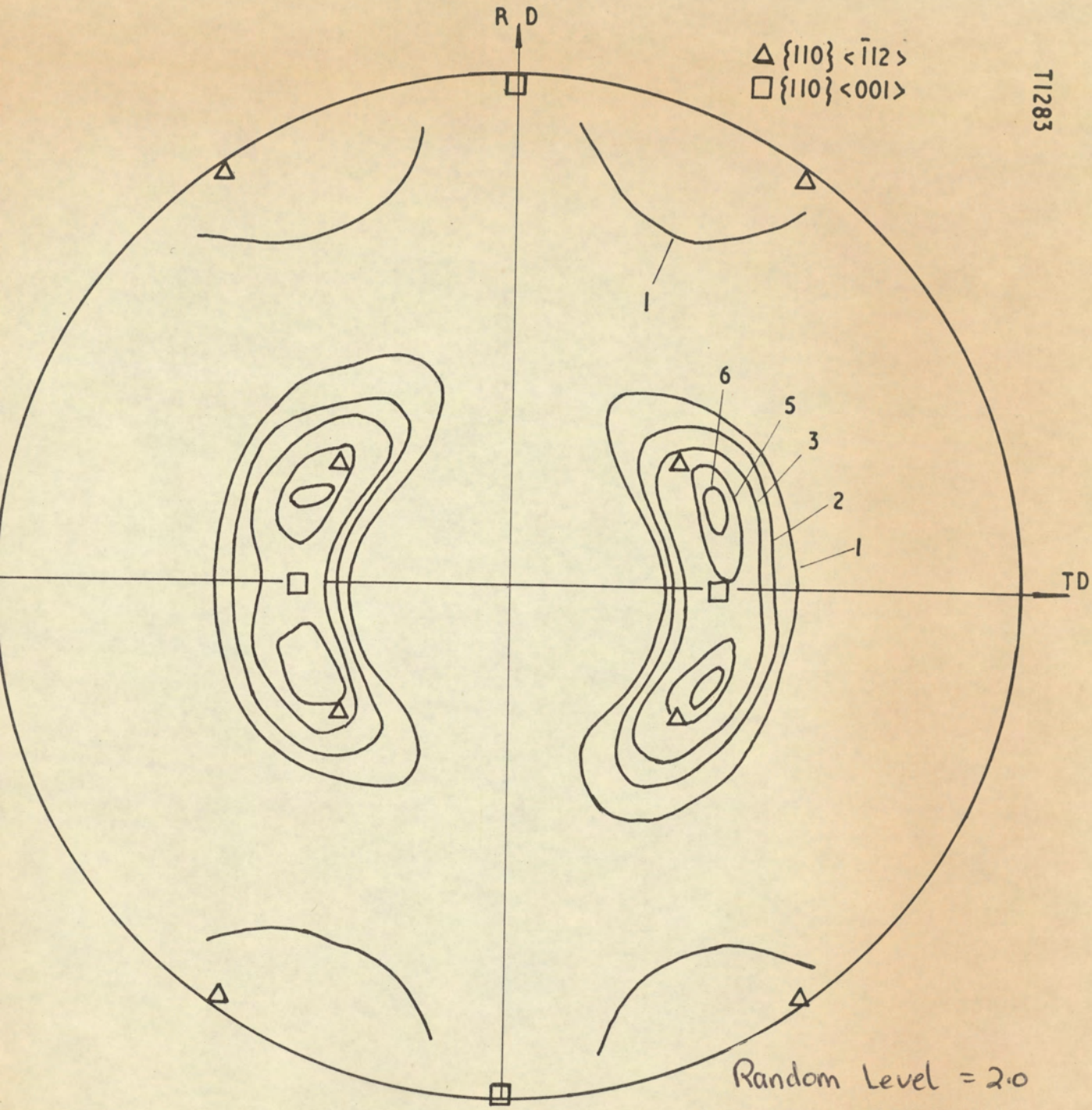

Figure 26 {200}γ pole figure of 18% Cr-12% Ni steel cold rolled to 93% reduction.

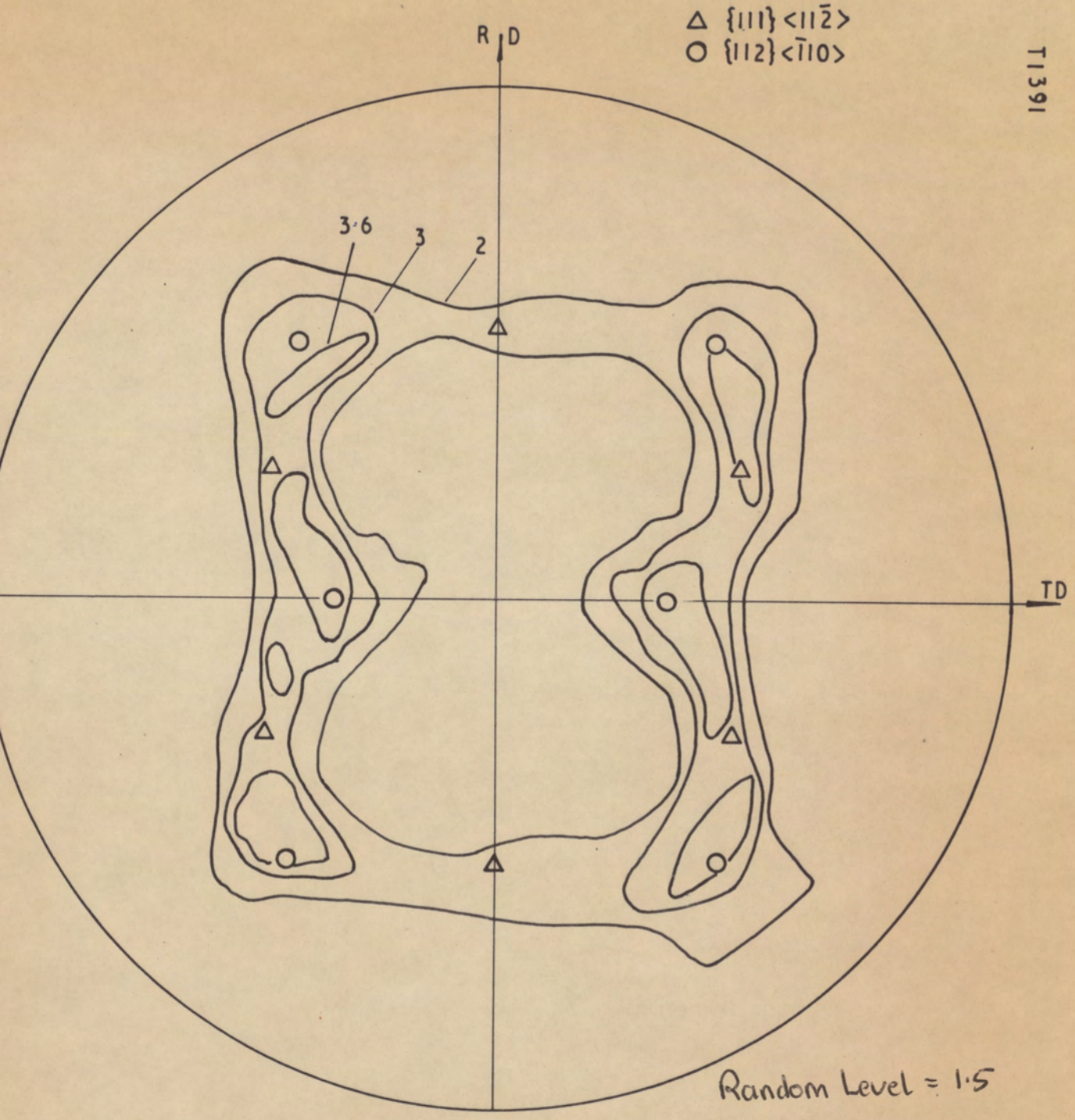

T1391

Figure 27 {200} α' pole figure of 18% Cr-12% Ni steel cold rolled to 93% reduction.

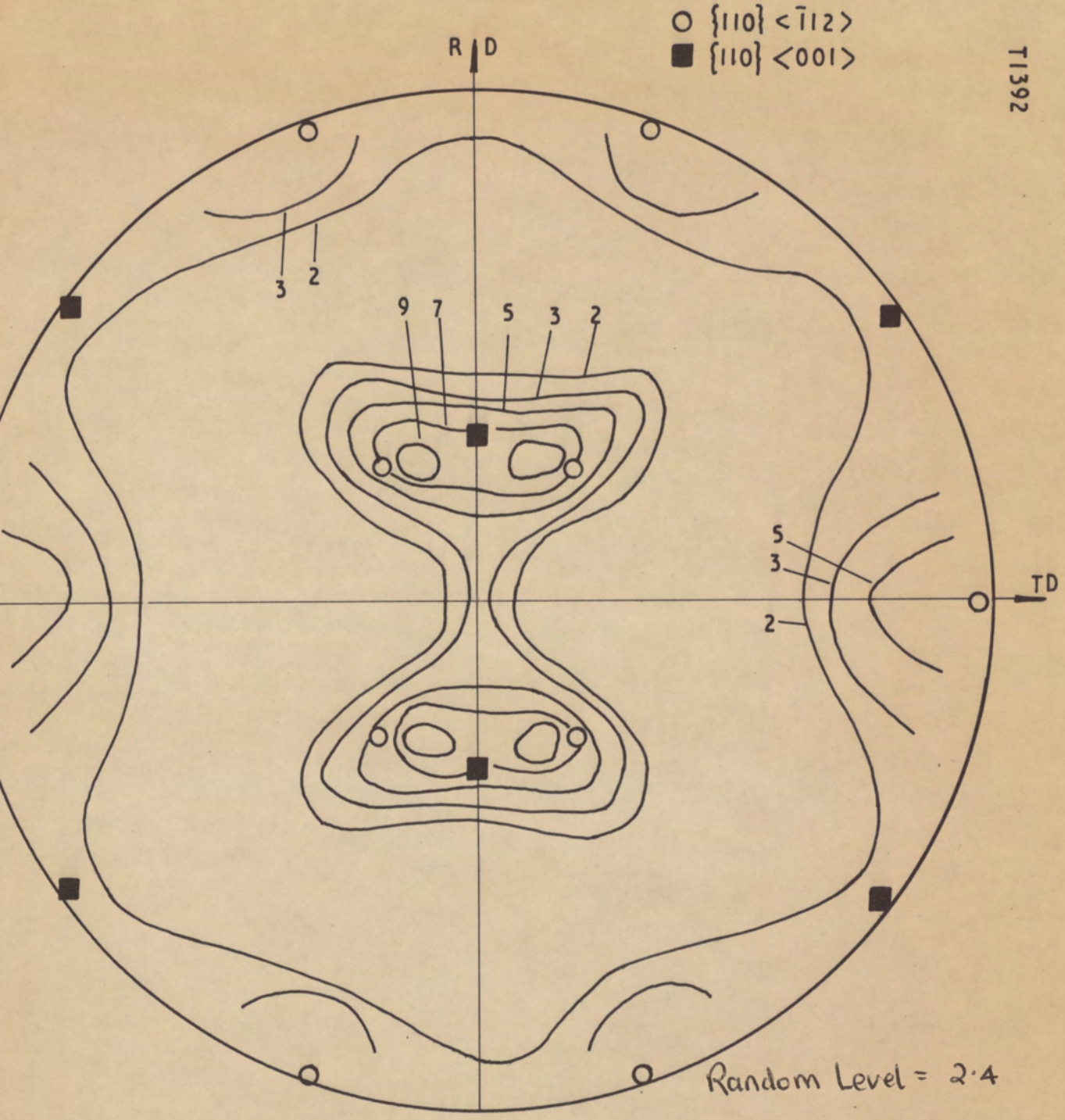

T1392

Figure 28 {111} γ pole figure of 18% Cr-12% Ni steel cold rolled to 93% reduction + 3 mins at 600° C.A.C.

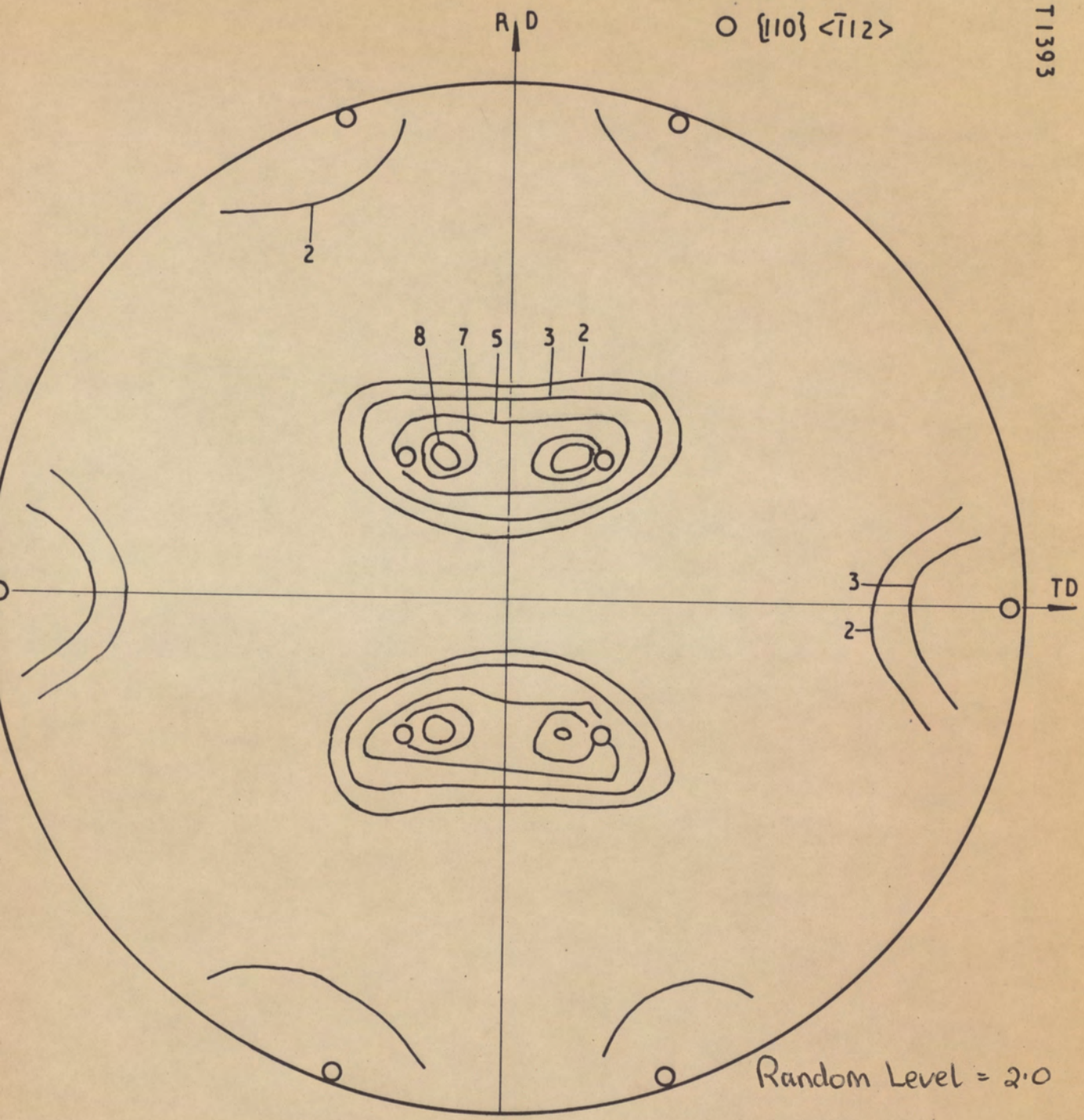

Figure 29 {111} γ pole figure of 18% Cr-12% Ni steel cold rolled to 93% reduction + 15 mins at 600° C. A.C.

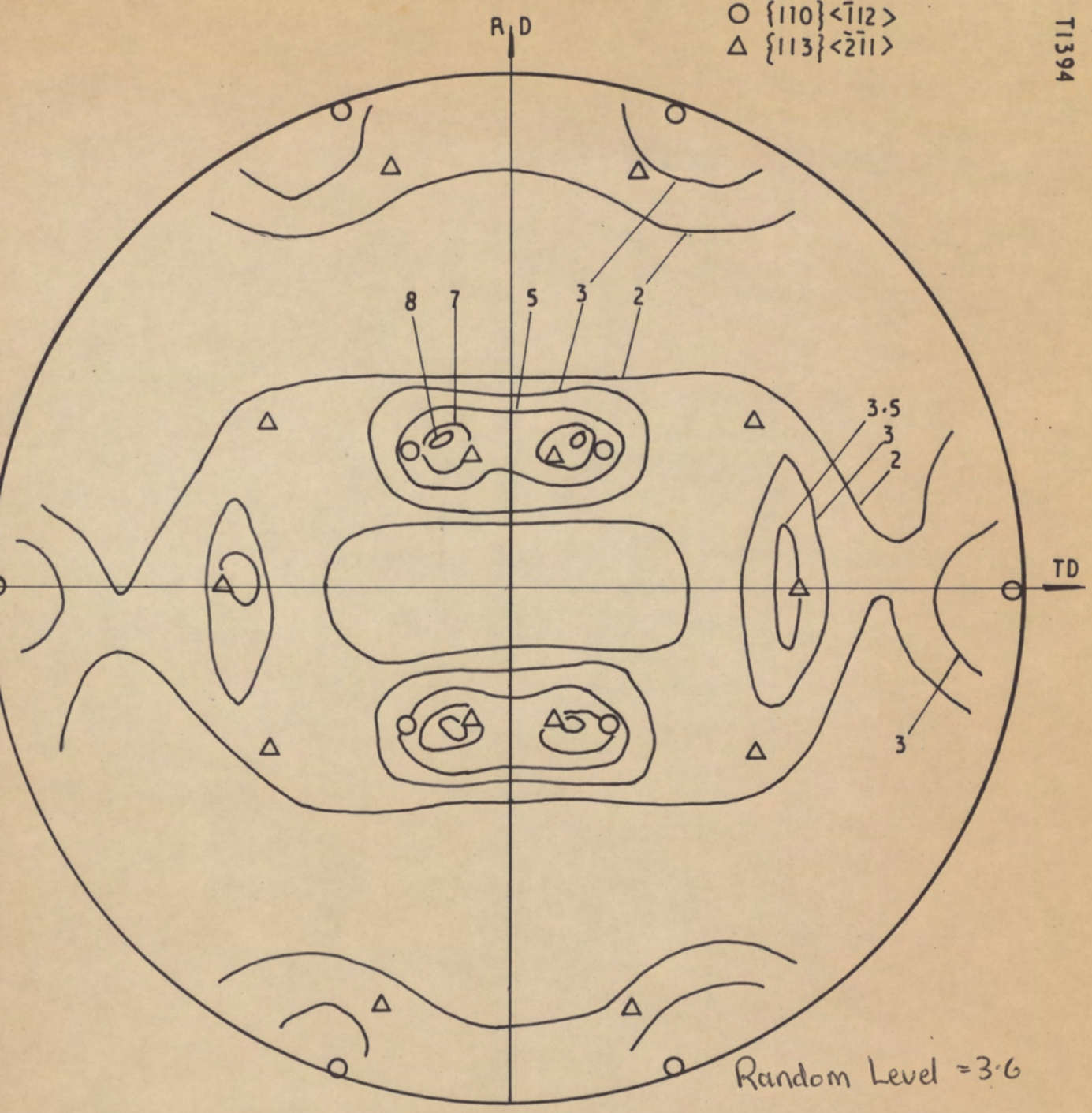

Figure 30 {111} γ pole figure of 18% Cr - 12% Ni steel cold rolled to 93% reduction + ½ h at 600° C. A.C.

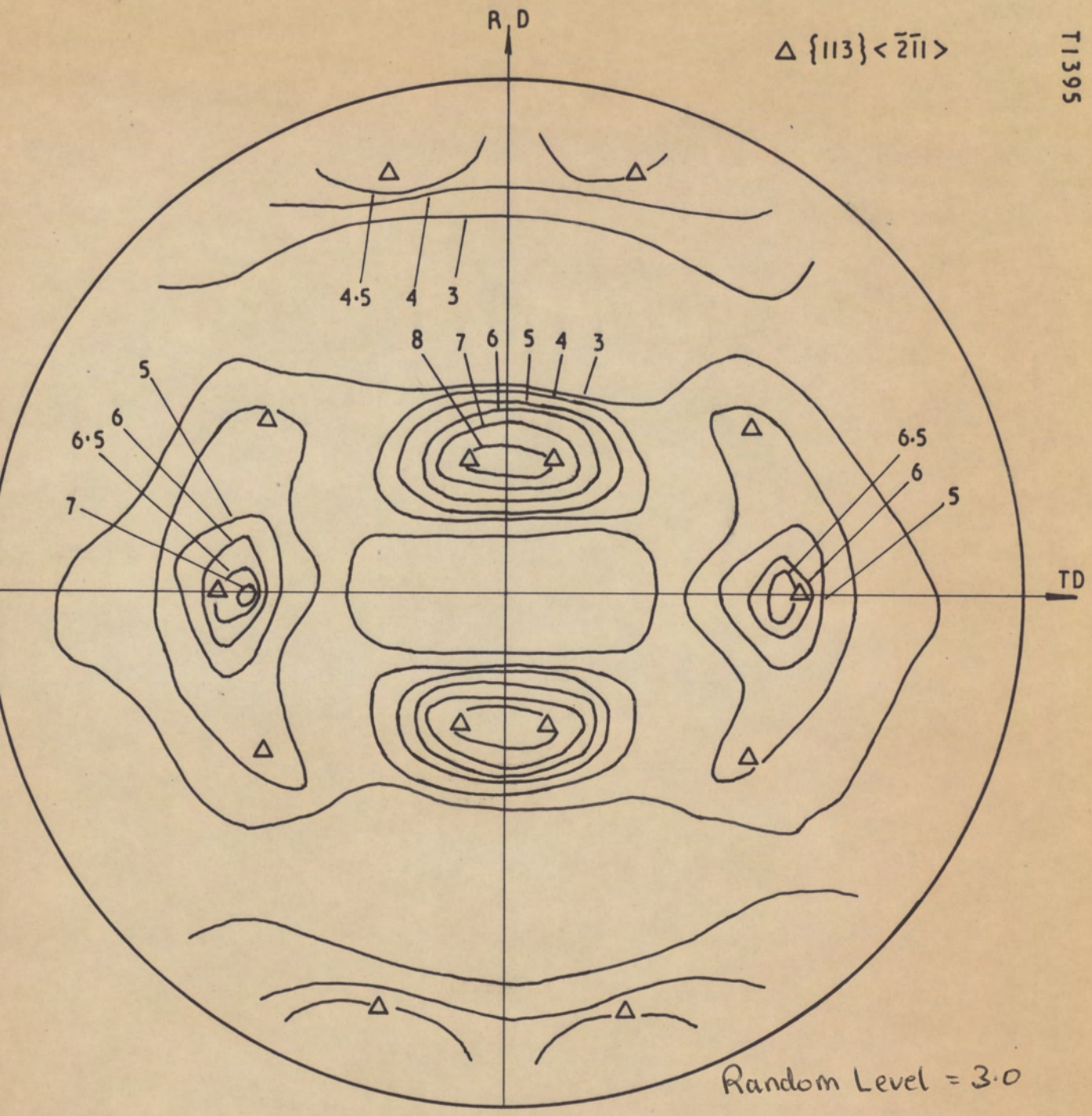

Figure 31 {111} γ pole figure of 18% Cr-12% Ni steel cold rolled to 93% reduction + ½h at 800° C. A.C.

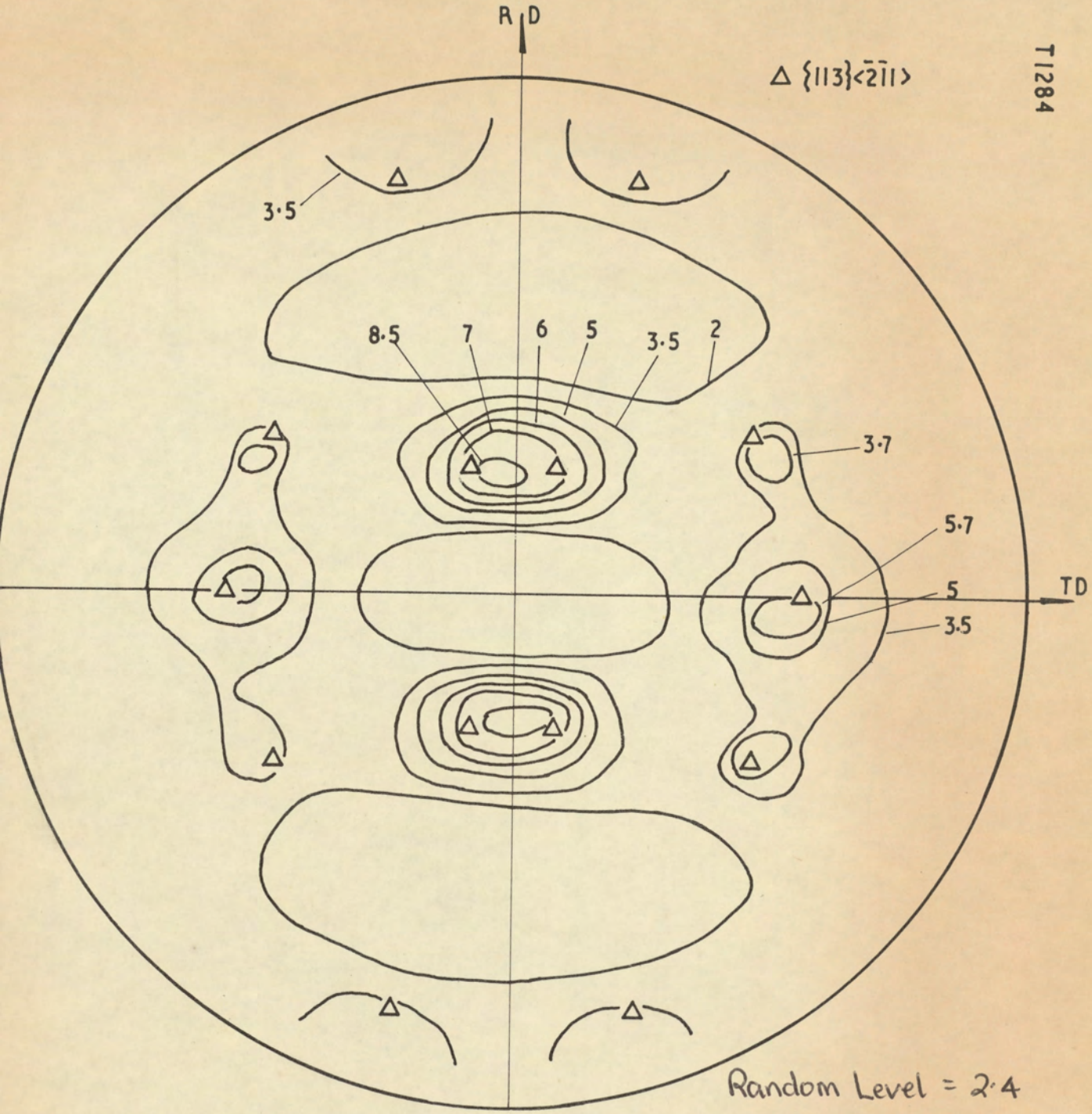

Figure 32 {111}γ pole figure of 18% Cr-12% Ni steel cold rolled to 93% reduction + ½h at 900°C. A.C.

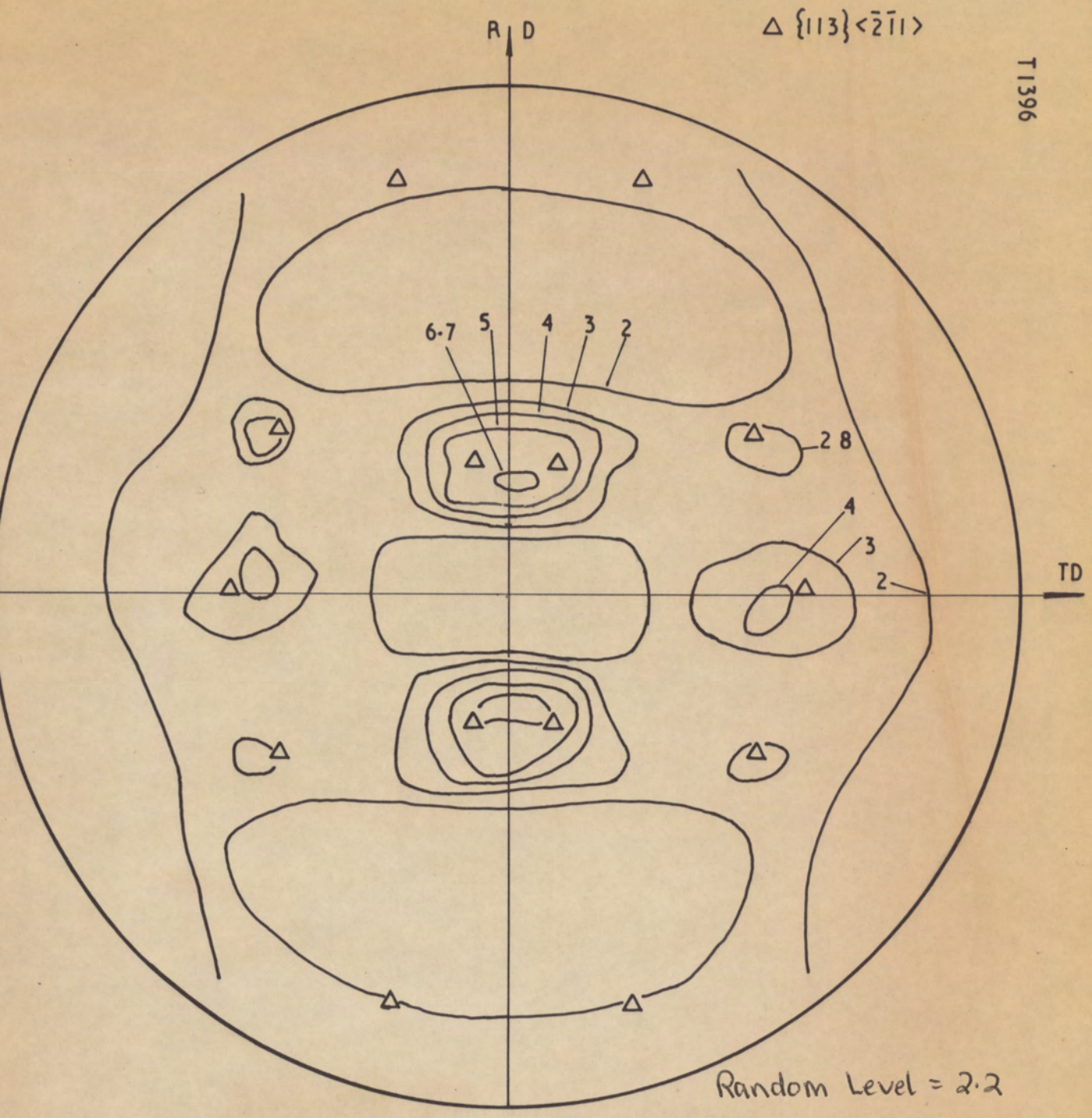

Figure 33 {111} γ pole figure of 18% Cr-12% Ni steel cold rolled to 93% reduction + 1 hour at 1000°C A.C.

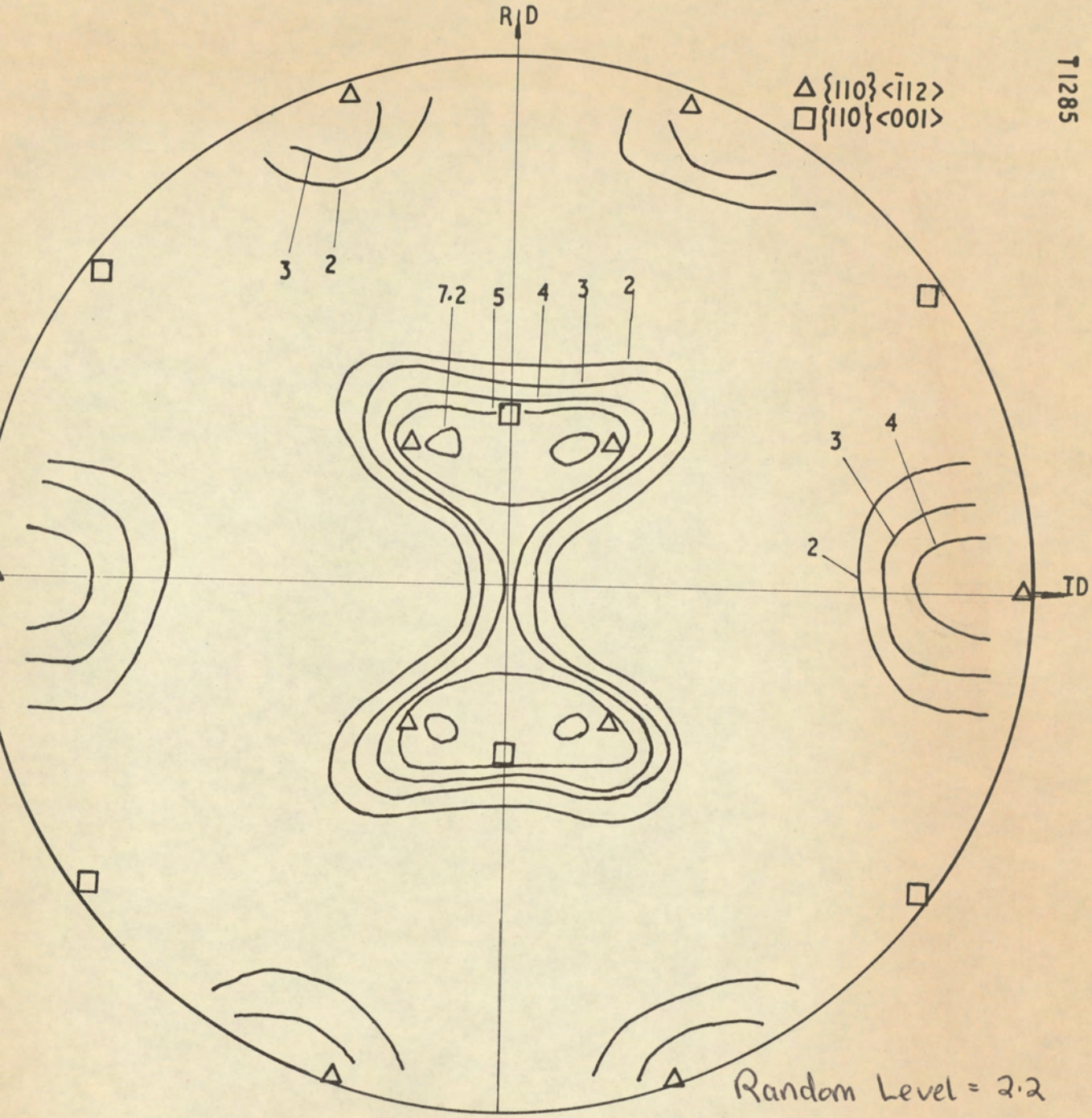

Figure 34 $\{111\}_\gamma$ pole figure of 18% Cr - 14% Ni steel cold rolled to 93% reduction.

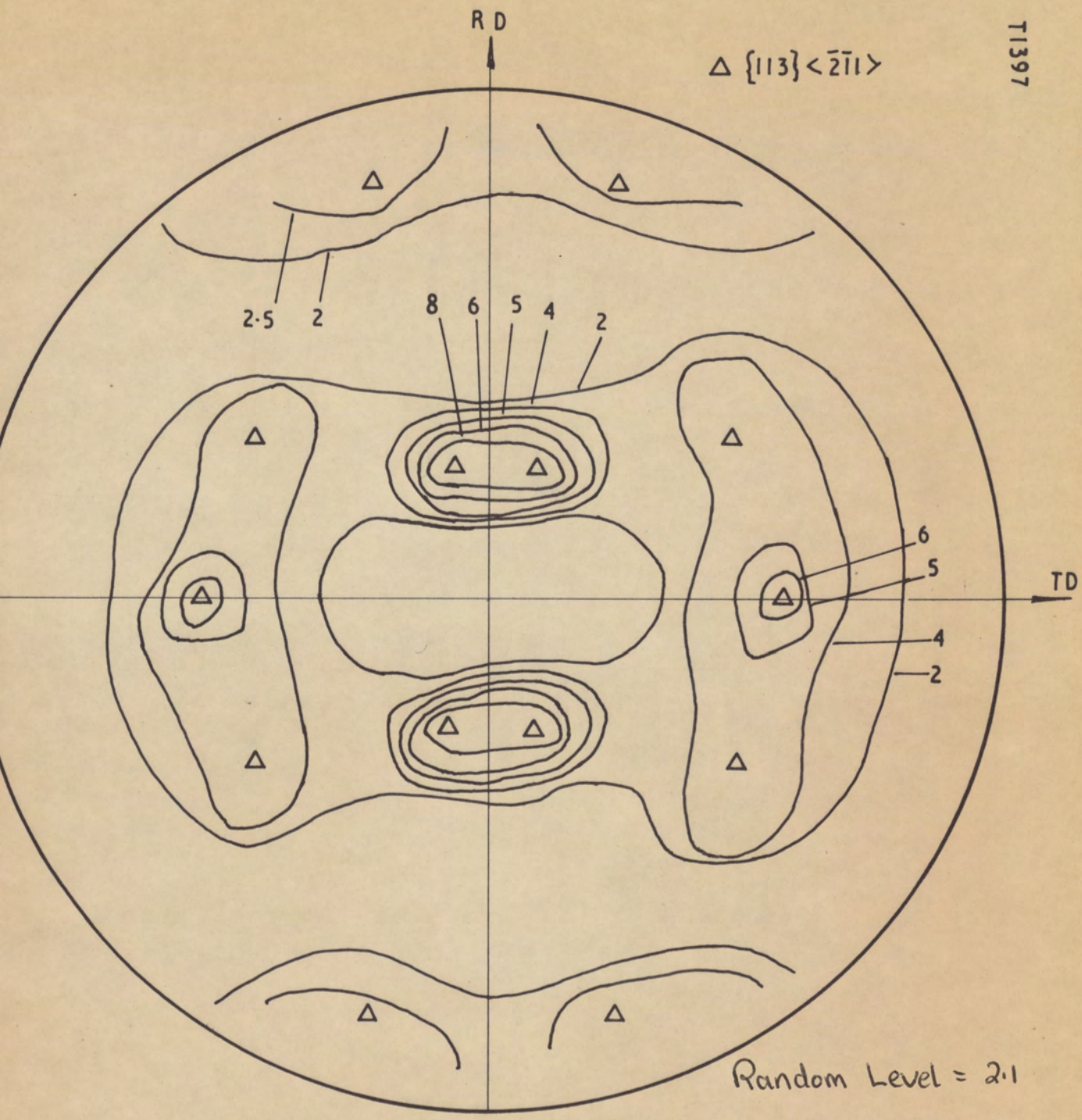

Figure 35 {111} γ pole figure of 18%Cr-14%Ni steel cold rolled to 93% reduction + ½ hour at 800°C AC.

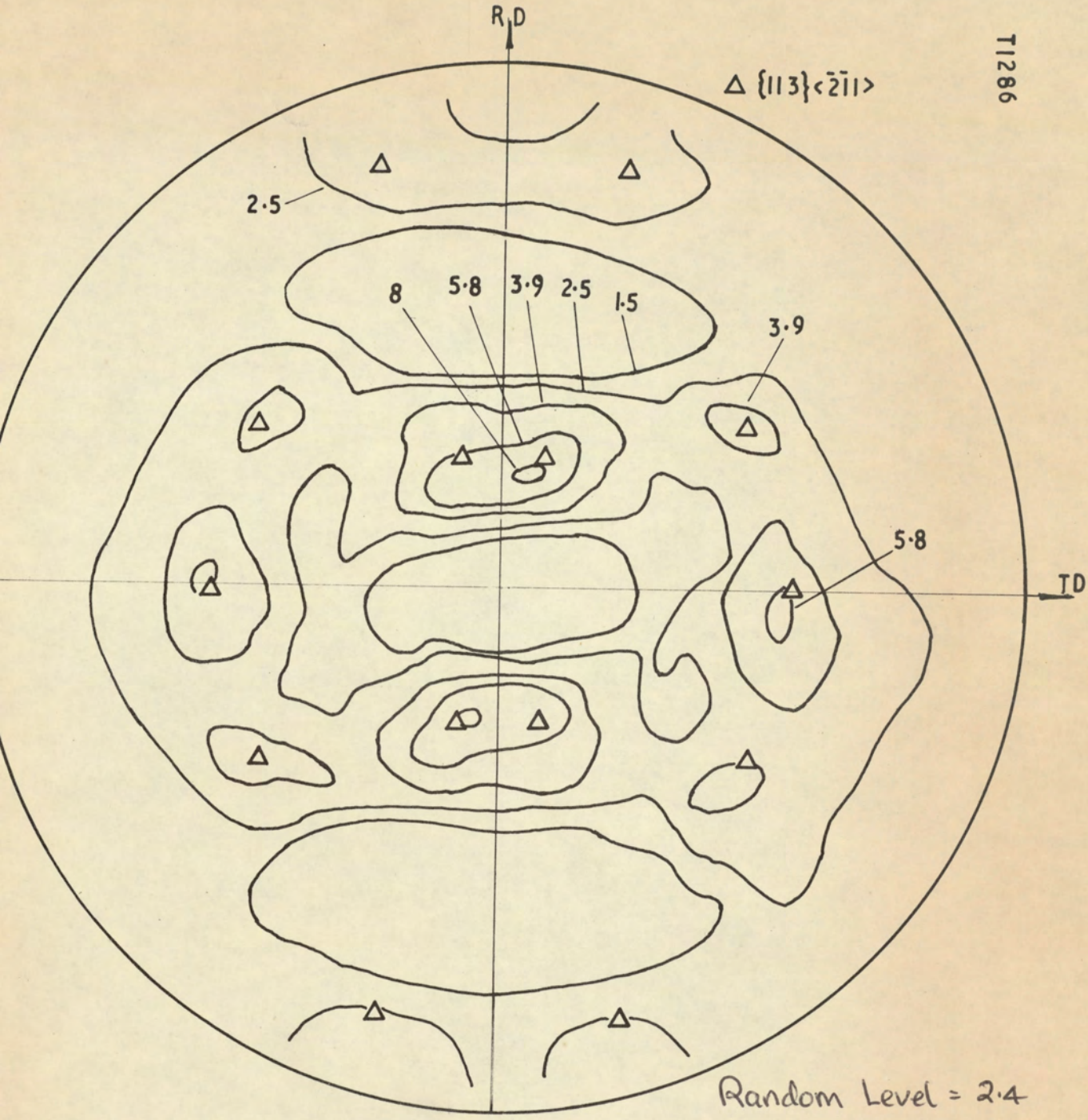

Figure 36 {111}γ pole figure of 18% Cr-14% Ni steel cold rolled to 93% reduction + ½h at 900° C, A.C.

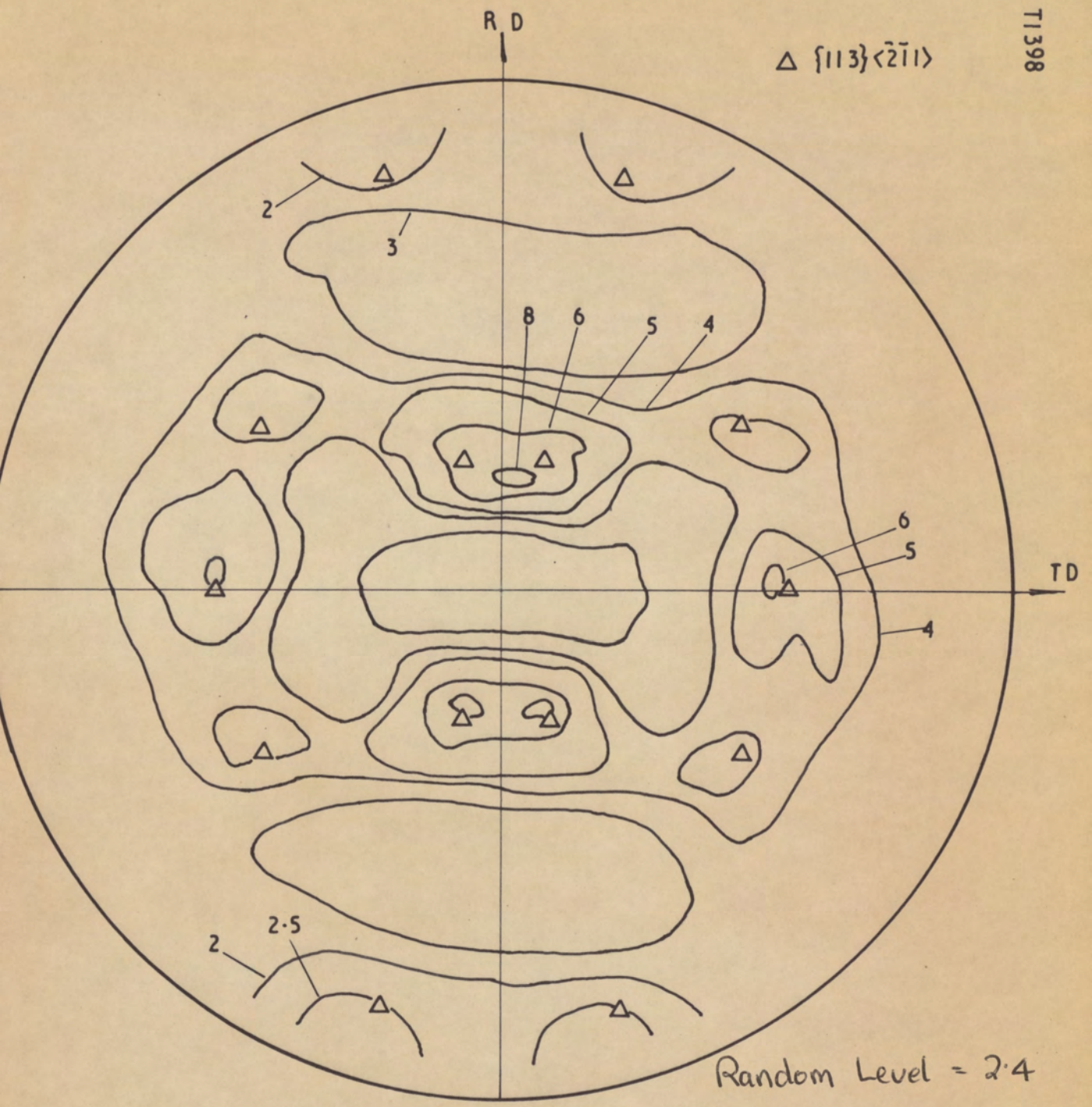

Figure 37 $\{111\}_\gamma$ pole figure of 18% Cr-14% Ni steel cold rolled to 93% reduction + 1hour at 1000° C. A.C.

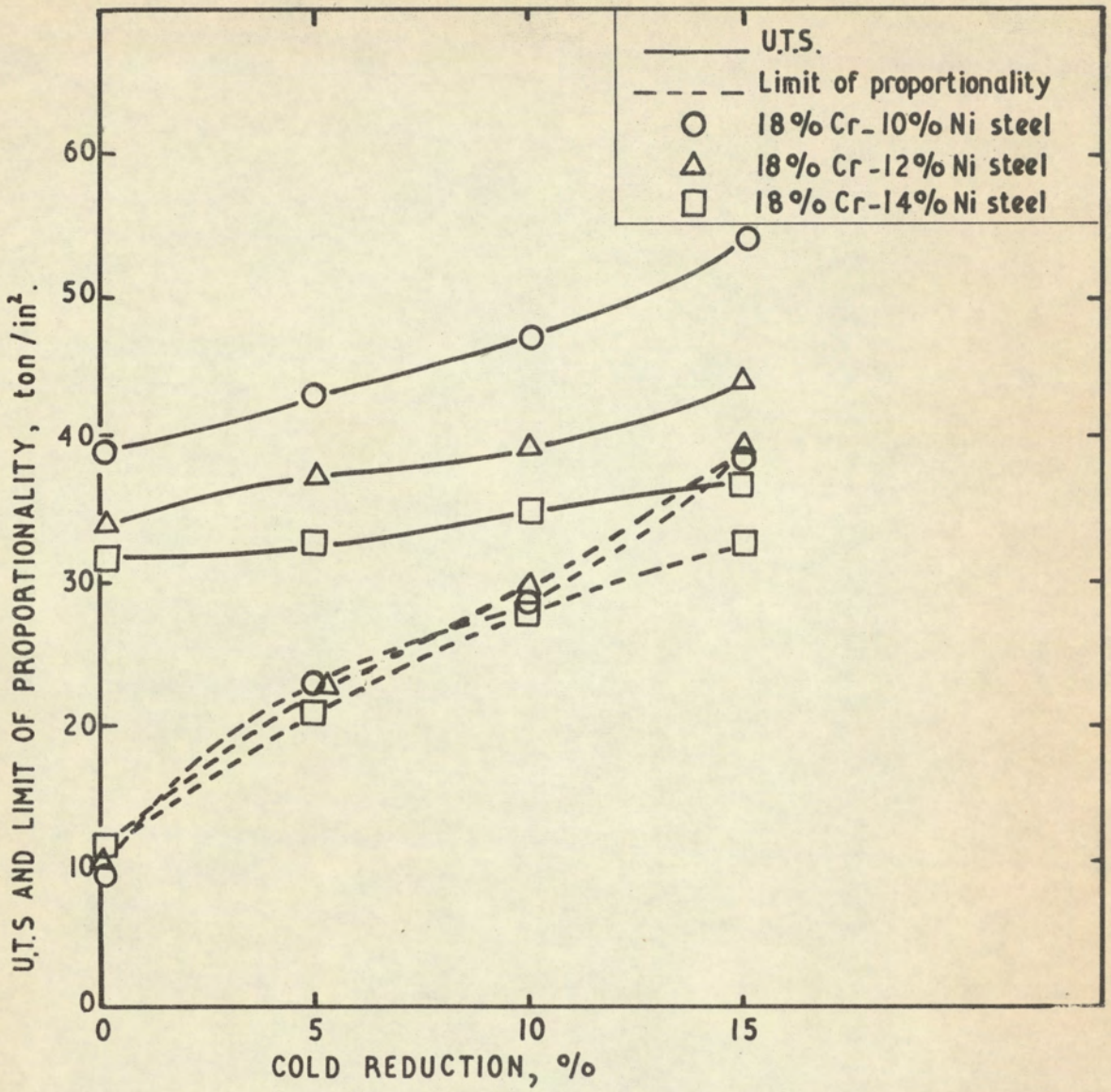

Figure 38 Effect of cold rolling on U.T.S. and limit of proportionality of 18% Cr steels containing 10-14% Ni

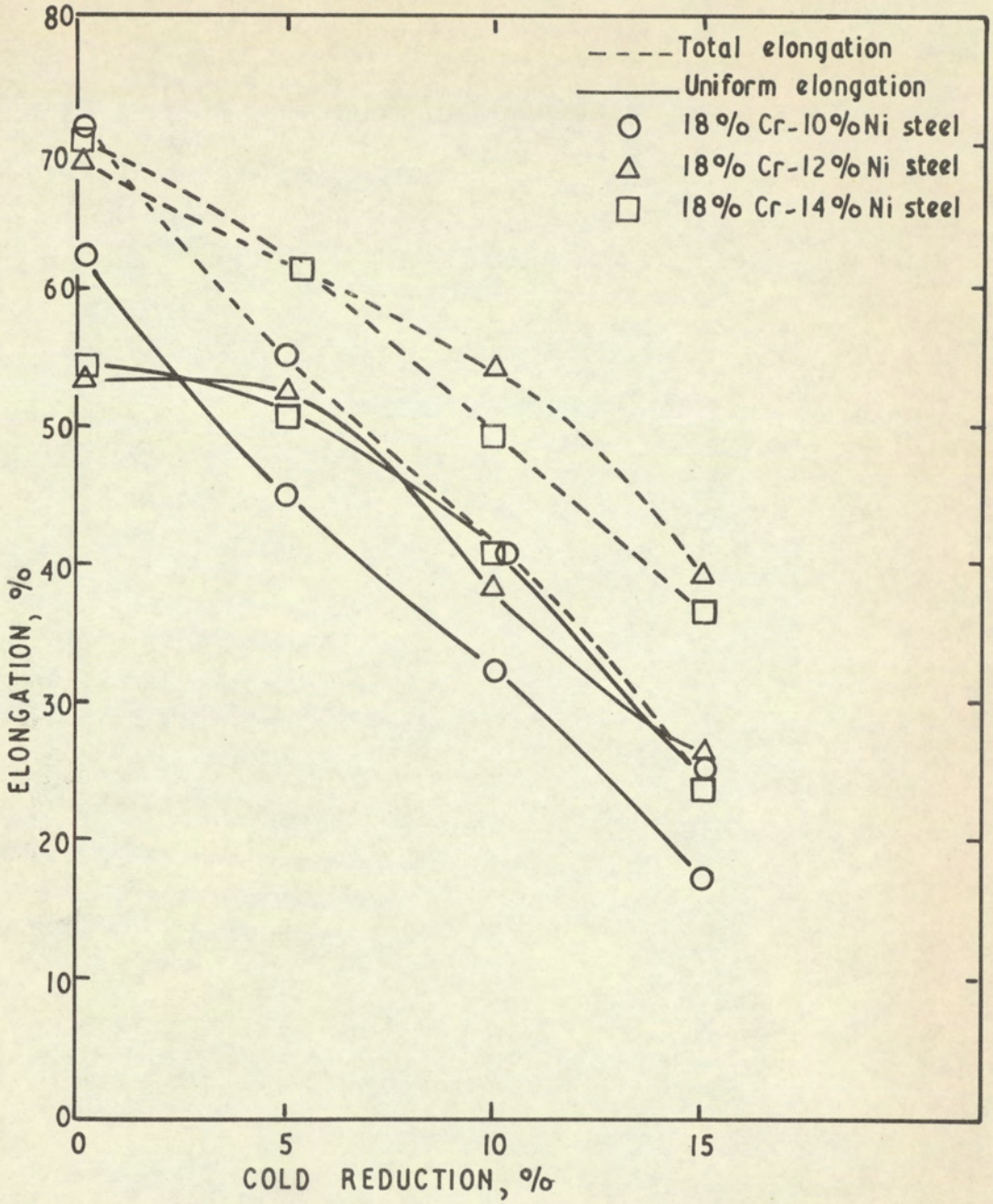

Figure 39 Effect of cold rolling on % elongation of 18% Cr steels containing 10-14% Ni.

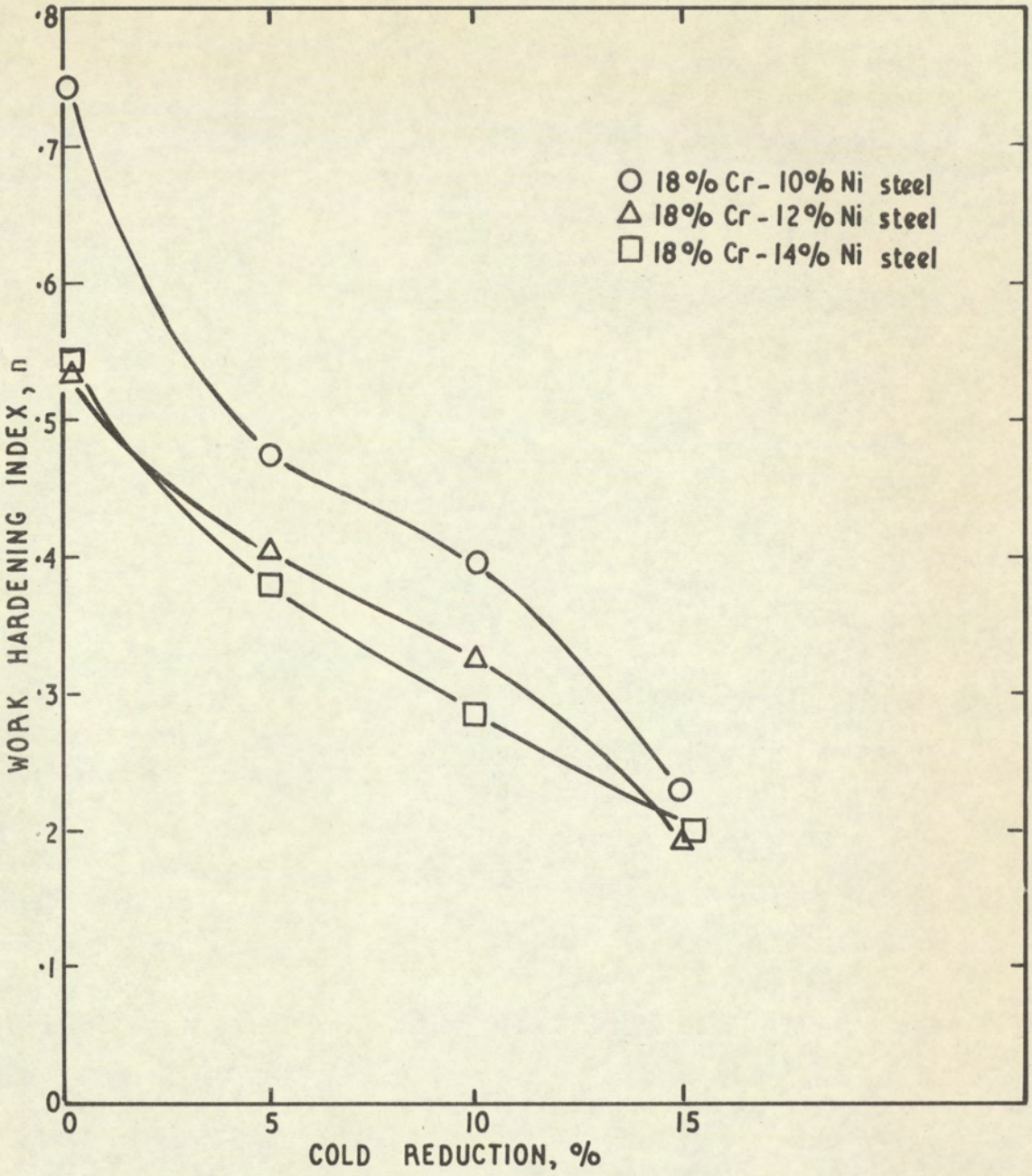

Figure 40 Effect of cold rolling on the rate of work hardening of 18% Cr steels containing 10-14% Ni.

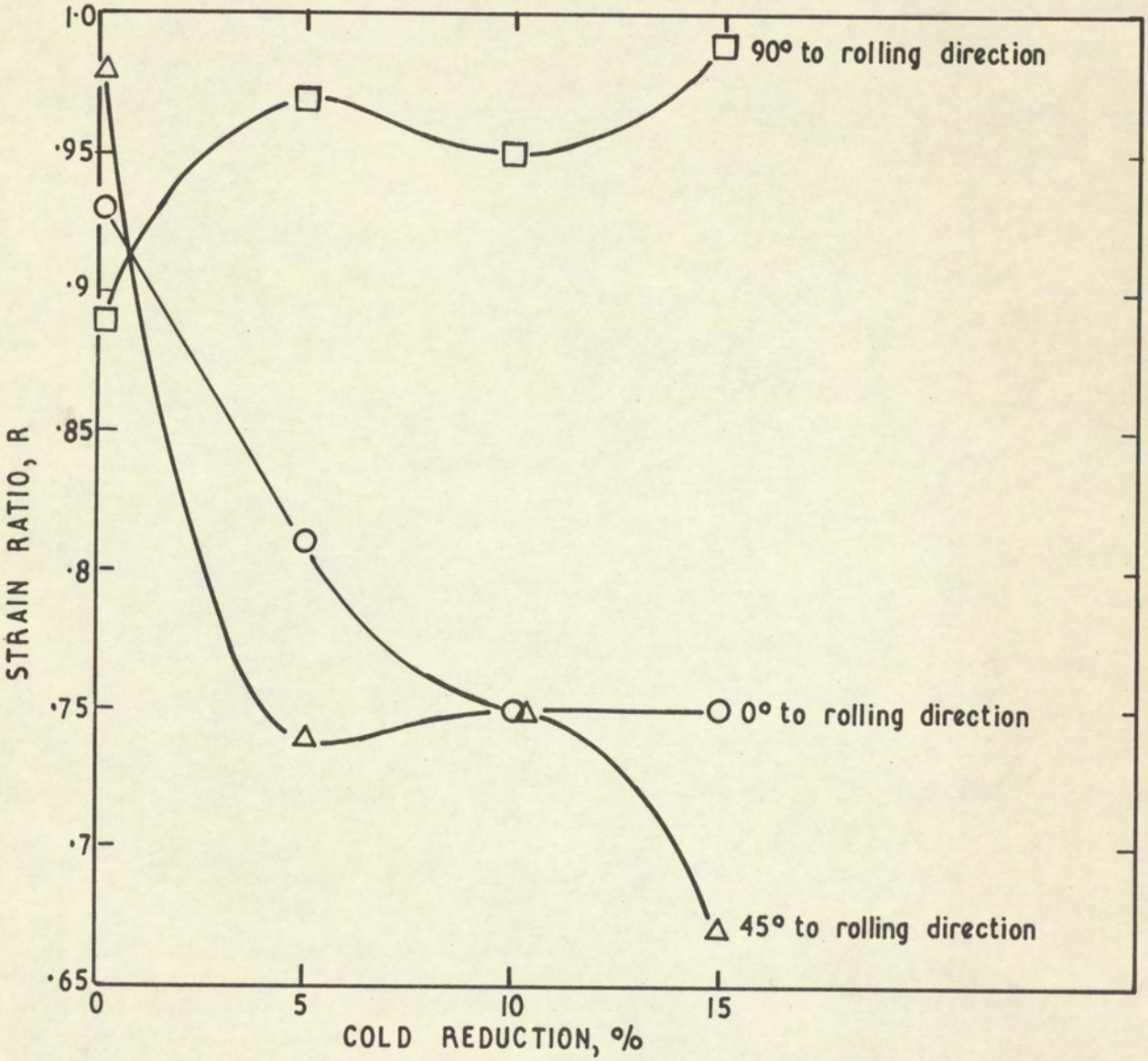

Figure 41 Effect of cold rolling on the strain ratio of 18% Cr - 10% Ni steel.

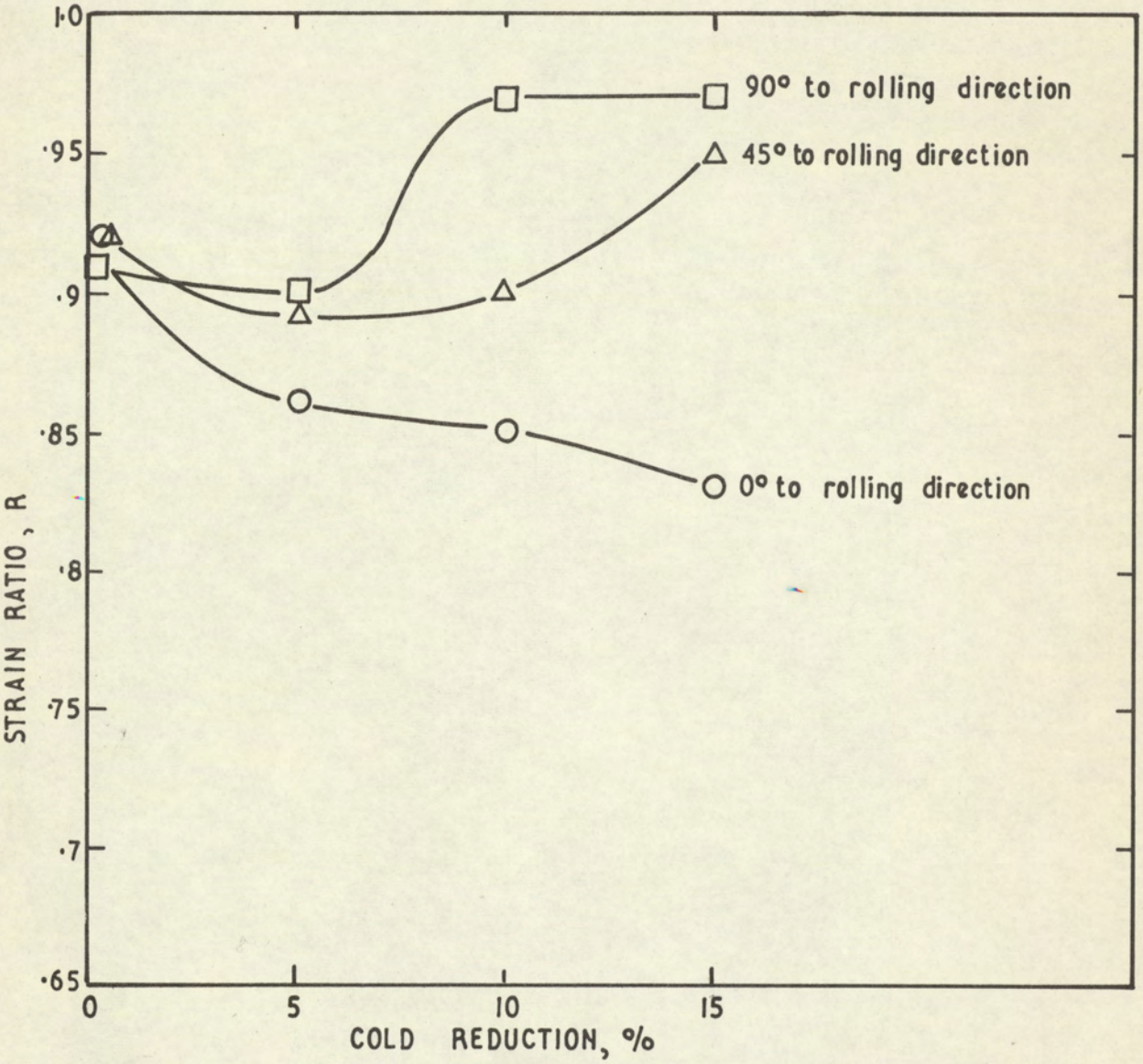

Figure 42 Effect of cold rolling on the strain ratio of 18% Cr-12% Ni steel.

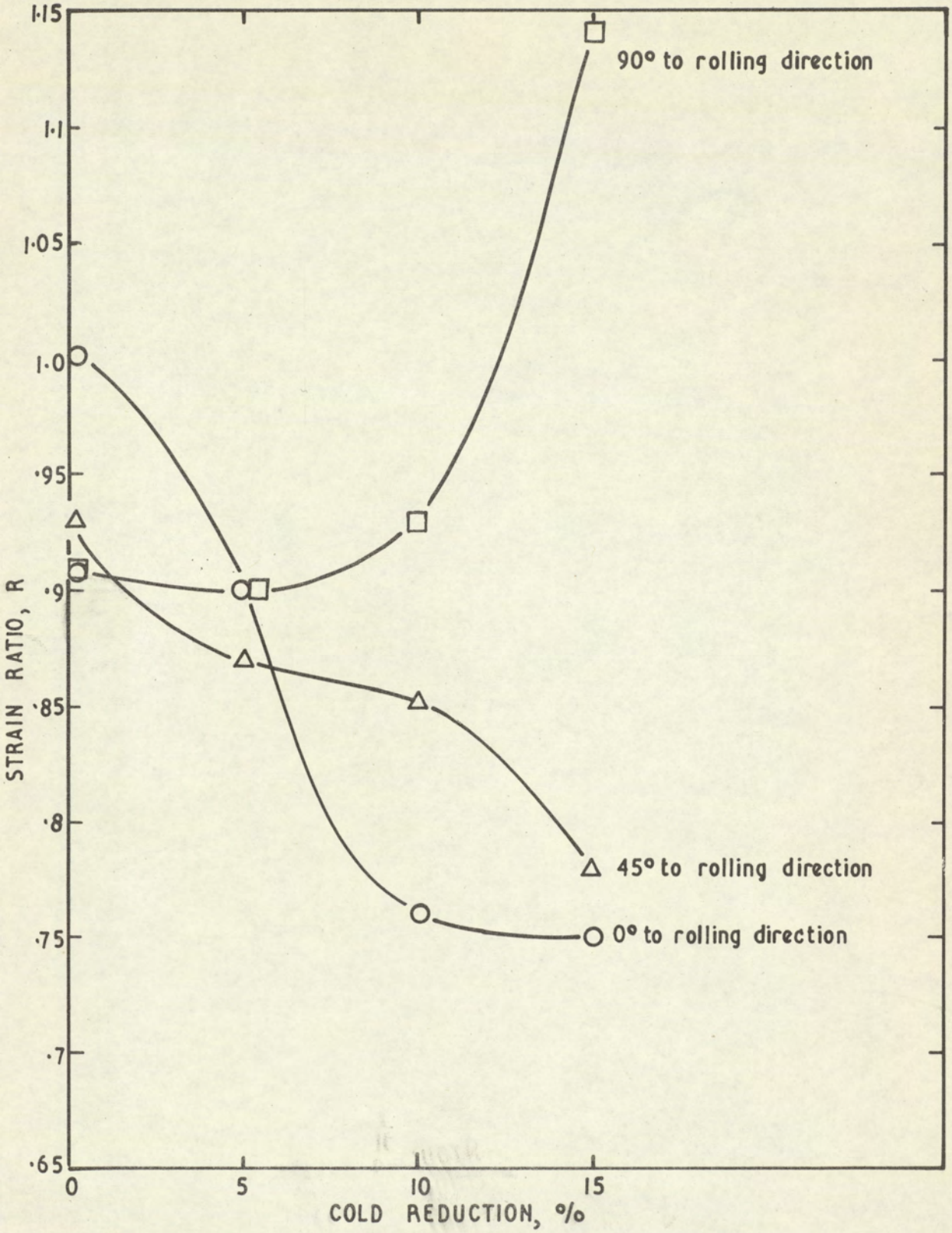

Figure 43 Effect of cold rolling on the strain ratio of 18% Cr-14% Ni steel.

T1279

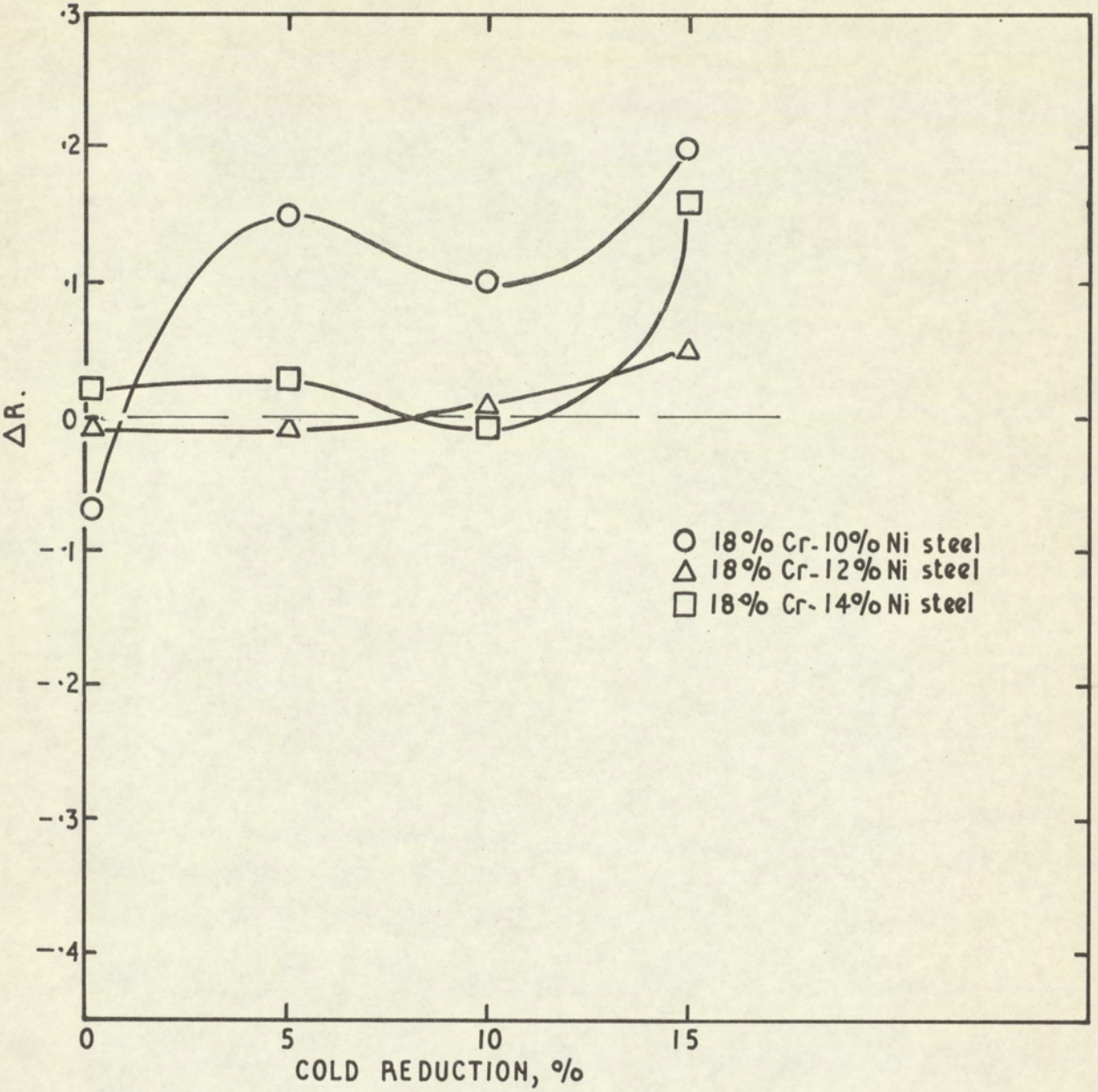

Figure 44 Effect of cold rolling on the planar variation in R, defined as $\Delta R = \frac{1}{2}(R_{0°} + R_{90°} - 2R_{45°})$.

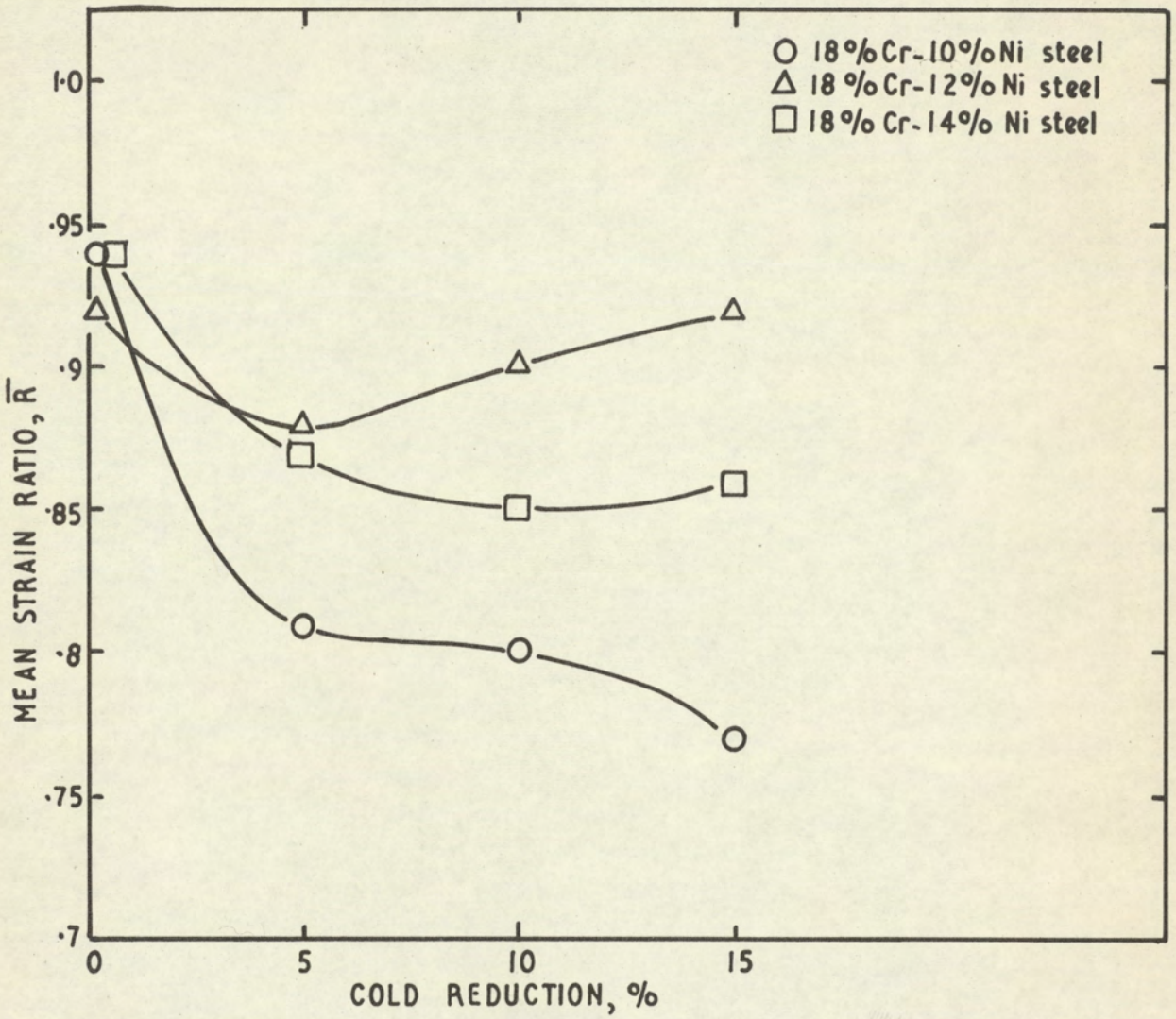

Figure 45 Effect of cold rolling on the mean strain ratio, $\bar{R}$, defined as $\bar{R} = \frac{1}{4}(R_{0°} + 2R_{45°} + R_{90°})$.

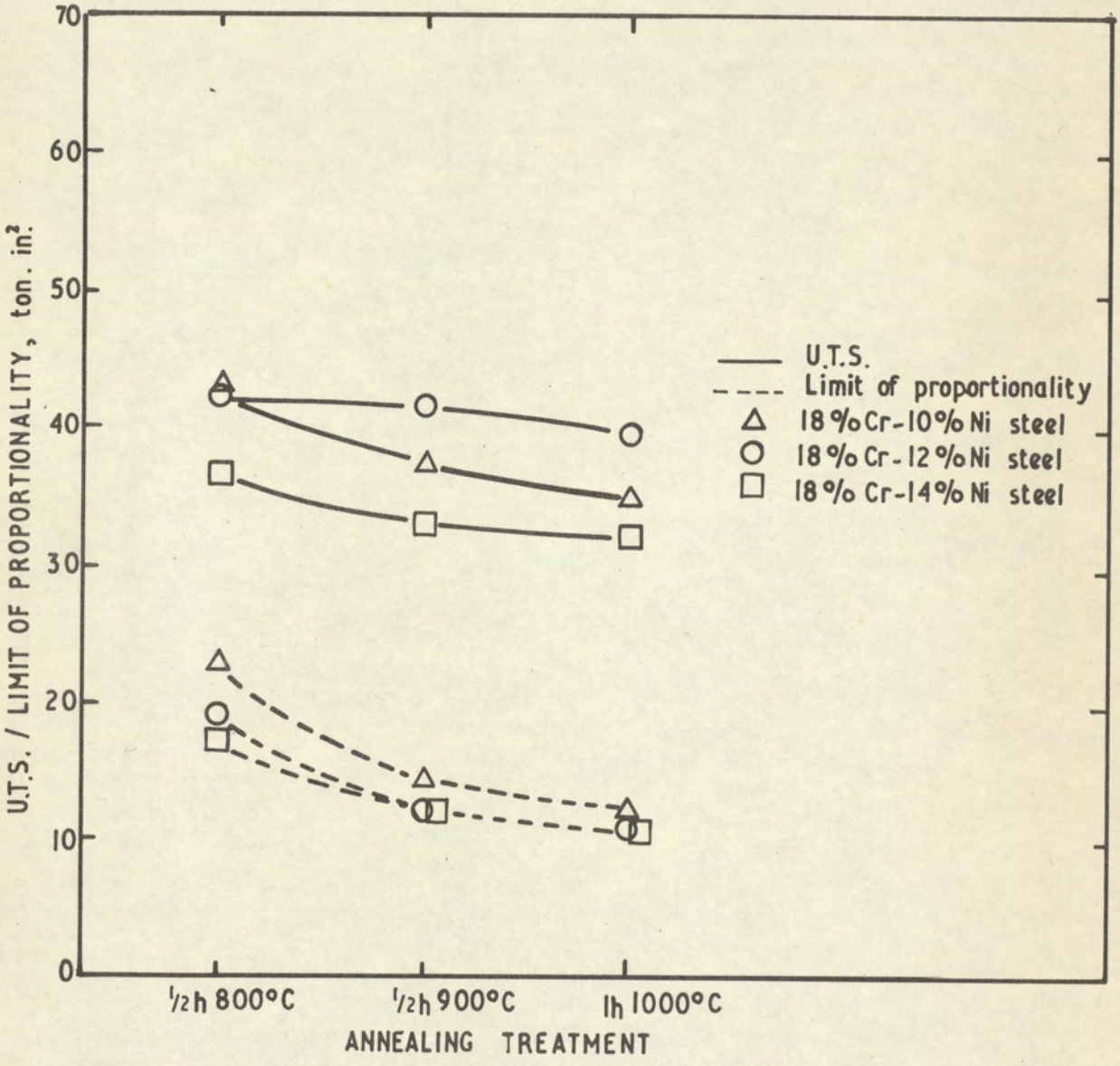

Figure 46 Effect of annealing treatment on U.T.S. and limit of proportionality of 18% Cr steels containing 10-14% Ni

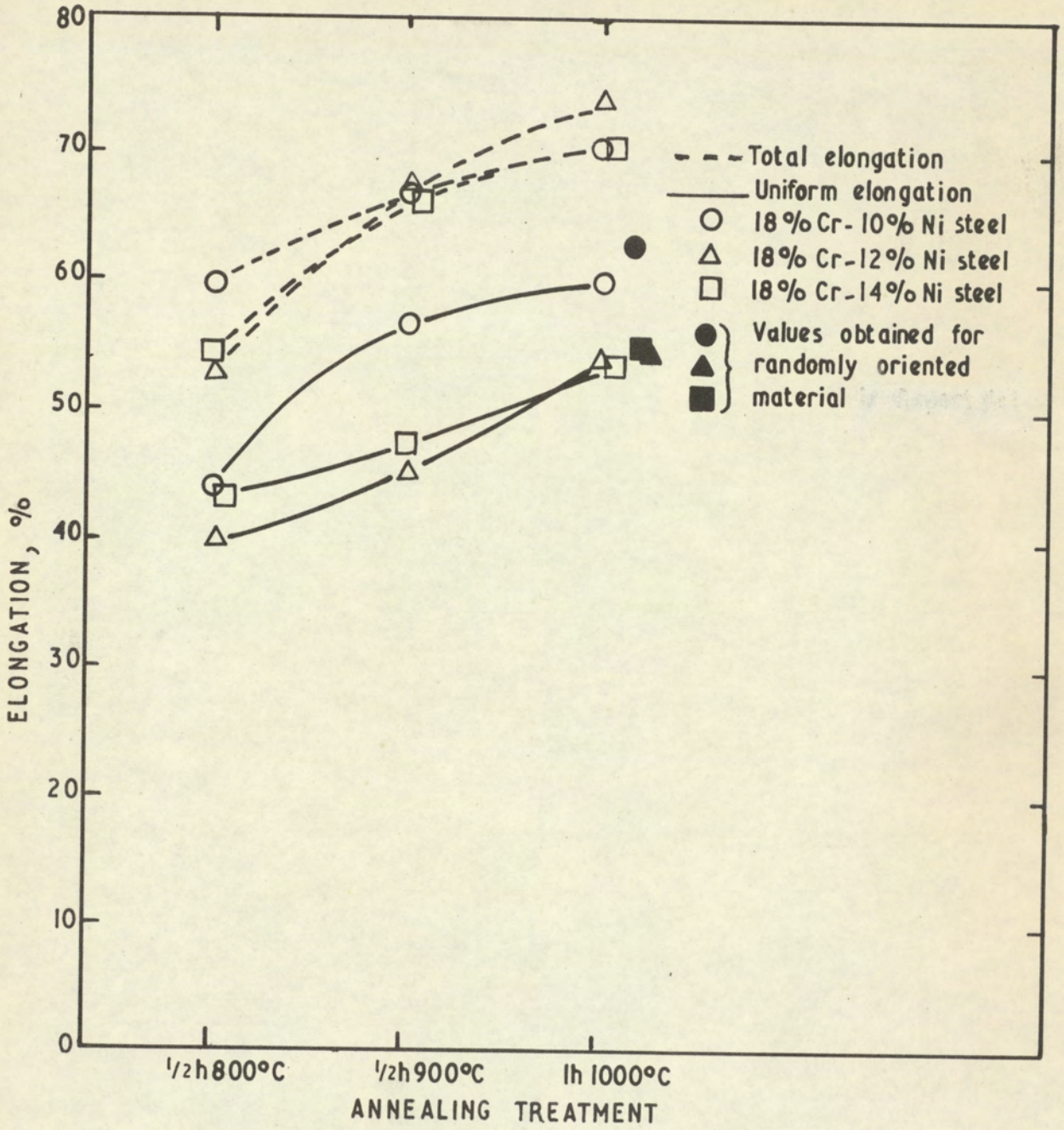

Figure 47 Effect of annealing treatment on % elongation of 18% Cr steels containing 10-14% Ni.

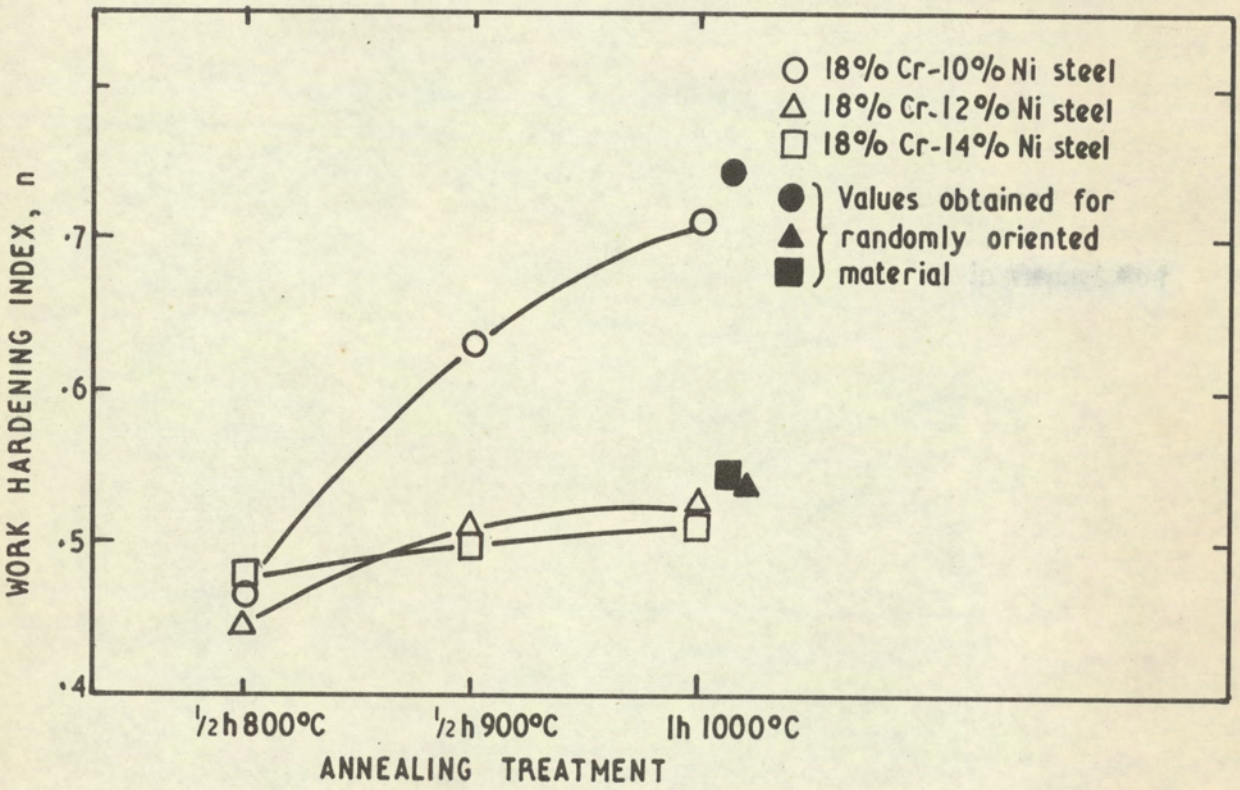

Figure 48 Effect of annealing treatment on the rate of work hardening of 18% Cr steels containing 10-14% Ni.

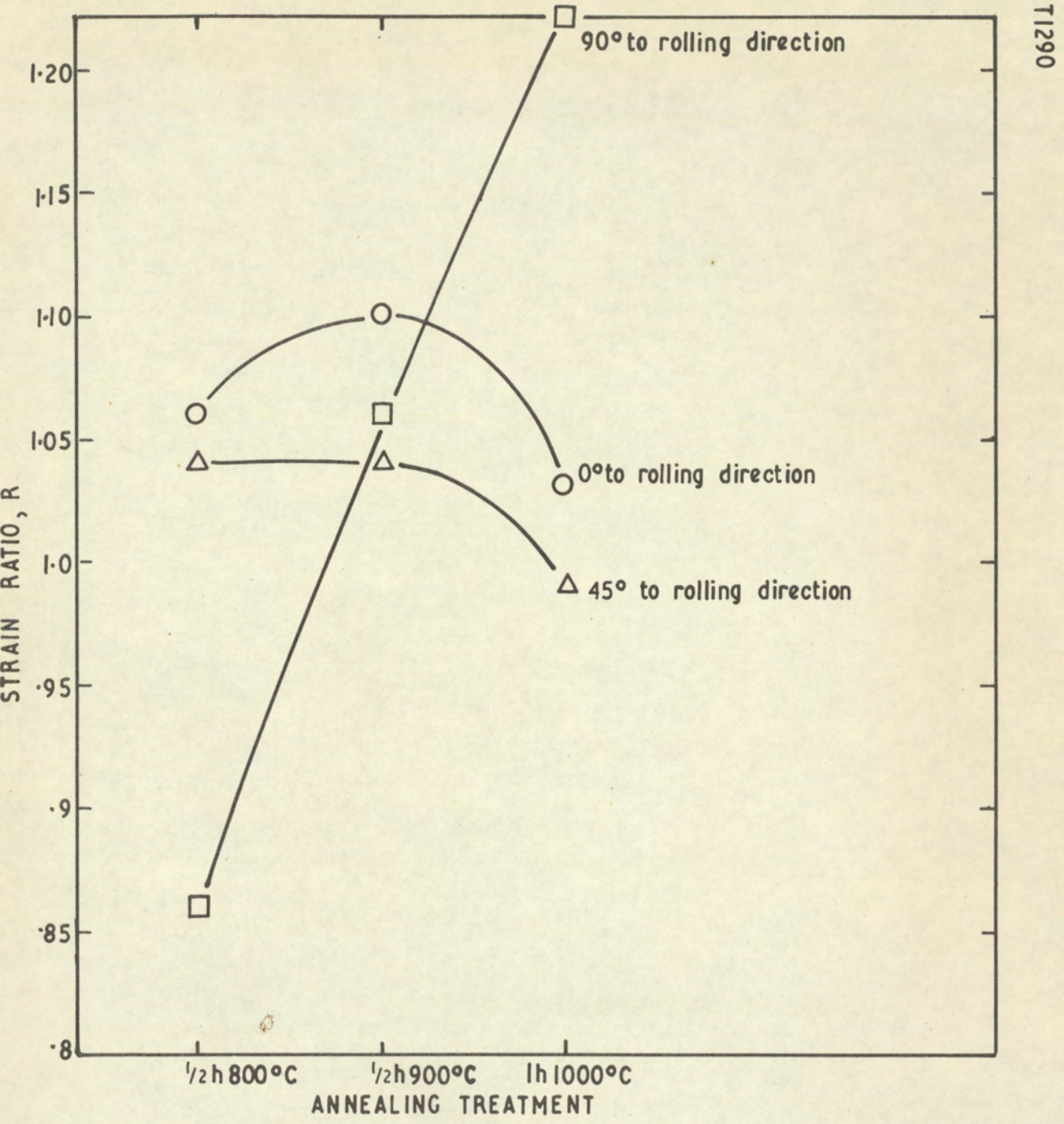

Figure 49 Effect of annealing treatment on the strain ratio of 18% Cr-10% Ni steel.

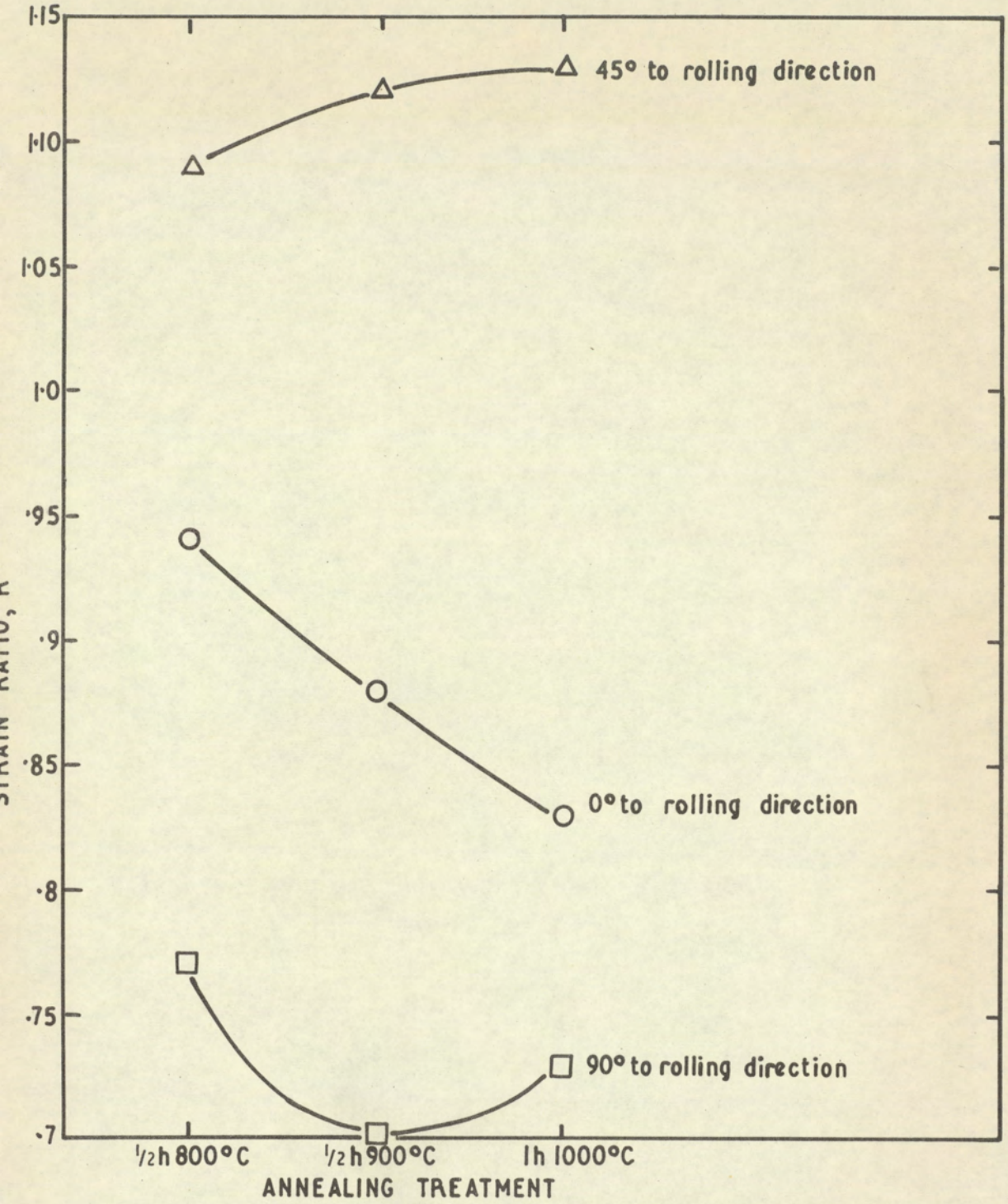

Figure 50 Effect of annealing treatment on the strain ratio of 18% Cr-12% Ni steel.

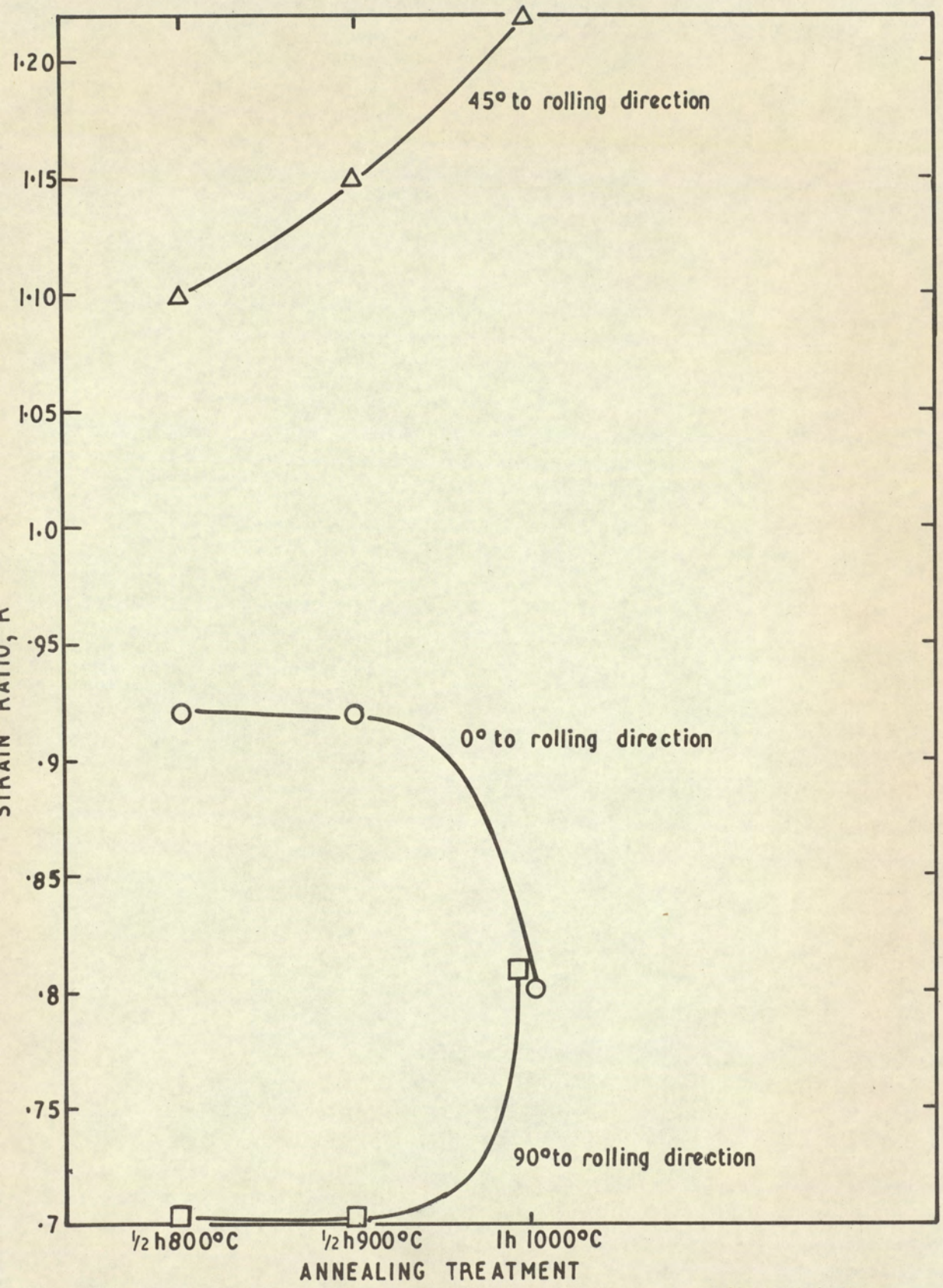

Figure 51 Effect of annealing treatment on the strain ratio of 18% Cr-14% Ni steel.

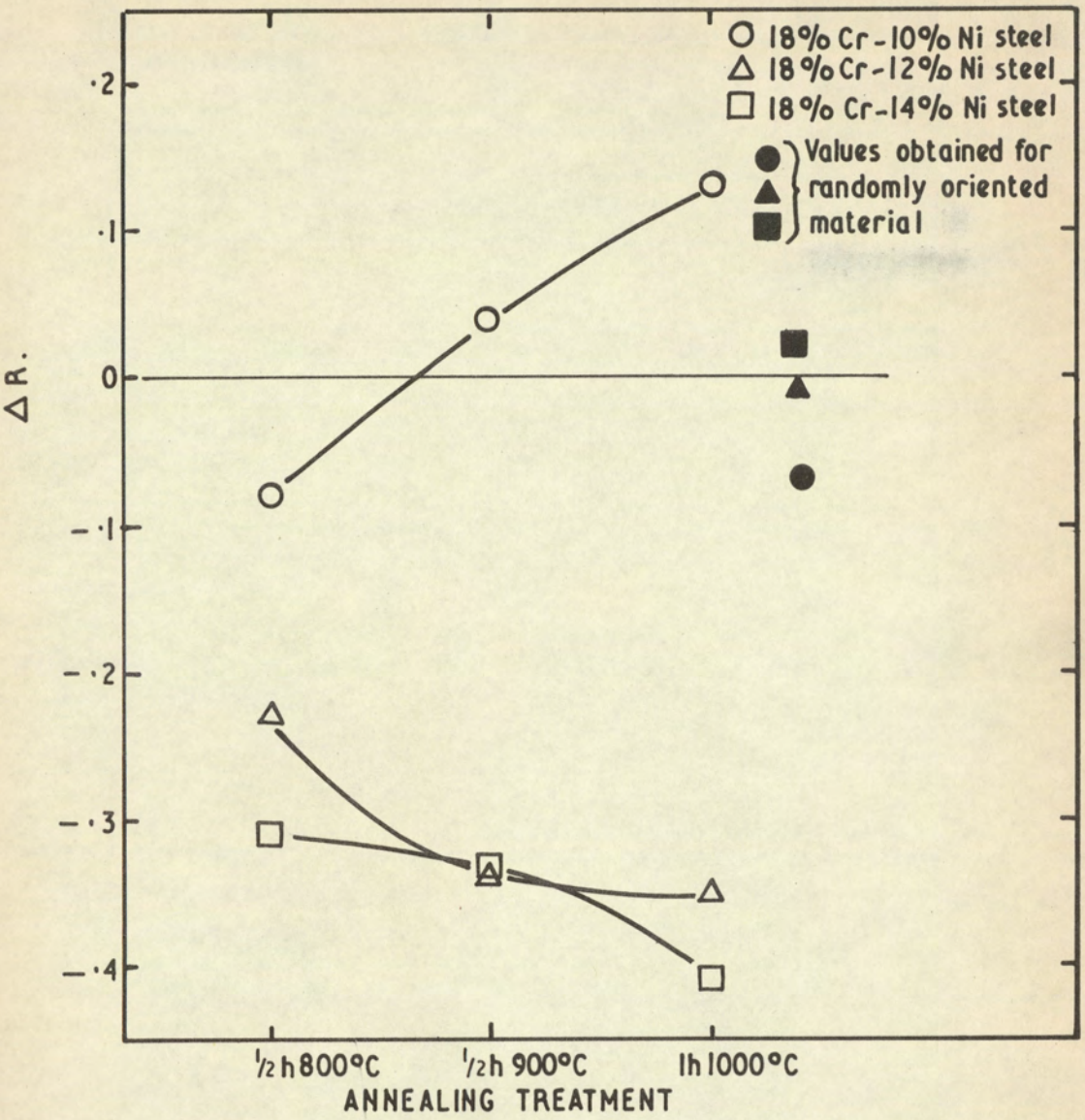

Figure 52. Effect of annealing treatment on the planar variation in R, defined as $\Delta R = \frac{1}{2}(R_{0°} + R_{90°} - 2R_{45°})$.

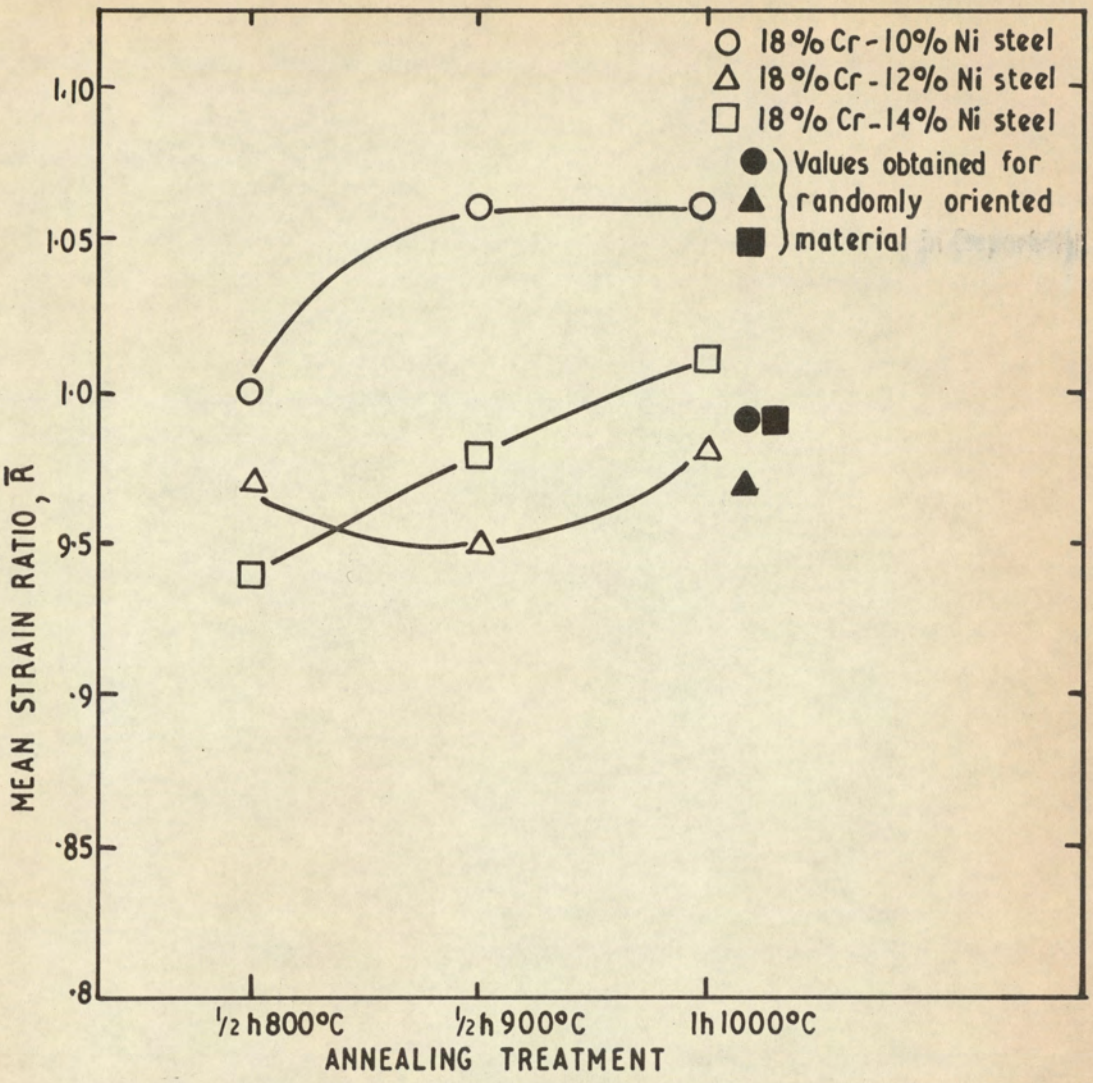

Figure 53 Effect of annealing treatment on the mean strain ratio, $\bar{R}$, defined as $\bar{R} = \frac{1}{4}(R_{0°} + 2R_{45°} + R_{90°})$.

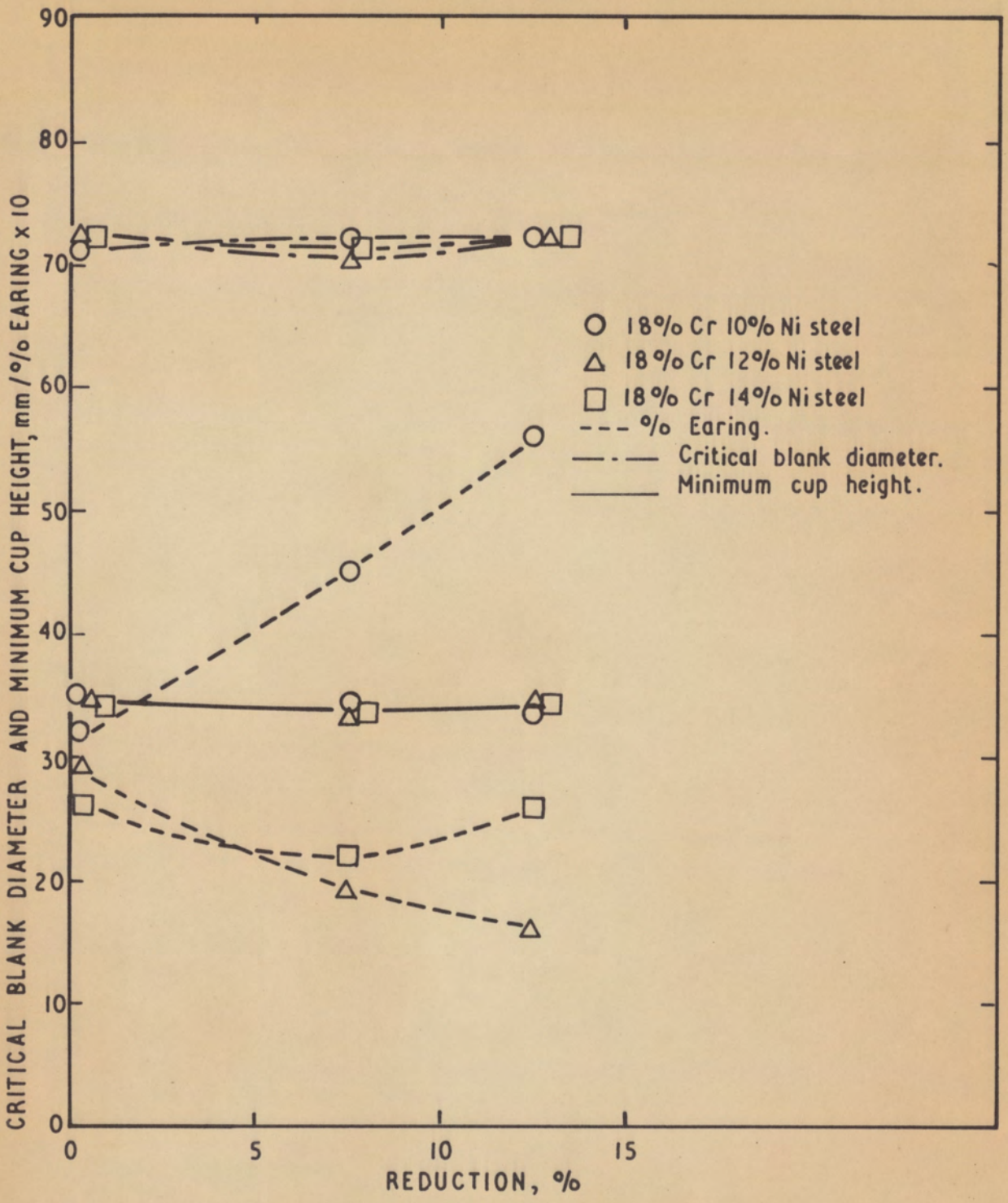

Figure 54 Effect of cold rolling on deep drawability and % earing of steels having an essentially random grain orientation.

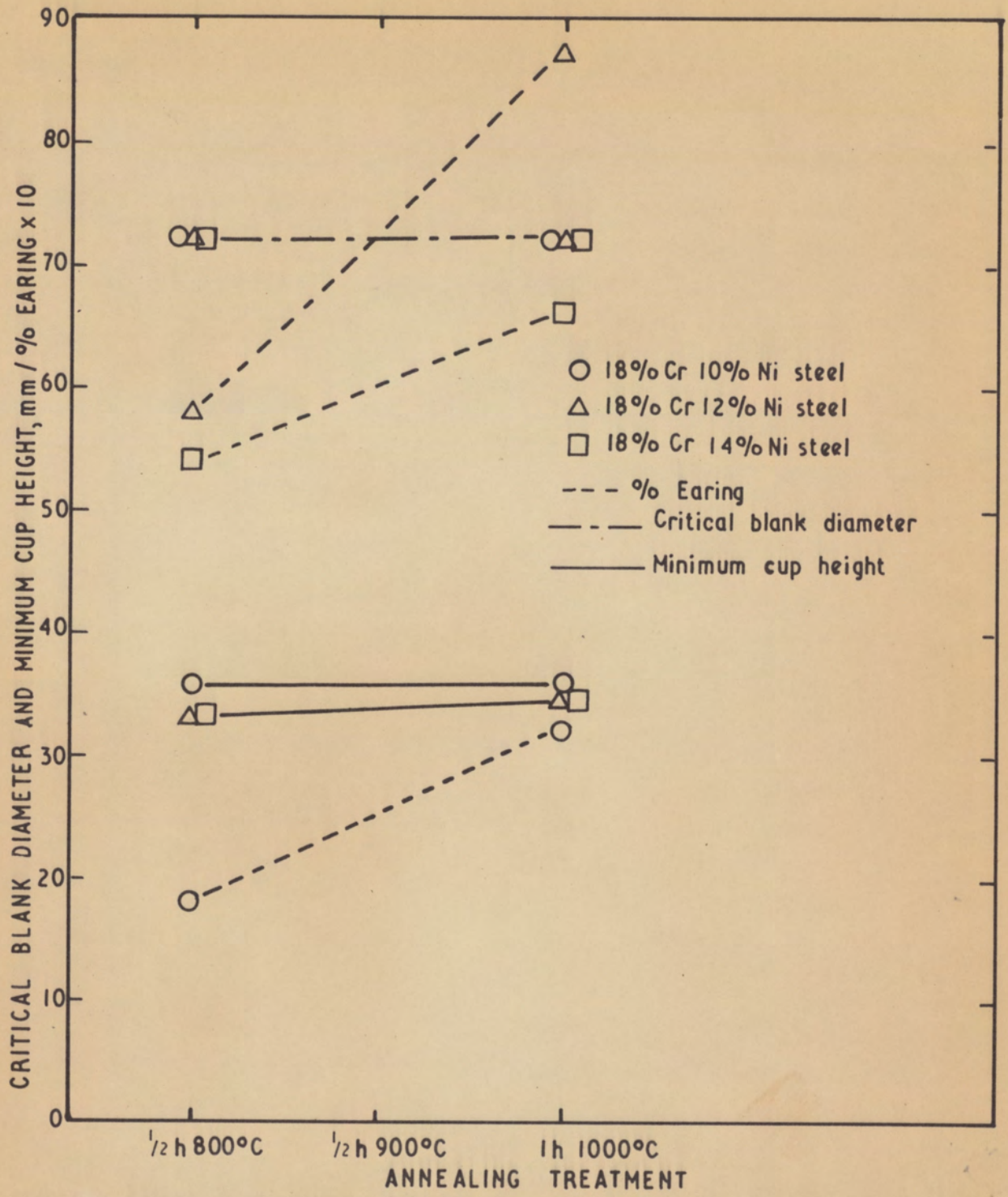

Figure 55 Effect of annealing treatment on deep drawability and % earing of steels having a primary recrystallisation texture developed by 93% cold rolling followed by the annealing treatment indicated.

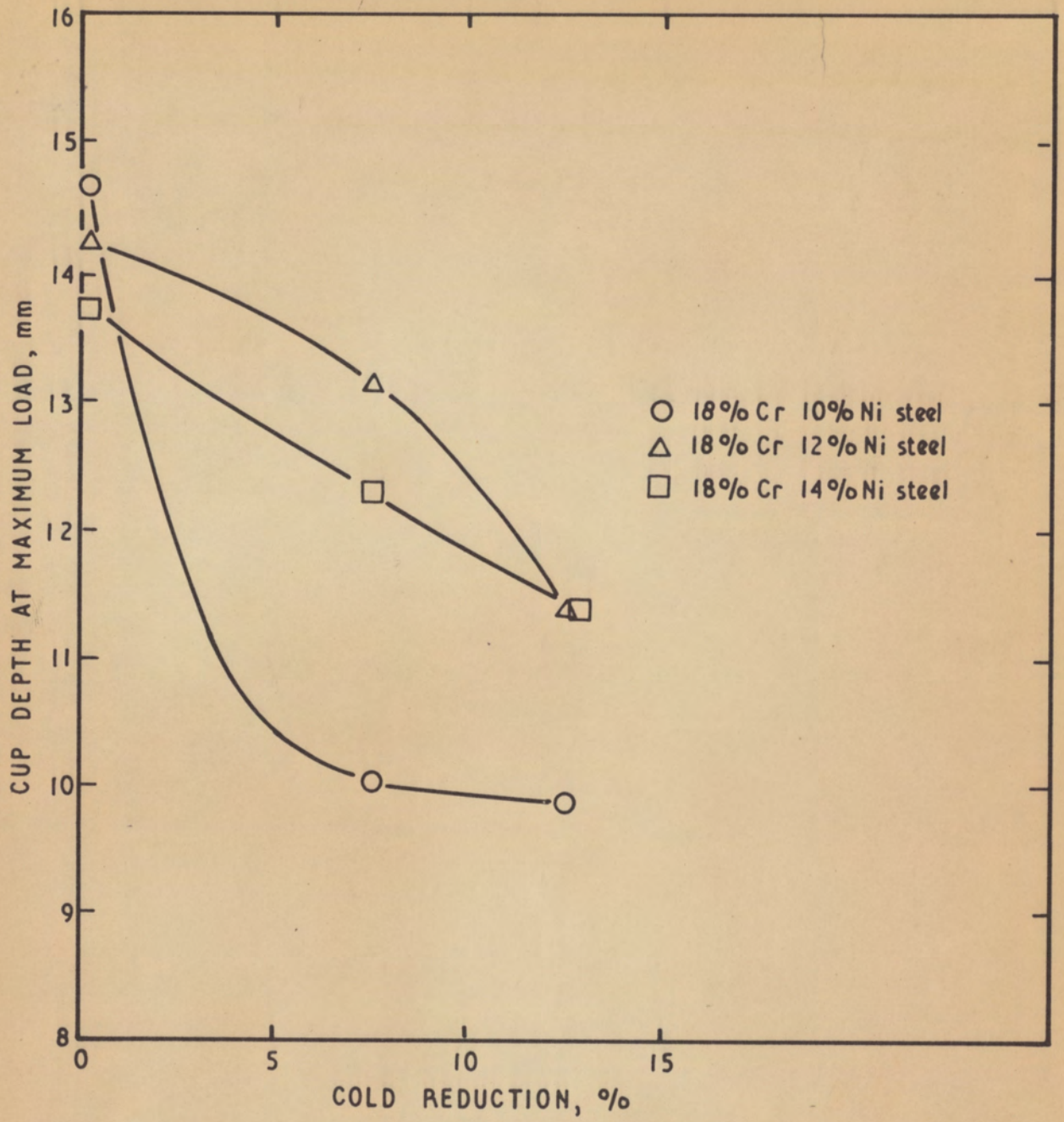

Figure 56 Effect of cold rolling on stretch formability of steels having an essentially random grain orientation.

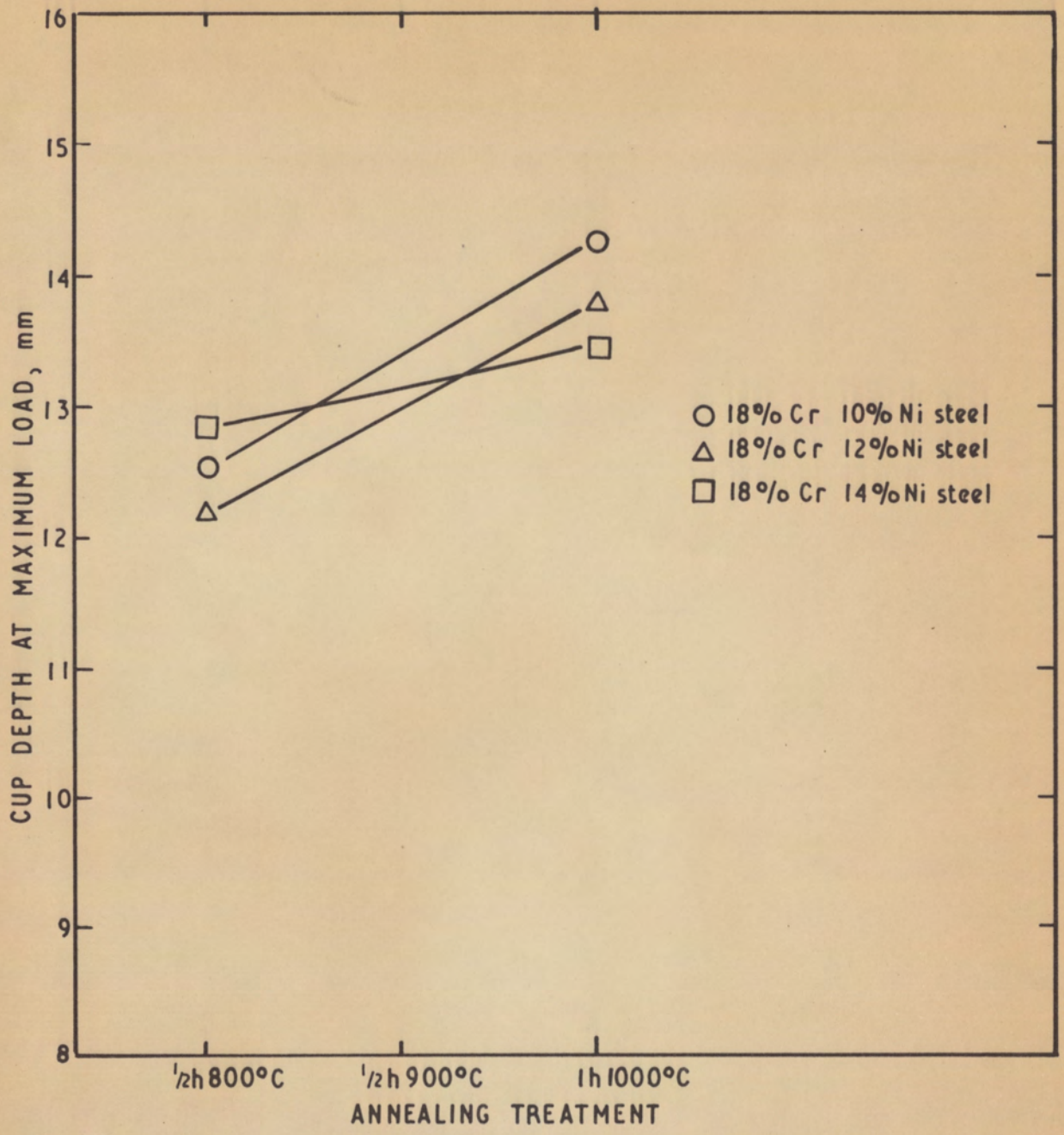

Figure 57 Effect of annealing treatment on stretch formability of steels having a primary recrystallisation texture developed by 93% cold rolling followed by the annealing treatment indicated.